Electronic Structure Calculations of Weak Intermolecular Interactions

by

Reza Hemmati

A dissertation submitted to the Graduate Faculty of
Auburn University
in partial fulfillment of the
requirements for the Degree of
Doctor of Philosophy

Auburn, Alabama
August 7, 2021

Keywords: quantum chemistry, intermolecular interactions, symmetry-adapted perturbation theory

Approved by

Konrad Patkowski, Chair, Associate Professor of Chemistry and Biochemistry
Vincent Ortiz, Ruth W. Molette Professor of Chemistry and Biochemistry
Evangelos Miliordos, Assistant Professor of Chemistry and Biochemistry
Rashad Karimov, Assistant Professor of Chemistry and Biochemistry
Andrew Adamczyk, Assistant Professor of Chemical Engineering

Abstract

This thesis focuses on a novel the application of Symmetry-Adapted Perturbation Theory (SAPT), Functional-group SAPT (F-SAPT), and F-SAPT difference analysis to chiral self-recognition. In addition to these, a variety of highly accurate ab initio electronic structure approaches were applied on the ethylene-oxygen complex to investigate the weak intermolecular interactions in the ground electronic state and several low-lying excited electronic states. SAPT decomposes the fundamental components of noncovalent interactions between two molecules into electrostatics, exchange, induction, and dispersion. These components can be split even more by a method called Functional-group SAPT, which provides the aforementioned separation of the total interaction energy into the contributions of pairs of functional groups. F-SAPT difference analysis transforms the effects of pairs of functional groups to the contributions of substituted functional groups.

We have applied SAPT, F-SAPT, and F-SAPT difference analysis methods to chiral complexes in order to elucidate the origin of chiral self-recognition and investigate the chirodiastaltic (chiral discrimination) energy, the energetic difference between homochiral and heterochiral diastereomers of a complex. For this matter, we chose propylene oxide (PO) as the simplest chiral molecule containing an epoxide ring and glycidol as one of chemical derivatives of PO. 12 possible dimer structures of PO and 14 complexes of glycidol were reoptimized and their interaction energies were computed at different levels of electronic structure theory and basis set up to the complete basis set (CBS) limit of the coupled-cluster approach with single, double, and perturbative triple excitations (CCSD(T)). Then, a variety of symmetry-adapted perturbation theory analyses were applied to both PO dimer structures and glycidol dimers including conventional SAPT, F-SAPT, and F-SAPT difference analysis. Our results showed that the largest diastereomeric energetic effects come from the electrostatic and dispersion SAPT contributions for PO and induction for glycidol in addition to electrostatic and dispersion contributions. To complement our findings, frequency computations were carried out to distinguish

the effect of chiral interactions on the vibrational frequencies of an isolated PO molecule and glycidol.

In another study, we picked an ethylene molecule and an oxygen molecule as a complex and studied their interaction energy at optimized geometry, both in ground state and a few low-lying excited states. In addition, the spin splitting and spin inversion for this complex is going to be performed which has important effects in biology.

Acknowledgments

I would like to thank my Ph.D. advisor Dr. Konrad Patkowski to help and support me to finish this step in my life at Auburn University.

I would also like to thank all the Professors of my committee, Dr. Vincent Ortiz, Dr. Evangelos Miliordos, and Dr. Rashad Karimov. This was a team work and without their help and assistance it was not possible to accomplish these studies.

I would also like to thank my office-mate Dr. Jonathan Waldrop for his time discussing about the projects.

Lastly, I would like to thank my family for providing me the time I needed to study more.

Table of Contents

List of Figures

List of Tables

Chapter 1

Introduction

Computational and theoretical chemistry is a field where all the individual fields of Mathematics, Physics, and Chemistry come together nicely to give the opportunity to formulate and model chemical phenomena that happen in wet labs. One can imagine that for computational chemistry, a computer resembles a lab and diverse softwares and methods play a role of all glassware. The methods used to simulate what occurs on the atomic and molecular levels have different computational complexity, and some of them used in this thesis are explained in the coming chapters. Noncovalent interactions, either intermolecular or intramolecular, as the name implies are interactions not leading to chemical bonds. They can be between different molecules or even between various functional groups in a molecule. The thermodynamics of weakly bonded molecules in the gas phase can be explained by van der Waals noncovalent interactions. In the crystal structure studies, noncovalent intermolecular forces play a crucial role in existence of molecular liquids, and understanding of these forces and interactions makes it possible to predict crystal structures.[1–3] Therefore, understanding their characteristics is crucial in many aspects of biochemistry,[4] surface chemistry,[5,6] thermodynamics, synthesis, and astrochemistry.[7] This thesis mainly focuses on the noncovalent interactions (NCI)[8] and their vital role in chiral discrimination and structural formation of dimers.[9–17]

Since there are many methods to study noncovalent interactions, we employed some of the most accurate and appropriate ones compatible to the chosen systems to elucidate their weak noncovalent interactions' nature in gas phase complexes.

To aim for this goal, one of the wave function-based methods used was the second-order Møller-Plesset (MP2) perturbation theory.[18] It accounts for the correlation energy which is missing in the Hartree-Fock method. MP2 is obtained from the Rayleigh-Schrödinger (RS)

perturbation theory where the unperturbed Hamiltonian is represented by the sum of Fock operators,

$$\hat{\mathrm{H}}^{(0)} = \sum_{\mathrm{i}} \hat{\mathcal{F}}(\mathrm{i}) = \sum_{\mathrm{i}} \hat{h}(\mathrm{i}) + \sum_{\mathrm{p,i}}^{\mathrm{p=N/2}} (2\hat{\mathcal{J}}_{\mathrm{p}}(\mathrm{i}) - \hat{\mathcal{K}}_{\mathrm{p}}(\mathrm{i})) \tag{1.1}$$

where $\hat{\mathcal{F}}$ is the Fock operator, $\hat{h}, \hat{\mathcal{J}}$, and $\hat{\mathcal{K}}$ are the one-electron Hamiltonian, Coulomb, and Exchange operators, respectively.[19,20] Coulomb and exchange operators are defined by their effect on spin orbitals ψ_i,

$$\begin{aligned} \hat{\mathcal{J}}_i(1)\psi_j(1) &= \left[\int d\vec{r_2}\psi_i^*(2) r_{12}^{-1}\psi_i(2)\right]\psi_j(1) \\ \hat{\mathcal{K}}_i(1)\psi_j(1) &= \left[\int d\vec{r_2}\psi_i^*(2) r_{12}^{-1}\psi_j(2)\right]\psi_i(1) \end{aligned} \tag{1.2}$$

In general, MP2 is less accurate than some other methods like coupled-cluster approach, but for the case of molecular systems presented in this work, it gives acceptable and reliable results and its output was used to construct our benchmark interaction energy values along with CCSD(T) and HF results.

The coupled-cluster method CCSD(T) was the second approximate approach utilized to describe the intermolecular interactions and establish the complete basis set (CBS) limit.[21,22] The benchmark interaction energy values were computed using MP2 extrapolated from two different bases with a higher-level correction from a coupled-cluster calculation in the aug-cc-pVTZ basis. The basis sets that were used in these studies are the Dunning-type augmented correlation consistent basis sets, denoted as aug-cc-pVXZ, where X can be D, T, Q, 5, ...[23–25] X is called cardinal number and displays the number of basis functions used in the valence orbitals. The mathematical formulation is described in more details in chapter 2.

Symmetry-adapted perturbation theory (SAPT)[26–31] is the next method used in this research and is one of the most robust methods that gives reliable results that are validated by experiments. SAPT not only gives the interaction energy (IE) of a molecular system, but it also decomposes the IE into individual pieces of contributions of electrostatics, induction, exchange, and dispersion. Therefore, from SAPT one can learn why a complex of interest is bound and what piece(s) of the interaction energy has the most significant contribution to the total interaction energy of the complex. In addition to SAPT, there are two partitions of SAPT,

(1) atomic SAPT (A-SAPT)[32] and (2) functional-group SAPT (F-SAPT),[33,34] of which the latter was used in this thesis. Functional-group SAPT (F-SAPT) indeed adds another layer to the SAPT approach to reveal the contribution of every user-defined functional group into the total interaction energy and its SAPT components. F-SAPT provides more fine-grained analysis of weak intermolecular interactions. F-SAPT was introduced and used for the first time by Dr. Sherrill's group to study organocatalysis and describe NCIs of reactions in transition states,[35] and we employed it to elucidate the influence of functional groups on the chiral discrimination energy in both propylene oxide and glycidol complex projects (Chapter 3).

Now we turn our attention to the density functional theory (DFT).[12–14] DFT is broadly and extensively used by computational chemists, physicists, and materials scientists because of its low cost and acceptable output accuracy. DFT was mainly used by solid state physics to calculate the electronic structure of materials and later in 1990s, it became popular in quantum chemistry. The main reason for its popularity is a good compromise between its accuracy and computational cost which enables this method to be applied to larger quantum systems without losing much of the accuracy. DFT mainly depends on the approximations to the exchange-correlation energy functional. There are hundreds of different proposed functionals and in practice this makes it difficult to chose an appropriate functional, which depends on the chemical system. The most useful and well-known DFT functionals we have used in this study are, PBE, PBE0, B3LYP, and BLYP. Among these functionals B3LYP and PBE0 are called hybrid functionals which were introduced first time by Axel Becke in 1993.[36] They incorporate a portion of the Hartree-Fock exact exchange together with portions of the exchange-correlation energy from nonhybrid DFT. For example, the popular PBE0[37] functional, which stands for Perdew–Burke-Ernzerhof, is constructed as a linear combination of the HF exact exchange functional and PBE exchange energy with a ratio of 1:3, along with the full PBE correlation term as,

$$E_{\mathrm{xc}}^{\mathrm{PBE0}} = \frac{1}{4} E_{\mathrm{x}}^{\mathrm{HF}} + \frac{3}{4} E_{\mathrm{x}}^{\mathrm{PBE}} + E_{\mathrm{c}}^{\mathrm{PBE}} \tag{1.3}$$

where $E_{\mathrm{x}}^{\mathrm{HF}}$, $E_{\mathrm{x}}^{\mathrm{PBE}}$, and $E_{\mathrm{c}}^{\mathrm{PBE}}$ are the HF exact exchange functional, the PBE exchange functional, and the PBE correlation functional, respectively. More details of the DFT functionals and their results are presented in chapter 3.

Doing computations and interpretation of results are different chapters from a book. In other words, after calculations and generating data, one needs statistical methods and tools for manipulating the obtained data. One of them that was extensively used in this research, is mean unsigned error (MUE) which is a measure of errors between pairs of values; in our case, one is the calculated value, E^{i}, and the other is the true value, $\mathrm{E}_{\mathrm{ref}}^{\mathrm{i}}$,. Mathematically, it can be written as,

$$\mathrm{MUE} = \frac{\sum_{\mathrm{i}=1}^{\mathrm{N}} |\mathrm{E}^{\mathrm{i}} - \mathrm{E}_{\mathrm{ref}}^{\mathrm{i}}|}{\mathrm{N}} \tag{1.4}$$

where N is the data set size.

One useful tool for investigating not only a molecular structure but also the interaction energies is a frequency profile of the structure under consideration because molecular vibrations act as a finger print for every specific structure and can reveal invaluable and unique information about the molecular complexes. Generally, a non-linear molecule with N atoms possesses $3N-6$ normal modes of vibration while for a linear molecule there are $3N-5$ normal modes. There are typically six different ways of vibration in molecules that include symmetric stretch, antisymmetric stretch, scissoring, rocking, wagging and twisting. To perform the accurate frequency calculations, there are some necessary prerequisites that must be fulfilled. The first condition that must be satisfied is that the underlying molecular structure must be in a stationary point. In a mathematical view, it means that all first derivatives of the energy with respect to nuclear coordinates must be zero. When molecules are isolated, their frequencies of normal modes are usually different from when they are in contact or interaction with another molecule. This difference in their frequencies is called frequency shift, which is classified into two categories, red-shift and blue-shift. When typical OH$\cdots$O H-bonds are formed, their stretches will undergo red-shift in their vibrational frequency because the O–H bond has a lower frequency in

a cluster compared to the isolated molecule,[38,39] which is the main characteristic of hydrogen bonds.

It can be concluded that vibrational normal modes are a direct outcome of potential energy surface. In other words, computation of vibrational frequencies requires an accurate potential energy surface (PES). Not only that, PES enables one to calculate zero-point energy (ZPE) of molecules; the lowest possible energy that an atom or a molecule may have. Indeed, a key quantity in the theoretical study of the interactions between two molecules/atoms is the potential energy surface. It maps the electronic interaction energy of a molecular cluster as a function of the intermolecular coordinates and of the relative orientation of fragments. When the PES is obtained for a particular system, it is feasible to calculate different quantities such as spectra, crystal parameters, and virial coefficients of the system of interest.

The other important concept in intermolecular interactions that must be taken into account is the monomer deformation. All molecular structures of the present study are in a dimer form and therefore the monomer deformation energy must be included in order to get a highly accurate binding energy. Indeed, when a geometry of a dimer structure is optimized, the monomer geometries are changed based on complexation.

1.1 Chiral Molecules and Significance of Chirality

In chemistry, if a molecule or ion cannot be superimposed on its mirror image by any rotations, translations, or a mixture of these two, that molecule or ion is called chiral. The geometric property of a molecule or ion is then called chirality. Chiral molecules or ions that are mirror images of one another are known as enantiomers. Chiral molecules do not have a plane of symmetry, that is, a plane that bisects a molecule in which the two halves are mirror images of each other. An example of such structure is an Alanine molecule. Most of the time in organic molecules, a carbon atom connected to four different substituents is the cause of chirality. In those cases, the carbon atom is called chiral or stereogenic center. This is not always the case; sometimes there are no chiral centers but the whole structures of molecules are chiral, such as the inherently chiral fullerene D_2-C_{76}. The two enantiomers of a chiral molecule are named based on their right-handedness (R) or left-handedness (S). Chirality is extremely important in our daily lives.

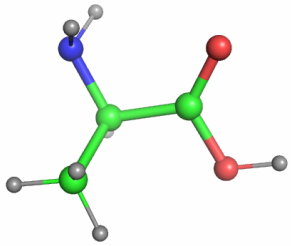

Figure 1.1: A R-alanine molecule as an example of a chiral molecule.

Usually only one enantiomer of a drug favors the desired effects and the other enantiomer is inactive or sometimes toxic. Indeed, all except one of the 20 amino acids from naturally occurring proteins are chiral and all of them are considered as left-handed. In addition, natural sugar molecules are all classified as right-handed. Therefore, chiral molecules and their interactions are significant in chemical and biological processes. Chiral recognition or chiral discrimination is defined as the ability of a chiral molecule or ion to recognize between the two enantiomers of another chiral molecule or ion. Therefore, to get inside into the chiral self-recognition, one of the main steps is the investigation of the interaction energies of the two enantiomeric forms of a chiral molecule to answer the questions such as, what are the driving forces for intermolecular interactions? how do they lead enantiomers to enantioselectivity in natural processes? The enantiomeric recognition has significant importance in chiral chromatography,[40] enantioselective synthesis (asymmetric synthesis),[41] and enantiomeric purity measurements using Nuclear Magnetic Resonance (NMR).[42]

1.2 Multireference methods

Multireference electron correlation methods such MRCI, are important for exploring static correlation effects. These methods can be utilized to compute highly accurate global potential energy surfaces (PESs) of ground and excited states. The HF method (see section 2.2 for more details) does not include electron correlation because it considers the average Coulombic interactions between electrons, and also it does not measure electron distributions and their quantum mechanical effects on the electron of interest. Therefore, the HF ground state wave function Φ_0 will be an approximate wave function. The HF ground state wave function encompasses a finite

set of spinorbitals if a finite basis set is used. For example, if a basis possesses M functions, it will generate M spatial wave functions and $2\mathrm{M}$ spinorbitals considering spin up and spin down electrons. Hence, for a quantum mechanical system with n electrons, the HF ground state wave function yields a finite set of n occupied spinorbitals

$$\Phi_0 = (1/n!)^{1/2} det|\phi_1(\vec{r_1})\phi_2(\vec{r_2})\cdots\phi_a(\vec{r_a})\phi_b(\vec{r_b})\cdots\phi_n(\vec{r_n})| \tag{1.5}$$

and therefore, there remain $2\mathrm{M}-\mathrm{n}$ spinorbitals unoccupied which are called virtual orbitals. Obviously, Φ_0 is one of the many Slater determinants that can be constructed from the $2\mathrm{M}$ spinorbitals. According to the ground state Slater determinant, it can be possible to classify all remaining determinants based on the number of transitions of electrons from occupied orbitals to virtual orbitals. As an example, a singly excited determinant corresponding to a single electron promotion from occupied spinorbital ϕ_{a} to a virtual spinorbital ϕ_{r} can be written as,

$$\Phi_a^r = det|\phi_1(\vec{r_1})\phi_2(\vec{r_2})\cdots\phi_r(\vec{r_a})\phi_b(\vec{r_b})\cdots\phi_n(\vec{r_n})| \tag{1.6}$$

Correspondingly, similar excited determinants can be formed and a symmetry-adapted linear combination of those Slater determinants is called a Configuration State Function (CSF). Later on to get an excited state wave function for a molecular system, these excited CSFs can be used. For this reason, the exact ground state or excited state wave functions can be represented as linear combinations of all possible n-electron Slater determinants. Therefore, the electronic wave function can be written in the form,

$$\Psi = \mathrm{c}_0\Phi_0 + \sum_{\mathrm{a,r}} \mathrm{c}_{\mathrm{a}}^{\mathrm{r}}\Phi_{\mathrm{a}}^{\mathrm{r}} + \cdots \tag{1.7}$$

This method is called Configuration Interaction (CI), which is one of the post-Hartree-Fock methods for solving the Schrödinger equation within the Born–Oppenheimer approximation.[43,44] The Born–Oppenheimer approximation assumes that the wave function of electrons and nuclei can be considered separately because of the fact that the masses of atomic nuclei are much larger than the mass of electron. The energy that comes from the CI method and the energy

coming from the HF method are different. This difference is called the correlation energy. Hence, the correlation energy, which is neglected in the HF method, is recovered by configuration interaction. One serious drawback of CI calculations is the lack of size-consistency. As outlined above, in the CI method the wave function is written as a linear combination of a set of many electron functions,

$$\Psi_{\mathrm{CI}} = \sum_{\mathrm{I}} \mathrm{C_I}\Phi_{\mathrm{I}} \tag{1.8}$$

where the coefficients $\mathrm{C_I}$ must be determined. If the set of $\{\Phi_{\mathrm{I}}\}$ encompasses the entire many-electron space, Ψ_{CI} is a full CI wave function. Unfortunately, even for small molecules, the total number of determinants can be dramatically large and it will be so expensive in terms of computational costs. In practice, one needs to truncate the full CI and this leads to size-consistency problem mentioned above. In simple words, a method is considered size-consistent if the sum of the energies of two subsystems A, B when they are far apart is equal to the energy of these two when they are treated as a supersystem using the same method. As the size of a molecular system increases, the magnitude of the size-consistency error rises. However, there are some corrections that can reduce this error such as the Davidson correction.[45]

In the CI methods, either the ground state wave function or excited states wave function can be represented as a linear combination of all possible n-electron Slater determinants built from a given set of spinorbitals. Therefore, for a full CI we can rewrite the eqn 1.8,

$$\Psi_{\mathrm{CI}} = \mathrm{a_0}\Phi_{\mathrm{HF}} + \sum_{\mathrm{i}}^{\mathrm{occ}}\sum_{\mathrm{r}}^{\mathrm{vir}} \mathrm{a_i^r}\Phi_{\mathrm{i}}^{\mathrm{r}} + \sum_{\mathrm{i<j}}^{\mathrm{occ}}\sum_{\mathrm{r<s}}^{\mathrm{vir}} \mathrm{a_{ij}^{rs}}\Phi_{\mathrm{ij}}^{\mathrm{rs}} + \cdots \tag{1.9}$$

where the a_ks are the expansion coefficients, indices i, j, ..., and r, s, ... are occupied and virtual molecular orbitals, respectively and the limits in the summation indices prevent generating a given excited state determinant twice. Also, the notation $\Phi_{\mathrm{i}}^{\mathrm{r}}$ shows all possible single electronic excitations where an electron from the occupied orbital i is excited and occupies the virtual orbital r, as such the second summation in the eqn. 1.9 represents all possible doubly excited electronic excitations. In this method, orbital wave functions (Slater determinants) are

held fixed and the expansion coefficients are optimized; but in the **Multiconfiguration Self-Consistent Field** method (MCSCF),[46,47] both CI coefficients and orbitals are optimized. This leads to the MCSCF methods, which can give accurate results even with a smaller number of CSFs. Like the SCF procedure, MCSCF is also an iterative method. When excited states computations are demanding, efficient MCSCF methods play an important role. The main procedure in MCSCF is the selection of CSFs and one of the popular approaches is the **Complete Active-Space Self-Consistent Field method** (CASSCF)[48] where the spinorbitals are classified into the following three classes for the selection of configurations,

- **inactive (core) orbitals** constructed by the lowest energy spinorbitals that always hold two electrons.
- **active orbitals** that are partially occupied and are energetically above the core orbitals.
- **virtual orbitals** composed of spinorbitals that are always unoccupied and are energetically above the other two inactive and active orbitals.

By this classification, the next step is to distribute all active electrons over all active orbitals in any possible ways in order to get the configuration state functions.

The reference wave function for the previous mentioned CI methods is the HF wave function, Φ_0, and the CSFs are generated by exciting electrons from occupied MOs of Φ_0 into unoccupied MOs. In **Multi-Reference Configuration Interaction** method (MRCI)[47,49,50] a set of reference configurations is generated, which correspond to all configurations from CASSCF. MRCI methods are not the only methods to calculate excited states of molecular systems. There are many different theoretical frameworks for computation of excited states which are out of the scope of the current dissertation.

Chapter 2

Methodology in electronic structure theory

The central part of all electronic structure methods is the Schrödinger equation which was introduced by Erwin Schrödinger in 1925,

$$i\hbar\frac{\partial}{\partial t}\Psi(\vec{r},t) = \hat{H(t)}\Psi(\vec{r},t) \tag{2.1}$$

where $\hat{H(t)}$ and $\Psi(\vec{r},t)$ are the time-dependent Hamiltonian operator and wave function of a system, respectively. This equation is a partial differential equation in which the first derivative of wave function, $\Psi(\vec{r},t)$, with respect to time depends on the second derivative of the wave function with respect to system coordinates. From general Physics, it is known that the Hamiltonian of a system is the sum of kinetic and potential energies. Therefore the explicit form of the Schrödinger equation can be written as,

$$i\hbar\frac{\partial\Psi(\vec{r},t)}{\partial t} = -\frac{\hbar^2}{2m}\nabla^2\Psi(\vec{r},t) + V(\vec{r})\Psi(\vec{r},t) \tag{2.2}$$

For the sake of simplicity we assume that potential energies are independent of time. Therefore, it is feasible to separate the above partial differential equation to two ordinary differential equations as follows. The wave function can be written

$$\Psi(\vec{r},t) = P(\vec{r})T(t) \tag{2.3}$$

which conveys that

$$i\hbar P(\vec{r})\frac{dT(t)}{dt} = \left[-\frac{\hbar^2}{2m}\nabla^2 P(\vec{r}) + V(\vec{r})P(\vec{r})\right]T(t) \tag{2.4}$$

By dividing both sides of the equation by $P(\vec{r})T(t)$, we can write,

$$i\hbar\frac{1}{T(t)}\frac{dT(t)}{dt} = \frac{1}{P(\vec{r})}\left[-\frac{\hbar^2}{2m}\nabla^2 P(\vec{r}) + V(\vec{r})P(\vec{r})\right] \tag{2.5}$$

because the two sides of the equation depend on various independent variables, it can only be true if each side equals a constant which is labeled E.

$$i\hbar\frac{dT(t)}{dt} = ET(t) \tag{2.6}$$

where its solution is

$$T(t) = ke^{-iEt/\hbar} \tag{2.7}$$

where k is a constant. The other equation which is known as the time-independent Schrödinger equation can be written as,

$$-\frac{\hbar^2}{2m}\nabla^2 P(\vec{r}) + V(\vec{r})P(\vec{r}) = EP(\vec{r}) \tag{2.8}$$

This is an eigenvalue equation which has different characteristics from equation (2.1), which describes the time evolution of the wave function $\Psi(\vec{r}, t)$.

The Schrödinger equation can only be solved exactly for a few model problems, but for real life situations it cannot be solved analytically. Therefore, to overcome this difficulty, we need to make approximate methods of solving this equation. One of them is the Born-Oppenheimer approximation which is the subject of the next section.

2.1 The Born-Oppenheimer Approximation

The Born-Oppenheimer (BO) approximation is based on the big difference in masses of electrons and nuclei in atomic and molecular systems.[43] Because nuclei are much heavier than the electrons, they cannot respond instantaneously to displacements of electrons and therefore they can be considered to be fixed. Hence, the electron and nuclear motions can be decoupled, and

electronic energies can be computed for fixed nuclear positions. In this approximation, the total wave function is written as a product of the electronic and nuclear wave functions.

For the case of molecules, the Hamiltonian of the time-independent Schrödinger equation contains five contributions to the total energy of the system. They include the kinetic energies of electrons and nuclei, the Coulomb potential between electrons and nuclei, the repulsion between electrons and between nuclei, respectively.

$$\mathrm{H} = -\sum_{\mathrm{i}=1}^{\mathrm{N}} \frac{\hbar^2}{2\mathrm{m_e}} \nabla_{\mathrm{i}}^2 - \sum_{\mathrm{k}=1}^{\mathrm{M}} \frac{\hbar^2}{2\mathrm{m_k}} \nabla_{\mathrm{k}}^2 - \sum_{\mathrm{i}=1}^{\mathrm{N}} \sum_{\mathrm{k}=1}^{\mathrm{M}} \frac{\mathrm{e}^2 \mathrm{Z_k}}{\mathrm{r_{ik}}} + \sum_{\mathrm{i}=1}^{\mathrm{N}} \sum_{\mathrm{j}>1}^{\mathrm{N}} \frac{\mathrm{e}^2}{\mathrm{r_{ij}}} + \sum_{\mathrm{k}=1}^{\mathrm{M}} \sum_{\mathrm{l}>\mathrm{k}}^{\mathrm{M}} \frac{\mathrm{e}^2 \mathrm{Z_k} \mathrm{Z_l}}{\mathrm{R_{kl}}} \tag{2.9}$$

where i and j run over electrons (N), k and l run over nuclei (M), $\hbar$ is Planck's constant divided by 2π, $\mathrm{m_e}$ and $\mathrm{m_k}$ are the mass of an electron and a nucleus, respectively, ∇^2 is the Laplacian operator, e is the charge of an electron, Z is the atomic number of an element, $\mathrm{r_{pq}}$ is the distance between an electron and a particle, and finally $\mathrm{R_{pq}}$ is the distance between two nuclei. Indeed, solving the Schrödinger equation analytically for many-particle molecular systems is extremely difficult because of the correlated motions of electrons and nuclei. In other words, the motion of any particle depends on the motion and position of all the other particles. Since nuclei are much heavier than the electrons, they move much more slowly. Therefore, to a good approximation, the motions of electrons and nuclei can be decoupled and one can consider the motions of electrons at the fixed nuclear positions. This is called the Born-Oppenheimer approximation. This approximation implies that the nuclear kinetic energy term is independent of the electrons. Therefore, the second term of equation (2.9), the nuclear kinetic energies, can be neglected and the last term, repulsion between nuclei, can be considered as a constant. Thus, the electronic Schrödinger equation can be written as,

$$\mathrm{H_{elec}} = -\sum_{\mathrm{i}=1}^{\mathrm{N}} \frac{\hbar^2}{2\mathrm{m_e}} \nabla_{\mathrm{i}}^2 - \sum_{\mathrm{i}=1}^{\mathrm{N}} \sum_{\mathrm{k}=1}^{\mathrm{M}} \frac{\mathrm{e}^2 \mathrm{Z_k}}{\mathrm{r_{ik}}} + \sum_{\mathrm{i}=1}^{\mathrm{N}} \sum_{\mathrm{j}>1}^{\mathrm{N}} \frac{\mathrm{e}^2}{\mathrm{r_{ij}}} = \hat{\mathrm{T}}_{\mathrm{e}} + \hat{\mathrm{V}}_{\mathrm{en}} + \hat{\mathrm{V}}_{\mathrm{ee}} \tag{2.10}$$

where the subscript "elec" emphasizes the electronic Hamiltonian. The solution to an electronic Schrödinger equation,

$$\mathrm{H_{elec}} \Phi_{\mathrm{elec}} = \mathrm{E_{elec}} \Phi_{\mathrm{elec}} \tag{2.11}$$

is the electronic wave function denoted by Φ_{elec},

$$\Phi_{\mathrm{elec}} = \Phi_{\mathrm{elec}}(\tilde{\mathrm{r}}; \tilde{\mathrm{R}}) \tag{2.12}$$

which shows the explicit dependence of the electronic wave function on the electronic coordinates ($\tilde{\mathrm{r}}$) and the implicit dependence (parametrically) on the nuclear coordinates ($\tilde{\mathrm{R}}$). Also the electronic energy, $\mathrm{E}_{\mathrm{elec}}(\tilde{\mathrm{R}})$, depends parametrically on the positions of nuclei.

2.2 Hartree-Fock Theory

Hartree-Fock theory is a fundamental concept in electronic structure theory. It is the basis of describing the motion of every single electron by a molecular orbital (MO); and molecular orbitals are made of linear combinations of atom-centered basis functions and the Hartree-Fock method tries to find the coefficients of these linear expansions.

Now the main problem is to solve the electronic Schrödinger equation which can be denoted simply as

$$(\hat{\mathrm{T}}_{\mathrm{e}} + \hat{\mathrm{V}}_{\mathrm{en}} + \hat{\mathrm{V}}_{\mathrm{ee}})\Psi_{\mathrm{e}} = \mathrm{E}_{\mathrm{e}}\Psi_{\mathrm{e}}. \tag{2.13}$$

It is impossible to solve this equation analytically except for a few systems with one electron. For many electron systems, one needs to make some assumptions and approximations to solve this equation computationally. One of the possible approximations is the Hartree-Fock (HF) method. Hartree-Fock assumes that an electron interacts with a mean field of the rest of electrons. Solutions to eqn.2.13 are called electronic wave functions, which include the spatial and spin coordinates of electrons. According to the Pauli principle for fermions, which includes electrons, the total electronic wave function must be antisymmetric by interchanging the spatial coordinates and spin states of any two electrons. By these characteristics, it is feasible to represent the N-electron wave function of a molecular system by the following determinant that

is known as Slater determinant,[51]

$$\Psi_e(\vec{r}_1, \vec{r}_2, \cdots, \vec{r}_N) = \frac{1}{\sqrt{N!}} \begin{vmatrix} \chi_1(\vec{r}_1) & \chi_2(\vec{r}_1) & \cdots & \chi_N(\vec{r}_1) \\ \chi_1(\vec{r}_2) & \chi_2(\vec{r}_2) & \cdots & \chi_N(\vec{r}_2) \\ \vdots & \vdots & \ddots & \vdots \\ \chi_1(\vec{r}_N) & \chi_2(\vec{r}_N) & \cdots & \chi_N(\vec{r}_N) \end{vmatrix} \tag{2.14}$$

where $\chi_N(\vec{r})$s are molecular spinorbitals and $\vec{r}$ denotes the position and spin of a single electron. Generally, a spinorbital is a product of spatial orbital ψ and a spin state function which is denoted by α for spin up and β for spin down. The HF method alone can recover 99% of the total energy of a system and the 1% remaining which is called correlation energy, $\mathrm{E_{corr}}$, varies across the potential energy surface (PES) of the system of interest. Correlation energy mathematically can be written as,

$$\mathrm{E_{corr}} = \mathrm{E_0} - \mathrm{E_{HF}} \tag{2.15}$$

where $\mathrm{E_0}$ is the exact energy. This is the main drawback of the HF method which limits its application in practice; nevertheless, it is the starting point of many advanced wave function methods and plays a vital role in so called post-HF methods.

2.2.1 Møller-Plesset (MP) perturbation theory

One the simplest post-HF methods is the Møller-Plesset (MP) perturbation theory.[18] It starts with HF determinant as a good approximation to the ground state and then tries to recover the missing correlation energy using a perturbation expansion. The Hamiltonian is partitioned into two terms,

$$\hat{H} = \hat{H}^{(0)} + \lambda \hat{V} \tag{2.16}$$

where $\hat{H}^{(0)}$ is the Hartree-Fock Hamiltonian,

$$\hat{H}^{(0)} = \sum_i (h(i) + v_{HF}(i)) \tag{2.17}$$

and λ is called the perturbation parameter. The perturbation term $\hat{V}$ is the difference in the electronic Hamiltonian and the HF potential,

$$\hat{V} = \sum_{i<j} 1/r_{ij} - v_{HF}. \tag{2.18}$$

We assume that the wave functions and energies can be expanded as,

$$\begin{aligned} \Psi_i &= \Psi_i^{(0)} + \lambda\Psi_i^{(1)} + \lambda^2\Psi_i^{(2)} + \cdots \\ E_i &= E_i^{(0)} + \lambda E_i^{(1)} + \lambda^2 E_i^{(2)} + \cdots \end{aligned} \tag{2.19}$$

The superscripts refer to the order of perturbation theory. Substitution the above expressions into the time-independent Schrödinger equation gives,

$$\begin{aligned} &\hat{H}^{(0)}\Psi_i^{(0)} + \lambda\left(\hat{V}\Psi_i^{(0)} + \hat{H}^{(0)}\Psi_i^{(1)}\right) + \lambda^2\left(\hat{V}\Psi_i^{(1)} + \hat{H}^{(0)}\Psi_i^{(2)}\right) + \cdots \\ &= E_i^{(0)}\Psi_i^{(0)} + \lambda\left(E_i^{(1)}\Psi_i^{(0)} + E_i^{(0)}\Psi_i^{(1)}\right) + \lambda^2\left(E_i^{(2)}\Psi_i^{(0)} + E_i^{(1)}\Psi_i^{(1)} + E_i^{(0)}\Psi_i^{(2)}\right) + \cdots \end{aligned} \tag{2.20}$$

Collection of the terms with the same powers of λ yields the equations below,

$$\begin{aligned} \hat{H}^{(0)}\Psi_i^{(0)} &= E_i^{(0)}\Psi_i^{(0)} \\ \hat{H}^{(0)}\Psi_i^{(1)} + \hat{V}\Psi_i^{(0)} &= E_i^{(0)}\Psi_i^{(1)} + E_i^{(1)}\Psi_i^{(0)} \\ \hat{H}^{(0)}\Psi_i^{(2)} + \hat{V}\Psi_i^{(1)} &= E_i^{(0)}\Psi_i^{(2)} + E_i^{(1)}\Psi_i^{(1)} + E_i^{(2)}\Psi_i^{(0)} \end{aligned} \tag{2.21}$$

Here we stop at the second-order perturbation and neglect the higher order terms. If we multiply each of the above equations by $\Psi_i^{(0)}$ from the left hand side and integrate over all space, the following expressions for different levels of energy are generated,

$$\begin{aligned} E_i^{(0)} &= \langle\Psi_i^{(0)}|\hat{H}^{(0)}|\Psi_i^{(0)}\rangle \\ E_i^{(1)} &= \langle\Psi_i^{(0)}|\hat{V}|\Psi_i^{(0)}\rangle \\ E_i^{(2)} &= \langle\Psi_i^{(0)}|\hat{V}|\Psi_i^{(1)}\rangle \end{aligned} \tag{2.22}$$

Therefore, the sum of the zeroth and first-order energies in the MP perturbation theory is the HF energy,

$$\begin{aligned} E_i^{(0)} + E_i^{(1)} &= \langle \Psi_i^{(0)} | \hat{H}^{(0)} | \Psi_i^{(0)} \rangle + \langle \Psi_i^{(0)} | \hat{V} | \Psi_i^{(0)} \rangle \\ &= \langle \Psi_i^{(0)} | \hat{H}^{(0)} + \hat{V} | \Psi_i^{(0)} \rangle \\ &= \langle \Psi_i^{(0)} | \hat{H} | \Psi_i^{(0)} \rangle \\ &= E_{HF} \end{aligned} \tag{2.23}$$

By following the standard perturbation theory, the second-order energy term in an orbital basis can be written as

$$E_{MP}^{(2)} = 2 \sum_{ijab}^{N/2} \frac{\langle ij|ab\rangle \langle ab|ij\rangle}{\epsilon_i + \epsilon_j - \epsilon_a - \epsilon_b} - \sum_{ijab}^{N/2} \frac{\langle ij|ab\rangle \langle ab|ji\rangle}{\epsilon_i + \epsilon_j - \epsilon_a - \epsilon_b}, \tag{2.24}$$

where $\epsilon_k,\ (k = i, j, a, b)$ are the orbital energies and indices $i, j, ...$ show occupied orbitals while virtual spin orbitals are labeled by $a, b, ...$ Also, the two-electron integrals over spin orbitals, $\langle ij|ab\rangle$, are written as,

$$\langle ij|ab\rangle = \langle \chi_i \chi_j | \chi_a \chi_b \rangle = \int d\vec{r}_1 d\vec{r}_2 \chi_i^*(\vec{r}_1) \chi_j^*(\vec{r}_2) r_{12}^{-1} \chi_a(\vec{r}_1) \chi_b(\vec{r}_2) \tag{2.25}$$

The lowest order of the MP method that gives correlation energy is the second-order. The MP2 model provides accurate results to the correlation problem in the electronic structure theory at low cost. Møller-Plesset perturbation theory is abbreviated by MPn notation in which n indicates the order at which the expansion series is terminated. Among the different orders of MP theory, the second-order Møller-Plesset (MP2) perturbation theory is the most used one and for purposes of our projects, MP2 was used to recover the correlation energy in the molecular systems of interest because it provides accurate results for the correlation energy in the electronic structure theory at relatively low cost. One notable result of MP2 is that the correlation energy is dominated by double excitations as shown in equation (2.24) which is used in many advanced electronic structure methods.

2.2.2 Coupled-Cluster theory

Another widely used post-HF method is the Coupled-Cluster (CC) theory.[52] CC method uses an exponential function ansatz to construct the exact wave function and mathematically it can be written as

$$\Psi_{\mathrm{cc}} = \mathrm{e}^{\mathbf{T}}\psi_0 \tag{2.26}$$

where ψ_0 is the HF determinant and $\mathbf{T}$ is the cluster operator and is written as

$$\mathbf{T} = \mathbf{T}_1 + \mathbf{T}_2 + \mathbf{T}_3 + ... \tag{2.27}$$

with

$$\mathbf{T}_1\psi_0 = \sum_{i}^{occ}\sum_{a}^{unocc} t_i^a\psi_i^a, \qquad \mathbf{T}_2\psi_0 = \sum_{i<j}^{occ}\sum_{a<b}^{unocc} t_{ij}^{ab}\psi_{ij}^{ab}, ... \tag{2.28}$$

The coefficients t_i^a are called single-excitation amplitudes, t_{ij}^{ab} double-excitation amplitudes, and so on which are determined by solving the Schrödinger equation.

The exponential operator, $e^{\mathbf{T}}$ can be expanded as a Taylor series,

$$e^{\mathbf{T}} = \mathbf{1} + \mathbf{T} + \frac{\mathbf{T}^2}{2!} + \frac{\mathbf{T}^3}{3!} + ... \tag{2.29}$$

which can be sorted by the level of excitation terms as

$$e^{\mathbf{T}} = \mathbf{1} + \mathbf{T}_1 + \left(\mathbf{T}_2 + \frac{\mathbf{T}_1^2}{2}\right) + \left(\mathbf{T}_3 + \mathbf{T}_1\mathbf{T}_2 + \frac{\mathbf{T}_1^3}{6}\right) + ... \tag{2.30}$$

When it operates on the wave function ψ_0, it not only yields terms of the form $\mathbf{T}_1\psi_0$, $\mathbf{T}_2\psi_0$, $\mathbf{T}_3\psi_0$, ..., but also generates the products of excitation operators such as $\mathbf{T}_1\mathbf{T}_1\psi_0$, $\mathbf{T}_1\mathbf{T}_2\psi_0$, $\mathbf{T}_1\mathbf{T}_2\mathbf{T}_3\psi_0$, ... As mentioned earlier, $\mathbf{T}_1\psi_0$ results in singly excited determinants, therefore $\mathbf{T}_1\mathbf{T}_1\psi_0$ term results in doubly excited determinants keeping in mind that the doubly excited determinants are also generated by $\mathbf{T}_2\psi_0$ term. But the important difference between the latter two excitation terms is hidden into their amplitudes. The double-excitation amplitudes t_{ij}^{ab} appear for $\mathbf{T}_2\psi_0$ whereas products of single-excitation amplitudes $t_i^a t_j^b$ are generated for $\mathbf{T}_1\mathbf{T}_1\psi_0$.

The physical meaning of these notations is that $\mathbf{T}_2\psi_0$ shows a connected double-excitation contribution while $\mathbf{T}_1\mathbf{T}_1\psi_0$ represents a disconnected double-excitation portion.

Based on the truncation level and terms in the Taylor expansion of $e^{\mathbf{T}}$ operator and selection of basis sets, a variety of of approximations can be made in CC applications such as coupled-cluster singles and doubles (CCSD) which includes $\mathbf{T}_1 + \mathbf{T}_2$ only and coupled-cluster singles, doubles, and triples (CCSDT) which keeps $\mathbf{T}_1 + \mathbf{T}_2 + \mathbf{T}_3$ in the $e^{\mathbf{T}}$ expansion series. In addition to those, there is another method that is called CCSD(T), which is often called the "Gold Standard" of the computational chemistry.[53–56] This method is based on a CCSD computation where the triples are added in a perturbative manner.[57] The CCSD(T) method provides high accuracy results compared to CCSD, and often matches the accuracy of CCSDT, and its computational cost is significantly lower compared to FCI, but in terms of some basis sets and molecular systems, it is too costly for many of them.

2.3 Density Functional Theory

One of the most dominant computational methods for molecular electronic structure computations is density functional theory (DFT). In contrast to the methods mentioned previously, DFT employs the electron probability density. In general, using DFT has several advantages. This approach uses a single 3D function for an N electron system without any constraints due to permutation symmetry. The other benefit of using DFT is that there is no cusps as seen in the N electron wave functions when electrons reach each other, because in DFT the electron density does not involve inter-electron distances explicitly. It also takes into account the electron correlation with low computational cost comparing to MP2, for example. One of the reasons for popularity of DFT is that it is feasible to do calculations on molecules with more than 100 atoms in less demanding computational time. The main idea behind DFT is that the energy of a system of N electrons can be written in terms of electron density (ρ). In other words, the electronic energy, E, of a system is said to be a functional of the electron density and is denoted $E[\rho]$, which implies that for a given electron density function, $\rho(\mathbf{r})$, there is a single energy value corresponding to it.

2.3.1 Kohn-Sham equations

There were some attempts to use density functional models for the energy of molecules but it was 1964 when P. Hohenberg and W. Kohn showed that there exists a unique functional of the electron density corresponding to the ground state of N electron systems interacting with each other.

Later in 1965, W. Kohn and L. Sham showed that the problem of many electron interacting systems in an external field can be modeled by a set of non-interacting electrons in an effective external field. Indeed the Kohn-Sham approach relies on the two published theorems by Hohenberg and Kohn.[58] The first one says all the properties of a molecule in its ground state are determined by a unique ground state electron density, $\rho_0(\mathbf{r})$, where $\mathbf{r}$ is the spatial coordinate. This theorem proves the existence of such a density functional and does not say anything about its shape or how to find it, and therefore finding a good functional is the main problem in DFT. The second theorem is similar to the variational theorem, and claims that any trial electron density will give an energy higher or equal than the true ground state energy. Mathematically it means,

$$E[\rho_t] \geq E[\rho_0] \tag{2.31}$$

where ρ_t is a trial electron density and $E[\rho_0]$ is the true ground state electronic energy pertinent to the true electron density function ρ_0. The equal sign happens when the right electron density is found and selected.

The DFT approach led to a set of self-consistent equations known as the Kohn-Sham equations:[58]

$$(-\frac{1}{2}\nabla^2 + v_{eff}(\vec{r}))\phi_i(\vec{r}) = \epsilon_i\phi_i(\vec{r}), \tag{2.32}$$

where $v_{eff}(\vec{r})$ is the effective potential written as

$$v_{eff}(\vec{r}) = v(\vec{r}) + \int \frac{\rho(\vec{r'})}{|\vec{r} - \vec{r'}|}d\vec{r'} + v_{xc}(\vec{r}), \tag{2.33}$$

where $v(\vec{r})$ is the external potential, $\rho(\vec{r})$ is the electron density, and $v_{xc}(\vec{r})$ is the exchange-correlation potential. For solving the Kohn-Sham (KS) equations, one needs to know the effective potential, and having the effective potential requires knowing the density. The electron density of the ground state can be written as

$$\rho(\vec{r}) = \sum_{i}^{occ} |\phi_i(\vec{r})|^2. \tag{2.34}$$

In the equation above, the sum is over occupied spin orbitals. For solving equation (2.32), an initial guess is needed for $\phi_i(\vec{r})$ to produce equation (2.34) and equation (2.33), respectively. Finally, these two equations are used in equation (2.32) for $\phi_i(\vec{r})$ until the $\phi_i(\vec{r})$ that comes from the solution reaches the consistency to $\phi_i(\vec{r})$ that is used to define the equations. This process is called a self-consistent method. At the end of the process, the energy of the ground state of the system can be written as

$$E[\rho(\vec{r})] = T[\rho(\vec{r})] + V_{ne}[\rho(\vec{r})] + V_{ee}[\rho(\vec{r})] + V_{xc}[\rho(\vec{r})], \tag{2.35}$$

where $T[\rho(\vec{r})]$ is the kinetic energy of the non-interacting electrons, $V_{ne}[\rho(\vec{r})]$ is the nuclear-electron interaction, $V_{ee}[\rho(\vec{r})]$ is the electron-electron repulsion energy, and $V_{xc}[\rho(\vec{r})]$ is the exchange-correlation potential energy.

For the evaluation of intermolecular interaction energies, one needs to employ dispersion-including density functional theory methods to have acceptable accuracy at the van der Waals minima. For this reason, DFT-D3 which is an atom-pairwise dispersion correction on top of standard DFT, can be used.[59] This correction is added to the KS-DFT energies:

$$E_{DFT-D3} = E_{KS-DFT} - E_{disp}, \tag{2.36}$$

where E_{KS-DFT} is the self-consistent KS energy and the E_{disp} is the dispersion correction energy, which is the sum of the two- and three-body contributions to the dispersion energy[12,60]

$$E_{disp} = E^{(2)} + E^{(3)}, \tag{2.37}$$

where the two-body term can be written as,

$$E^{(2)} = \sum_{AB} \sum_{i=6,8,\ldots} s_i \frac{C_i^{AB}}{r_{AB}^i} f_{d,i}(r_{AB}), \tag{2.38}$$

where s_i is a ith scaling factor, C_i^{AB} denotes the ith-order dispersion coefficient for the atom pair AB, r_{AB} is the interatomic distance, and $f_{d,i}$ is a damping function. The damping function can be of any form and some types of if can be found in Refs.61 and 62. Finally, the nonadditive energy contribution, $E^{(3)}$, can be written as,[12]

$$E^{(3)} = \sum_{ABC} f_{d,(3)}(\bar{r}_{ABC}) E^{ABC}, \tag{2.39}$$

where the sum spans all atom triples ABC in a molecular system of interest, $\bar{r}_{ABC}$ is the geometrically averaged radius of ABC, and E^{ABC} is the leading nonadditive dispersion interaction term known as Axilrod–Teller–Muto (or triple-dipole),[63]

$$E^{ABC} = \frac{C_9^{ABC}(3\cos\theta_i \cos\theta_j \cos\theta_k + 1)}{(r_{AB} r_{BC} r_{CA})^3}, \tag{2.40}$$

where $\{\theta_s\}$ are a set of the internal angles of the triangle created by a set of $\{r_{KL}\}$ distances, and C_9^{ABC} is the triple-dipole interaction coefficient and is given by,

$$C_9^{ABC} = \frac{3}{\pi} \int_0^\infty d\omega \;\; \alpha^A(i\omega)\alpha^B(i\omega)\alpha^C(i\omega), \tag{2.41}$$

where $\alpha(i\omega)$ is the atomic dynamic dipole polarizability for the ground state at an imaginary frequency ($i\omega$).[64,65] Therefore, the DFT-D3 energy correction considers all pairs of atoms and triplets of atoms to account for three-body effects.

2.4 Symmetry-Adapted Perturbation Theory

Throughout this thesis, symmetry-adapted perturbation theory (SAPT) was used. SAPT provides a solid framework to understand intermolecular interactions and also make predictions of interaction energies. Nowadays SAPT calculations can be employed for large systems of

molecules. It provides tools to directly compute the non-covalent interactions between two monomers. In SAPT, the interaction operator between two molecules is considered as a perturbation.

$$\mathrm{H} = \mathrm{F_A} + \mathrm{W_A} + \mathrm{F_B} + \mathrm{W_B} + \mathrm{V} \tag{2.42}$$

where $\mathrm{F_A}$ and $\mathrm{F_B}$ are the Fock operators for monomers A and B, respectively, and $\mathrm{W_A}$ and $\mathrm{W_B}$ are fluctuation potentials (correlation operators) for each monomer A and B, and V is the interaction potential. When expanding the eqn. (2.42) in perturbation theory, the electrostatic and exchange interactions appear at first-order of V while induction and dispersion pop up in the second-order in V. As usual in approximate methods, several truncations of the SAPT expansion are possible. The ones which were used in this thesis and implemented in PSI4,[66] are SAPT0 and SAPT2+3 that can be represented mathematically as,[67]

$$E_{SAPT0} = E_{elst}^{(10)} + E_{exch}^{(10)} + E_{ind,resp}^{(20)} + E_{exch-ind,resp}^{(20)} + E_{disp}^{(20)} + E_{exch-disp}^{(20)} + \delta E_{HF}^{(2)} \tag{2.43}$$

$$\begin{aligned} E_{SAPT2+3} = E_{SAPT2+(3)} + E_{exch-ind,resp}^{(30)} + E_{ind,resp}^{(30)} + E_{exch-disp}^{(30)} + E_{ind-disp}^{(30)} + \\ E_{exch-ind-disp}^{(30)} - \delta E_{HF}^{(2)} + \delta E_{HF}^{(3)} \end{aligned} \tag{2.44}$$

where $E_{SAPT2+(3)}$ is expressed by the following formula,

$$\begin{aligned} E_{SAPT2+(3)} = E_{SAPT0} + E_{elst,resp}^{(12)} + \left(E_{exch}^{(11)} + E_{exch}^{(12)}\right) + \left(E_{ind}^{(22)} + E_{exch-ind}^{(22)}\right) + \\ \left(E_{disp}^{(21)} + E_{disp}^{(22)}\right) + \left(E_{elst,resp}^{(13)} + E_{disp}^{(30)}\right) \end{aligned} \tag{2.45}$$

As can be seen from the equations above, SAPT can decompose the total interaction energy into the physically meaningful components such as, electrostatics, exchange, induction, and dispersion contributions. In the above expressions, l in the notation $E^{(lm)}$ indicates the intermolecular interaction operator order and m shows the order of the intramonomer correlation operator, respectively. The additional subscript "$resp$" in some of the terms represents the inclusion of response (relaxation) effects, and the $\delta E_{HF}^{(2)}$ term is known as the Hartree-Fock correction and

encompasses higher-order induction and exchange-induction effects and is expressed as,

$$\delta E_{HF}^{(2)} = E_{IE}^{HF} - \left(\left[E_{elst}^{(10)} \right]_{elst} + \left[E_{exch}^{(10)} \right]_{exch} + \left[E_{ind,resp}^{(20)} + E_{exch-ind,resp}^{(20)} \right]_{ind} \right) \tag{2.46}$$

and finally, the third-order induction terms are represented by $\delta E_{HF}^{(3)}$ as follows,

$$\delta E_{HF}^{(3)} = E_{IE}^{HF} - \left(\left[E_{elst}^{(10)} \right]_{elst} + \left[E_{exch}^{(10)} \right]_{exch} + \left[E_{ind,resp}^{(20)} + E_{exch-ind,resp}^{(20)} + E_{ind,resp}^{(30)} + E_{exch-ind,resp}^{(30)} \right]_{ind} \right) \tag{2.47}$$

- The electrostatic contribution in SAPT includes Coulombic interactions, charge penetration, and it can be generally stabilizing (attractive) or destabilizing (repulsive).
- Exchange is a repulsive force which originates from the Pauli exclusion principle.
- Induction encompasses charge transfers from each monomer as well as polarization of one monomer in response to the other's electric field, which is an attractive contribution.
- Dispersion is an attractive force arising from the correlation between electron motions in the two monomers.

2.5 Basis Sets

One of the key tools in theoretical chemistry of electronic structure of molecules is the basis set. It is a set of mathematical functions, called basis functions, to expand molecular orbitals. Basis functions play the role of unit vectors in 3D vector space. They are used to construct molecular orbitals by forming linear combinations of atomic orbitals centered on atoms. In general, a basis set can be composed of atomic orbitals or plane waves. In the case of basis sets of atomic orbitals, several options are available; the popular ones are,

- Slater-type orbitals
- Gaussian-type orbitals

The general form of Slater-type orbitals (centered at the origin) in the spherical coordinate system is as follows,

$$\psi_{\zeta,n,l,m}(r,\theta,\phi) = NY_{l,m}(\theta,\phi)r^{n-1}e^{-\zeta r} \tag{2.48}$$

where n is the principal quantum number, l the angular momentum, and m the z component of the angular momentum, respectively. The coefficient N is the normalization coefficient and the parameter ζ controls the width of a specific orbital, small ζ gives diffuse functions while large ζ makes functions tight and sharp. Because of the $e^{-\zeta r}$ term which makes integration difficult and time consuming, Slater-type orbitals (STOs) are less popular than Gaussian-type orbitals. In practice, Gaussian-type orbitals (GTOs), which were introduced by Boys in 1950, are preferred because the computation of molecular integrals is efficient with the $e^{-\zeta r^2}$ term. Some quantum chemistry packages use the Cartesian form of GTOs,

$$g(\vec{r}) = Nx^l y^m z^n e^{-\zeta \vec{r}^2} = Nx^l y^m z^n e^{-\zeta(x^2+y^2+z^2)} \tag{2.49}$$

where $L = l + m + n$ is referred to as the angular momentum. On the other hand, some programs use the Spherical from of GTOs,

$$g(\vec{r}) = NY_{l,m}(\theta,\phi)r^l e^{-\zeta r^2} \tag{2.50}$$

Cartesian and Spherical primitive GTOs, which are defined as single Gaussian functions, are indeed the same for up to $l = 1$ and differ little for $l = 2$ and higher angular momenta. Some main properties of GTOs are as follows,

- they decay faster than STOs at infinity
- unlike s-type STOs, Gaussian s-types do not have a nuclear cusp
- computation of integrals is much easier than in STOs

Basis set types that were used in our studies are the Dunning-type correlation-consistent basis sets, denotes as cc-pVXZ (X = D, T, Q, 5, ...),[23,24] which imply Dunning correlation-consistent, polarized valence with X-zeta basis. For this type of basis sets, functions are added in shells,

for example, cc-pVDZ for O atom has 3s2p1d orbital functions while cc-pVTZ consists of 4s3p2d1f. Interactions between molecular systems are long-ranged, sensitive to the tails of the electron densities, and therefore basis sets should reflect this interaction by inclusion of diffuse basis functions which cover larger spatial distances. For Dunning-type basis sets, a prefix "aug" shows that one set of diffuse functions has been added to each angular momentum function. For instance, the aug-cc-pVDZ basis set for O atom will have the diffuse functions of s, p, and d type.

2.6 Noncovalent Interaction Computations

With the computer power and efficient computational methods available today, it is feasible to perform highly accurate calculations on different molecular systems with different sizes. Of particular interests to our group are noncovalent interactions (NCI) between molecules of different types. These interactions are ubiquitous and subject of many experimental and theoretical studies.[68,69] Noncovalent interactions play a vital role in biological systems because of their nature. They do not lead to any bond forming, but they have extremely important role in determining the shape of molecules in gas phases, liquids, and solid states as well as in crystal structures.[70]

In general, regardless of molecular systems of interest, there are two main approaches to computing interaction energies (IE) between two molecules; the supermolecular and perturbative approaches. In the supermolecular approach for computing the noncovalent interaction energies, the interaction energy is calculated as the energy of the dimer minus the energies of each isolated monomer,

$$\mathrm{E_{int}} = \mathrm{E_{Dimer}} - \mathrm{E_{monomerA}} - \mathrm{E_{monomerB}} \tag{2.51}$$

The equation above gives the "interaction energy" of the dimer, which is negative when the dimer is more stable than infinitely isolated monomers. Dispersion-corrected density functional theory (DFT-D),[11,12] second-order Møller-Plesset perturbation theory (MP2), and coupled-cluster theory are examples of widely used supermolecular approaches. The "binding energy"

is the negative of the interaction energy, the amount of energy required to disperse the fragments. If there are more than two fragments in a cluster, one must take into account the effect of all two-body, three-body, ..., terms into the interaction energy by computing all possible dimers, trimers, ..., within the complex. The second option for computation of intermolecular interactions is to compute them "directly". One commonly used example of this type is SAPT, in which the interaction between fragments is considered as a perturbation to the total Hamiltonian of the system. One of the main difficulties in the computation of intermolecular interaction energies is the accuracy, especially when the effects of London dispersion forces are significant. In this regard, one challenge is Basis Set Superposition Error (BSSE), where one monomer "borrows" basis set functions from the other monomer, artificially increasing the attraction of two monomers and therefore improving the interaction energy value. Overestimating binding energy due to BSSE is a big challenge especially in dispersion dominant clusters. Several solutions have been proposed to cancel or lower this error,

- the use of large basis sets in order to compensate the inadequacy of the monomer small basis sets
- methods to mitigate or cancel the BSSE such as the Boys-Bernardi counterpoise (CP) correction[71]

CP is the most used correction to eliminate the BSSE. The typical uncorrected interaction energy of two adjacent interacting fragments A and B can be computed as,

$$\Delta E_{\text{int}} = E_{\text{AB}}^{AB}(AB) - E_{\text{A}}^{A}(A) - E_{\text{B}}^{B}(B) \tag{2.52}$$

where $E_{\text{Y}}^{Z}(X)$ indicates the energy of a subsystem X computed at the geometry Y with basis set Z. Therefore, $E_{\text{A}}^{A}(A)$ shows the energy of monomer A computed in the monomer basis at the monomer A geometry. In this method, the BSSE is present in the energy of the monomer A in the dimer, as an example, by including the monomer B basis sets without involving the nuclei and electrons of the monomer B. Then, the CP-corrected interaction energy can be explicitly written as the dimer energy subtracting out the energy of each monomer as computed in the

dimer basis set.

$$\Delta E_{\text{int}}^{CP} = E_{\text{AB}}^{AB}(AB) - E_{\text{A}}^{AB}(A) - E_{\text{B}}^{AB}(B) \tag{2.53}$$

In addition to BSSE, the other barrier in the accurate computation of noncovalent interactions is the dispersion forces. They are attractive forces that result when electrons of one monomer interact with those of another monomer making temporary fluctuating dipoles. Therefore, they are generated by correlated motions of electrons. Unfortunately, these electron correlations are not included in the Hartree-Fock computation procedure, and one must use methods that take into account the electron correlation such as MP2 or coupled-cluster singles and doubles (CCSD). It is obvious that the use of correlated wave function methods is computationally expensive and does not necessarily lead to the exact answers. For example, using the CCSD method tends to drastically underbind the dispersion bonded π complexes.[67] Hence, for this type of systems, CCSD(T) which is known as "gold standard" gives accurate results. However, if large basis sets are used, getting the accurate CCSD(T) results is very difficult because the computational cost of CCSD(T) is on the order of $\mathcal{O}(N^7)$ scaling with the system size of N, which makes CCSD(T) unfeasible for systems with more than approximately 40 atoms.

Chapter 3

Chiral Self-Recognition in Propylene Oxide Complexes and Glycidol Dimers

Chiral molecules and chirality are the subject of chemistry research for decades. It stems from the importance of chirality in our daily lives. Especially, the importance of chirality in biological systems has attracted a lot of attention during the past years. From the food we eat to many biological reactions occurring in our bodies, all depend on chiral molecules and chiral synthesis. Therefore, it is vital to get to know intermolecular interaction energies between this type of molecules and try to understand how big are the chiral differences and where they come from. For the first project of this type, we chose a small and rigid propylene oxide (PO) molecule, a simple chiral molecule with the formula C_3H_6O and the IUPAC name (2R)-2-Methyloxirane/(2S)-2-Methyloxirane (Fig. 3.1). Propylene oxide has a chirality center where

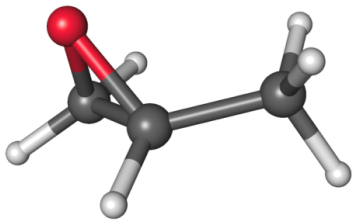

Figure 3.1: The propylene oxide molecule

four different functional groups or atoms are attached to it. It is one of the important compounds in industry and its main application is in the production of polyether polyols in order to make polyurethane plastics. In recent years due to the detection of the propylene oxide molecule in the interstellar medium,[72] much more attention has been given to the interactions of this molecule.[73] For the first time, Su and co-workers[74] took the propylene oxide dimer and tried to understand chiral self-recognition in propylene oxide clusters using spectroscopic detection of

the homochiral and heterochiral complexes of propylene oxide in the gas phase. They described rotational spectroscopic chiral self-recognition of the propylene oxide dimer using high-level *ab initio* studies that were available at the time. The propylene oxide complexes are bound weakly by secondary hydrogen bonds of the oxygen atom of the epoxide ring and the $\cdots$H–C group of the other PO monomer. Su et al. have found 12 stable PO complexes consisting of six homochiral and six heterochiral conformers, where each monomer in a dimer acts as a hydrogen bond donor and an acceptor, simultaneously. Su et al. performed Fourier Transform Microwave (FTMW) Spectroscopy[74] to identify spectral lines for the heterochiral dimers and to measure the intensity of homo- and heterochiral complexes. What distinguishes our study is that it is not limited to spectroscopy and rotational spectra of PO dimers. Importantly, SAPT and F-SAPT difference analysis were performed on these chiral clusters along with various DFT methods.

In the other project which followed the PO study, one of the chemical derivatives of propylene oxide was chosen. It is called glycidol (oxiranemethanol) with the formula $C_3H_6O_2$, in which one of the hydrogen atoms of the methyl group in PO is replaced by a hydroxyl functional group (–OH). One big difference of glycidol over the propylene oxide is its more degrees of freedom of hydroxyl group as it can rotate when making H-bonds with other adjacent molecules. As we will see, the monomer deformation is not negligible for glycidol as it is for the PO monomer in a dimer. Another difference between PO and glycidol is that there exist two monomer conformations for glycidol based on its –OH group position with respect to the epoxide ring (Fig. 3.2). Theoretically, many conformations are feasible for glycidol, but the lowest energy structures are shown in Fig. 3.2. Indeed, different rotamers of glycidol are distinguished by the rotation of the OH group around the C–C bond; the structure where the hydroxyl group is above the oxirane ring is called H-bond inner and the rotamer where the OH group is outside the oxirane ring is called H-bond outer next to the C–O bond. In 1973 Oki and Murayama,[75] by means of infrared spectroscopy, showed that oxirane derivatives such as glycidol favor conformers with intramolecular H-bonds in CCl_4 solutions. Later in 1975 Brooks and Sastry[76] studied the microwave spectrum, dipole moment, and structure of glycidol and assigned that the ground state of the glycidol molecule is the H-bond inner conformer, Fig. 3.2(b). Finally,

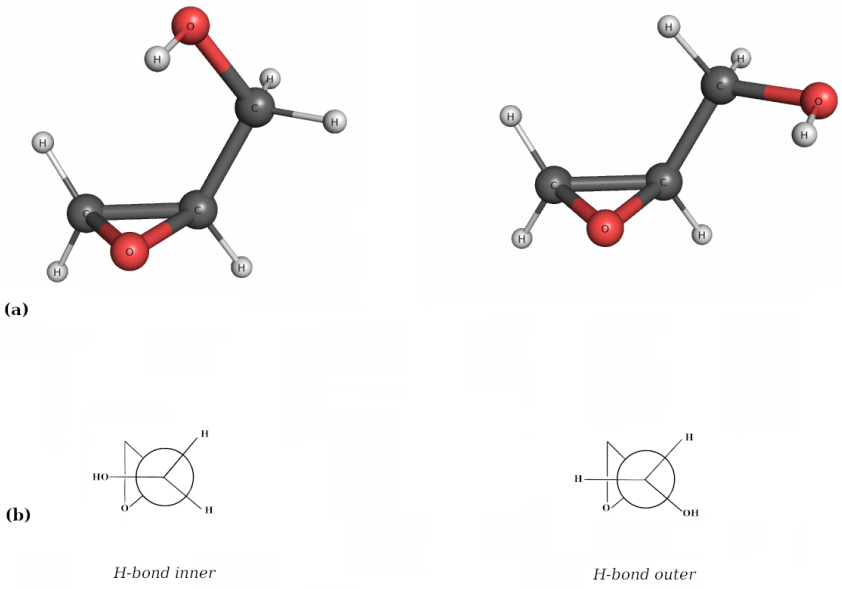

Figure 3.2: Two most stable conformations of glycidol monomers

Marstokk and co-workers showed[77] that only the H-bond inner and H-bond outer rotamers exist experimentally. By following their nomenclature, the H-bond inner conformer is the most stable one, stabilized by an intramolecular H-bond of the hydroxyl group H atom and the oxygen atom of the oxirane ring. By performing microwave spectroscopy, Marstokk et al. showed and assigned the next low-energy conformer as H-bond outer. This rotamer is thought to be stabilized by an internal hydrogen bond between the hydrogen atom of hydroxyl group and the pseudo-π-electrons, i.e. the electrons involved in the formation of the C-O bond of the epoxide ring. It has been revealed that the latter conformer is almost 3.6 kJ/mol higher in energy than the H-bond inner conformer. Theoretically, the third conformer is possible where the OH group is in the para-position with respect to the oxygen atom of the epoxide ring, but this roamer has not been confirmed experimentally.[77]

For our studies, we chose small molecules as prototype models to better understand the driving forces for the intermolecular interactions and chiral discrimination energy. One of the main quantities to compute in the interaction of chiral molecules is the chirodiastaltic energy,[78] defines as the energy difference between the homochiral (RR/SS) and heterochiral (RS/SR) complexes. The chirodiastaltic (chiral discrimination) energy has been the subject of many studies, both experimentally and theoretically including but not limited to, the propylene oxide

dimer,[74] glycidol dimer,[79,80] butan-2-ol dimer,[81] and propylene oxide-glycidol[82] complexes. Generally, the previous *ab initio* calculations of chiral discrimination energies were performed either with density functional theory or using the second-order Møller-Plesset perturbation theory (MP2). In one of the recent studies on chiral molecules with high-level *ab initio* methods which were performed by Korona and co-workers,[83–85] the SAPT and F-SAPT approaches are applied on three important drug molecules, ibuprofen, norepinephrine, and baclofen, interacting with two chiral phenethylamine or proline molecules. In addition, the interacting quantum atoms (IQA)[86,87] approaches was applied to analyze the interaction between atoms and atomic groups and its results were compared to the F-SAPT results. Based on the F-SAPT results, it is shown that the interaction energy differences between RR and RS complexes are noticeable for structures interacting with phenethylamine but this is not necessarily the case for those interacting with proline. Therefore, Korona et al. concluded that the interaction energy differences between the homochiral (RR) and heterochiral (RS) complexes are very important for structures containing phenethylamine but not necessarily for those with proline.

Computing the chirodiastaltic energy using only supermolecular approaches such as MP2, DFT, and CCSD(T)[57] may provide little insight into the nature and function of chiral recognition. Therefore, with robust and accurate approaches available today, it is a worthwhile task to decompose the chiral discrimination energy into the physically meaningful components using SAPT, which splits the total interaction energy into the well-defined electrostatics, induction, exchange, and dispersion contributions. It is also possible to go beyond SAPT and even further split these components based on the functional groups from which they come, using F-SAPT and atomic-SAPT (A-SAPT)[32,33,35] approaches. The final step in this series was utilizing the F-SAPT difference analysis.[88] This recent development adds another layer to the F-SAPT method in such a way that it provides the effects of substituting atoms or functional groups into the interaction and chiral discrimination energies. For example, in the case of the PO dimer, we start with an achiral ethylene oxide complex and see how different SAPT components change when we substitute hydrogen atoms by methyl groups one at a time, and then the interaction energies in the PO dimer are compared to the ethylene oxide dimer.

3.1 Methods and computational details

In all of our calculations, MOLPRO[89] and PSI4[66] were used to study the lowest energy structures for both PO and glycidol dimers. The propylene oxide dimer structures of Ref. 74 were re-optimized at the MP2 complete basis set limit, utilizing the MP2/(aTZ,aQZ) level of theory and basis set, where MP2/(aTZ,aQZ) is the short-hand notation for the $\mathrm{E}_{\mathrm{int}}^{\mathrm{MP2}}$(aug-cc-pVTZ,aug-cc-pVQZ) extrapolation. In the next study, all 14 glycidol complexes of Ref. 90 were reoptimized using the DF-MP2/aTZ level, where aTZ≡aug-cc-pVTZ denotes the augmented correlation consistent triple-zeta Dunning basis.[23,24] In addition, for both the PO and glycidol projects, different electronic structure approaches were used in the counter poise-corrected supermolecular fashion. In other words, the interaction energy for these clusters is calculated as,[91]

$$\mathrm{E}_{\mathrm{int}} = \mathrm{E}_{\mathrm{AB}} - \mathrm{E}_{\mathrm{A}} - \mathrm{E}_{\mathrm{B}}, \tag{3.1}$$

where $\mathrm{E}_{\mathrm{x}}(\mathrm{x} = \mathrm{AB}, \mathrm{A}, \mathrm{B})$ is the total energy of a dimer and the energies of monomers A and B, respectively, all computed in the complete basis set of the interacting dimer. Our benchmark interaction energies are calculated as,

$$\mathrm{E}_{\mathrm{int}}^{\mathrm{benchmark}} = \mathrm{E}_{\mathrm{int}}^{\mathrm{MP2}}(\mathrm{aug{-}cc{-}pVQZ}, \mathrm{aug{-}cc{-}pV5Z}) + \Delta\mathrm{E}_{\mathrm{int}}^{\mathrm{CCSD(T)}}(\mathrm{aug{-}cc{-}pVTZ}) \tag{3.2}$$

according to the standard practice,[92] and $\Delta\mathrm{E}_{\mathrm{int}}^{\mathrm{CCSD(T)}}$ is called the coupled-cluster correction energy and is written as,

$$\Delta\mathrm{E}_{\mathrm{int}}^{\mathrm{CCSD(T)}} = \mathrm{E}_{\mathrm{int}}^{\mathrm{CCSD(T)}} - \mathrm{E}_{\mathrm{int}}^{\mathrm{MP2}} \tag{3.3}$$

In the above description, the notation (basis1, basis2) in the benchmark interaction energy computation implies that the bases "basis1" and "basis2" have been used in the standard X^{-3} correlation energy extrapolation for a given method.[93,94] All 12 PO dimres and all 14 glycidol complexes are shown in Fig. 3.3 and Fig. 3.4, respectively.

As can be seen in Fig. 3.3, each PO monomer in a dimer acts as a proton donor and an acceptor for two C–H$\cdots$O contacts, and therefore, in each PO dimer there are four secondary

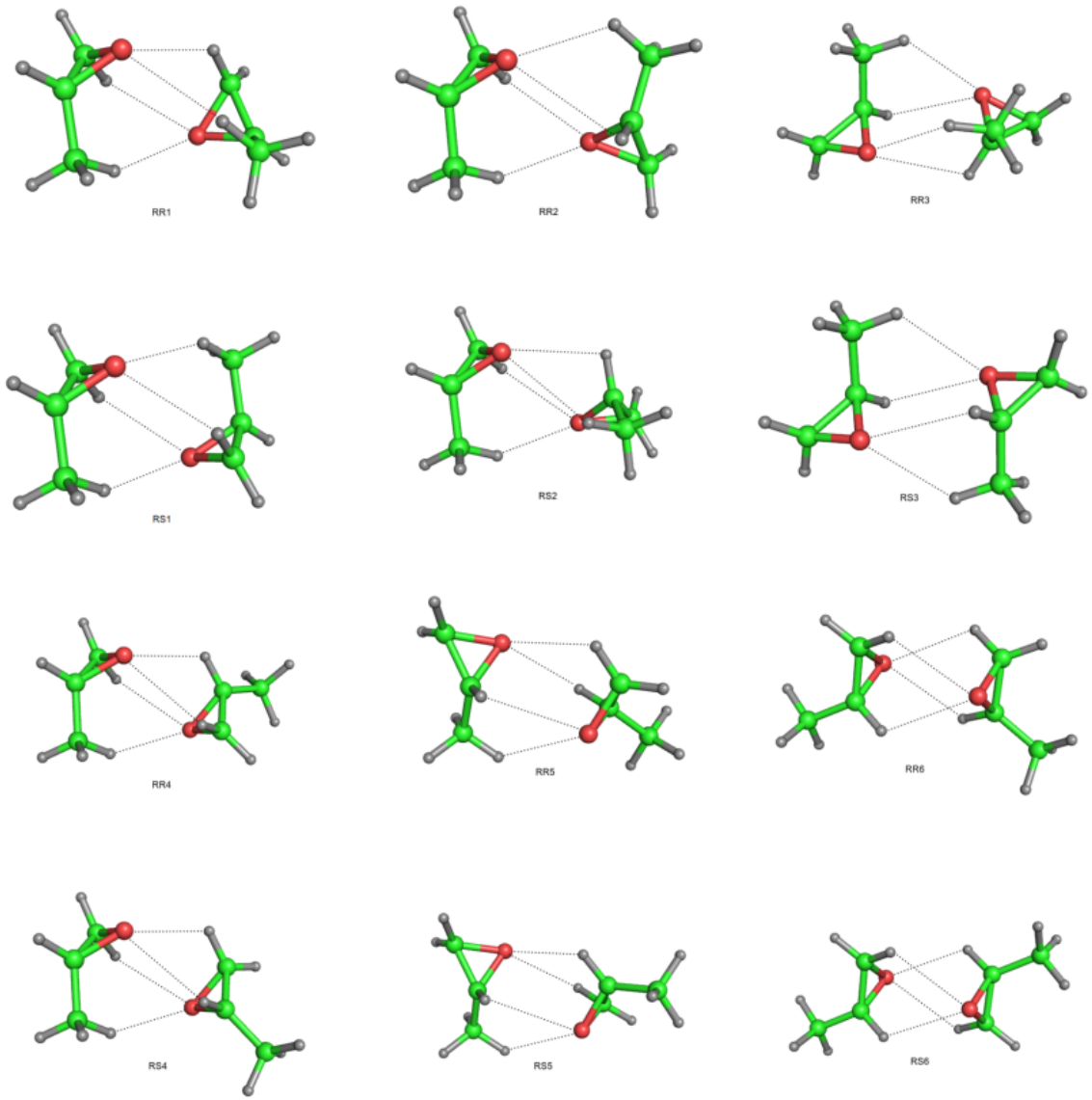

Figure 3.3: Optimized geometries of six homochiral and six heterochiral conformers of the propylene oxide dimers.

hydrogen bonds keeping the PO monomers adjacent to each other to form a dimer configuration. We have denoted six PO homochiral configurations by RR1-RR6 and the heterochiral configurations by RS1-RS6. For the glycidol dimers, the nomenclature is not as simple as it was for PO complexes. In Fig. 3.4, two classes of configurations are distinguished, where one class has 5-membered heavy atom rings (HOM5xx, HET5xx) (including C and O atoms) and the other possesses 8-membered heavy atom rings (HOM8xx, HET8xx).

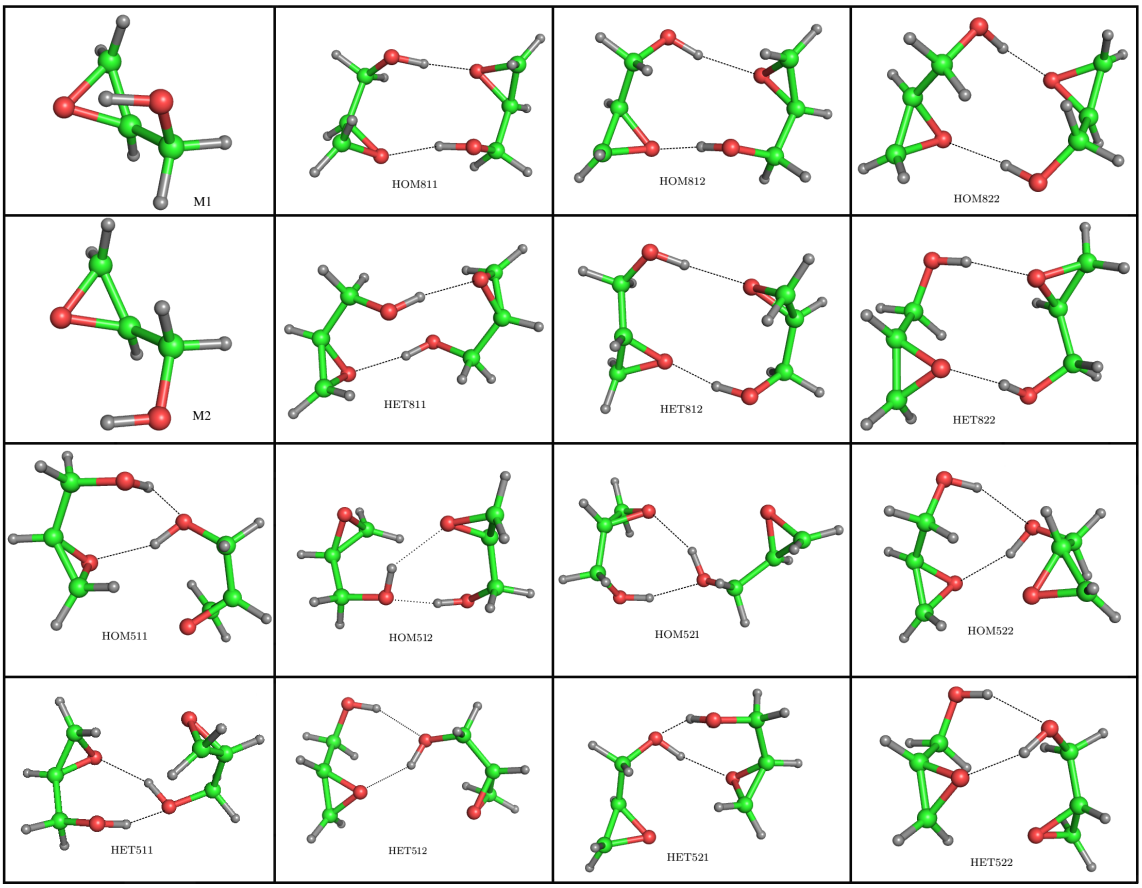

Figure 3.4: Optimized geometries of seven homochiral and seven heterochiral conformers of the glycidol dimers.

3.2 Interaction energies of propylene oxide dimers and glycidol dimers

Geometry optimization is the first and important step in quantum chemistry computations. It is the process of seeking a particular arrangement of atoms and molecules where the energy has a global or local minimum. For the PO dimer, we took the initial and already optimized geometries from Ref. 74 and reoptimized them using higher level of theory and basis sets. There were 12 propylene oxide dimer structures consisting of two different enantiomers in each. From the general chemistry, it is known that every chiral molecule can be in the so called "R" or "S" configuration. It is also known that R and S enantiomers have the same energy, as such, the RR and SS enantiomers have the same energy in the form of a dimer structure. But RS/SR configurations have different energy that of either RR/SS. And this is the critical starting point to distinguish between homochiral (RR/SS) and heterochiral (RS/SR) diastereomers. The current study adds several layers of high accuracy *ab initio* computations to the original study

such as SAPT, F-SAPT, and the DFT approaches to get more essential insight into the interaction and chirodiastaltic energies. The main goal of this study was investigating the chiral self-recognition in PO complexes by calculating the chirodiastaltic energy, which is defined as the energy difference between a homochiral and its counterpart heterochiral structure. In addition, it was informative to characterize the different normal modes of motion of each of these structures when they were at their local minimum energy. For the glycidol complexes, the initial 14 geometries were given by Maris et al. in Ref. 90.

Tables 3.1 and 3.2 show the benchmark interaction energies for all 12 propylene oxide and 14 glycidol complexes, respectively. All 12 PO structures were reoptimized to minimize the counterpoise-corrected MP2/(aTZ,aQZ) energy. The monomer deformation contributions to the interaction energy were about 0.09-0.15 kcal/mol and these values were considered very small compared to the total interaction energy values (but large compared to the chiral discrimination energies). Nevertheless, the monomer deformation effects contribute very little (less than 0.018 kcal/mol) between the homo- and heterochiral of PO–PO diastereomers and therefore they were ignored in Table 3.1 and in all subsequent results.

Table 3.1: Benchmark interaction energies (in kcal/mol) of the propylene oxide dimer.

System	MP2/(aQZ,a5Z)	ΔCCSD(T)	Benchmark	ΔE_{chir} [a]
RR1	-5.185	0.094	-5.091	-0.133
RS1	-5.050	0.092	-4.958	
RR2	-5.081	0.163	-4.918	-0.027
RS2	-5.042	0.151	-4.891	
RR3	-4.881	0.247	-4.634	-0.049
RS3	-4.789	0.203	-4.585	
RR4	-5.020	0.042	-4.978	0.048
RS4	-5.075	0.049	-5.026	
RR5	-4.842	0.112	-4.730	-0.002
RS5	-4.828	0.100	-4.728	
RR6	-4.940	-0.006	-4.946	-0.002
RS6	-4.936	-0.008	-4.944	

[a] Defined as $\Delta E_{chir} = E^{int}_{RRx} - E^{int}_{RSx}$

All 14 geometries of the glycidol dimer were reoptimized using the DF-MP2/aTZ level by minimizing the counterpoise-corrected interaction energy with the inclusion of the monomer deformation corrections.

Structure	DF-MP2/CBS	ΔCCSD(T)	Benchmark	ΔE_{chir}^{int}
HOM811	-14.499	0.144	-14.355	1.620
HET811	-16.059	0.084	-15.975	
HOM812	-12.702	0.135	-12.567	-1.469
HET812	-11.251	0.153	-11.098	
HOM822	-11.987	0.185	-11.802	-0.181
HET822	-11.813	0.192	-11.621	
HOM511	-10.235	0.187	-10.048	1.474
HET511	-11.663	0.142	-11.522	
HOM512	-10.154	0.174	-9.980	-0.093
HET512	-9.998	0.111	-9.887	
HOM521	-10.374	0.115	-10.259	0.737
HET521	-11.174	0.178	-10.996	
HOM522	-12.404	0.155	-12.249	-0.409
HET522	-11.972	0.132	-11.839	

Table 3.2: Benchmark DF-MP2/(AVQZ,AV5Z)+ΔCCSD(T)/AVTZ interaction energies (in kcal/mol) for the glycidol dimer.

As seen in Tables 3.1 and 3.2, the interaction energies are larger for glycidol complexes and this was predicted because glycidol can make a true H-bond with the adjacent monomer with its rotating hydroxyl group, while this is not the case for PO dimers. Also, the sign of chiral discrimination energy is important and shows which diastereomer is favored over the other. The monomer deformation contributions to the interaction energy for the PO dimer are negligible because of the rigidity of the propylene oxide molecule, but they are large enough (1.26–6.43 kcal/mol) for glycidol complexes and were taken into account in all calculations including benchmark binding energies.

Next, we listed the MUE values obtained from various dispersion-corrected DFT variants in the aug-cc-pVTZ basis set relative to the benchmark both for the interaction energy and the chiral discrimination energy (Figures 3.5 and 3.6, respectively). As Fig. 3.5 shows, the B3LYP-D3 and B3LYP-D3M functionals perform well for the PO complexes while the BLYP-D3M and PBE0-D3 functionals display good results in addition to the B3LYP-D3 functional for the glycidol dimer structures.

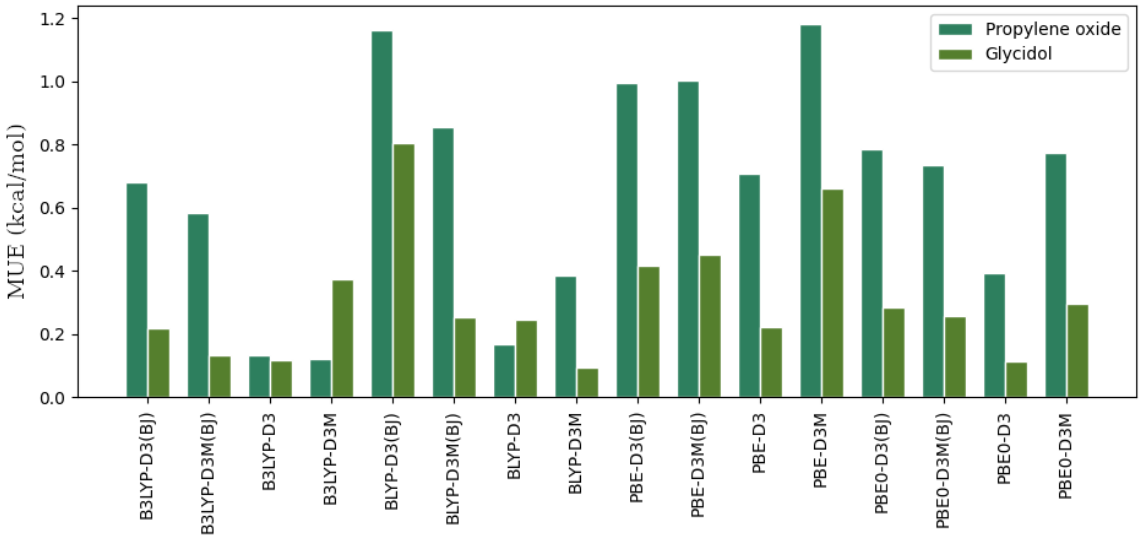

Figure 3.5: Mean unsigned error of the interaction energy (kcal/mol) for all structures of propylene oxide and glycidol complexes in the aTZ basis set using various DFT-based methods.

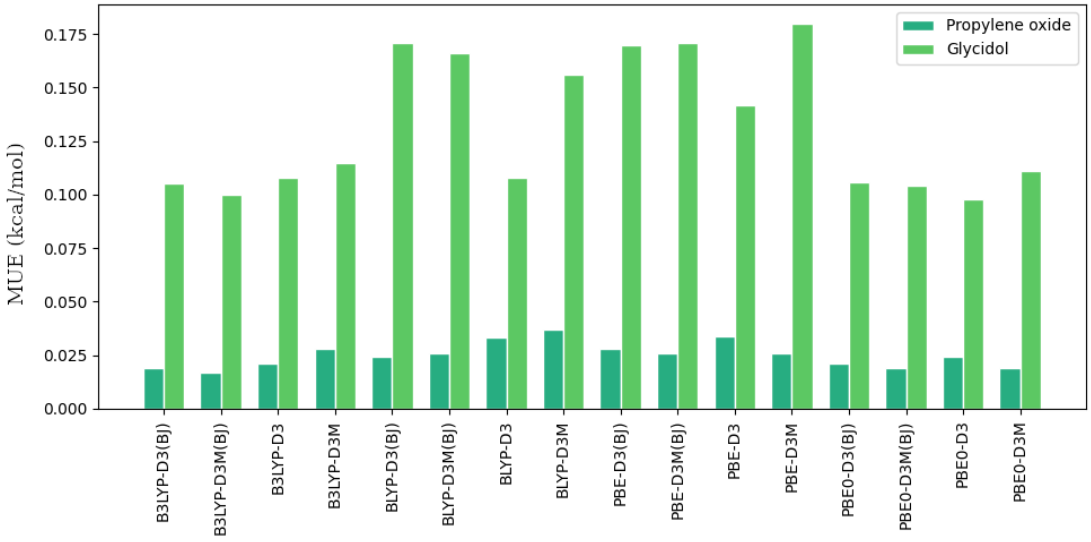

Figure 3.6: Mean unsigned error of the chiral discrimination energy (kcal/mol) for all structures of propylene oxide and glycidol complexes in the aTZ basis set using various DFT-based methods.

Figure 3.6 shows the MUE values for chirodiastaltic energies. As can be seen, some DFT variants show a more complete error cancellation between the homochiral and heterochiral diastereomers of both PO and glycidol dimer structures, resulting in lower MUE values. The details can be found in Refs. 39 and 95.

One of the important parts of the analysis of chiral self-recognition origins comes from the SAPT and F-SAPT results. They give clear picture of the role and function of different functional groups in the propylene oxide and glycidol molecules, and represent how the hydroxymethyl group of glycidol or methyl group of PO lead to the chiral recognition effects. The decomposed interaction energies at the SAPT0/aTZ and SAPT2+3/aTZ levels are shown in Table 3.3 for PO dimer structures.

Structure	Elst	Exch	Ind	Disp	SAPT0	ΔE_{chir}
RR1	-5.748	6.878	-1.496	-6.065	-6.431	-0.141
RS1	-5.618	6.476	-1.405	-5.743	-6.290	
RR2	-5.423	6.392	-1.405	-5.777	-6.213	-0.016
RS2	-5.394	6.352	-1.389	-5.765	-6.197	
RR3	-4.592	5.521	-1.150	-5.627	-5.848	-0.107
RS3	-4.539	5.349	-1.114	-5.438	-5.741	
RR4	-5.474	6.266	-1.344	-5.656	-6.208	0.063
RS4	-5.537	6.360	-1.364	-5.730	-6.271	
RR5	-4.888	5.506	-1.160	-5.407	-5.950	-0.017
RS5	-4.918	5.519	-1.173	-5.360	-5.933	
RR6	-5.262	5.795	-1.191	-5.461	-6.119	-0.004
RS6	-5.260	5.788	-1.190	-5.453	-6.115	

A similar table, Table 3.4, is available for glycidol dimer structures.

Structure	Elst	Exch	Ind	Disp	SAPT2+3	ΔE_{chir}
RR1	-5.535	8.083	-1.600	-6.469	-5.522	-0.137
RS1	-5.397	7.633	-1.504	-6.117	-5.385	
RR2	-5.166	7.447	-1.487	-6.068	-5.273	-0.009
RS2	-5.157	7.427	-1.477	-6.057	-5.264	
RR3	-4.326	6.350	-1.189	-5.767	-4.932	-0.067
RS3	-4.301	6.236	-1.168	-5.632	-4.865	
RR4	-5.268	7.457	-1.460	-6.090	-5.361	0.050
RS4	-5.330	7.562	-1.480	-6.163	-5.411	
RR5	-4.622	6.515	-1.242	-5.698	-5.048	-0.009
RS5	-4.651	6.531	-1.257	-5.662	-5.039	
RR6	-5.060	7.025	-1.330	-5.931	-5.296	-0.004
RS6	-5.057	7.018	-1.329	-5.924	-5.292	

Table 3.3: Different components of the PO-PO interaction energy, in kcal/mol, computed with SAPT0 (top) and SAPT2+3 (bottom) in the aTZ basis set. The ΔE_{chir} values pertain to the total SAPT energies.

Structure	Elst.	Exch.	Ind.	Disp.	SAPT0	ΔE^{int}_{chir}
HOM811	-20.652	19.683	-7.612	-8.523	-17.104	1.725
HET811	-22.677	21.663	-8.703	-9.111	-18.829	
HOM812	-19.296	19.755	-7.082	-8.450	-15.073	-1.196
HET812	-16.537	16.152	-6.110	-7.382	-13.877	
HOM822	-18.655	20.836	-6.711	-9.471	-14.002	0.044
HET822	-18.090	19.411	-6.437	-8.930	-14.046	
HOM511	-17.543	20.400	-6.194	-8.688	-12.025	1.890
HET511	-20.058	22.614	-6.890	-9.582	-13.915	
HOM512	-15.277	16.209	-5.012	-7.743	-11.824	-0.069
HET512	-16.241	16.933	-5.516	-6.931	-11.755	
HOM521	-18.162	19.766	-6.637	-7.136	-12.168	0.968
HET521	-19.145	22.034	-6.934	-9.091	-13.136	
HOM522	-19.539	20.807	-6.378	-9.704	-14.814	-0.686
HET522	-18.767	20.866	-6.248	-9.978	-14.128	

Structure	Elst.	Exch.	Ind.	Disp.	SAPT2+3	$\Delta E^{\text{int}}_{\text{chir}}$
HOM811	-19.869	23.280	-8.367	-9.813	-14.769	1.690
HET811	-21.922	25.509	-9.546	-10.499	-16.459	
HOM812	-18.629	23.218	-7.791	-9.753	-12.955	-1.391
HET812	-15.378	18.819	-6.614	-8.391	-11.564	
HOM822	-18.480	24.654	-7.452	-10.938	-12.216	-0.206
HET822	-17.616	22.964	-7.122	-10.235	-12.010	
HOM511	-17.685	24.304	-6.946	-10.053	-10.380	1.575
HET511	-19.872	26.570	-7.643	-11.010	-11.955	
HOM512	-15.088	19.158	-5.550	-8.816	-10.296	-0.209
HET512	-15.893	19.937	-6.103	-8.028	-10.087	
HOM521	-17.998	23.250	-7.359	-8.386	-10.492	0.877
HET521	-19.241	26.151	-7.754	-10.526	-11.369	
HOM522	-19.125	24.476	-7.064	-11.064	-12.778	-0.452
HET522	-18.624	24.696	-6.961	-11.437	-12.326	

Table 3.4: Interaction energy components for all 14 optimized glycidol structures computed with SAPT0 (top) and SAPT2+3 (bottom) in the AVTZ basis set, along with the resulting chirodiastaltic energies. All values are in units of kcal/mol.

As can be seen, for all 12 PO dimer structures the electrostatic component is almost as large in magnitude as the total interaction energy for every PO complex. This component is larger in magnitude for the glycidol dimer structures because of the electronegative oxygen atom in the hydroxyl group. Therefore, the Coulomb interaction plays a bigger role in glycidol than PO. On the other hand, in both cases of PO and glycidol, these electrostatic energies are quenched by the unfavorable first-order exchange energies. This implies that the monomer wave functions have considerable overlap. Also, these tables show that the largest favorable contribution to the total interaction energy of the PO dimers come from the attractive dispersion interaction, while this is different for the glycidol complexes where in addition to the dispersion interaction, the induction components play a constructive role contributing to the total interaction energy.

Another informative and useful chiral discrimination energy analysis can be obtained by looking at F-SAPT differences,[39,88,95] where the effect of substituted fragments is taken into account. For example, in the case of PO dimer structures, we start from achiral ethylene oxide–ethylene oxide (EO–EO) complexes and substitute hydrogen atoms of EO by methyl functional

group one at a time to reach PO–PO dimers. Therefore, the physical origins of chiral discrimination energy can be obtained and analyzed by investigating the roles of substituted methyl group in PO dimers and hydroxymethyl group in glycidol complexes. Mathematically, the complete SAPT component of the PO–PO interaction energy for a given RRx/RSx complex can be written as,

$$\mathrm{E}_{\mathrm{SAPT}}^{\mathrm{PO-PO}} = \mathrm{E}_{\mathrm{SAPT}}^{\mathrm{EO-EO}} + \Delta_{\mathrm{SAPT}}\mathrm{E}^{(\mathrm{EO-PO})} + \Delta_{\mathrm{SAPT}}\mathrm{E}^{(\mathrm{PO-PO})}, \tag{3.4}$$

where $\Delta_{\mathrm{SAPT}}\mathrm{E}^{(\mathrm{EO-PO})} = \mathrm{E}_{\mathrm{SAPT}}^{\mathrm{EO-PO}} - \mathrm{E}_{\mathrm{SAPT}}^{\mathrm{EO-EO}}$ and $\Delta_{\mathrm{SAPT}}\mathrm{E}^{(\mathrm{PO-PO})} = \mathrm{E}_{\mathrm{SAPT}}^{\mathrm{PO-PO}} - \mathrm{E}_{\mathrm{SAPT}}^{\mathrm{EO-PO}}$. In addition, F-SAPT difference analysis approach was used to even further partition the Δ_{SAPT} terms into the direct and indirect energetic effects of the H→CH_3 change. We define direct energetic effect as the difference between the interaction of a methyl group with the entire other molecule and the interaction of its substituent, i.e. a hydrogen atom, with the entire other molecule. The indirect energetic effect is defined as the change in interaction energy caused by the part of the molecule whose geometry does not change by the H→CH_3 substitution but the electron density does. The relevant tables and results can be found in Appendix A, Figure 3. In the subfigures of Fig. 3, the analysis and computation start from achiral ethylene dimer structures where the two methyl groups of both PO monomers were cut and replaced with hydrogen atoms in the same position and direction as the carbon atom of the methyl group, but with the optimized distance from the stereogenic center of a PO monomer. Because of the symmetry in the O$\cdots$H contacts in all 12 PO dimer complexes, it does not matter which ethylene monomer is chosen first for H/CH_3 replacement. The results for RR6/RS6, as an example in Figure 3, showed that the two methyl groups contribution to the total interaction energy is very small. This was expected as the two methyl groups were far away from each other and they contributed less than 1.0 kcal/mol in magnitude. Structures of RR4, RS4, RR5, and RS5 PO dimer complexes are different than the remaining ones, where one of the methyl groups is far away from the adjacent interacting PO monomer and this is reflected in the total noncovalent interaction energy. Addition of one of the methyl groups increases the total interaction energy more than

the addition of the other methyl group. This is also shown in the direct and indirect contributions of F-SAPT difference analysis. For the remaining structures RR1–RS3, both methyl groups are engaged directly in the intermolecular interactions and the H→CH_3 replacement leads to stronger binding energies by a similar amount. It can also be concluded from Figure 3 that the PO complexes are generally more stable than their ethylene oxide counterparts, which is mainly an effect of the increases in the attractive electrostatic and dispersion interactions and repulsive exchange interaction in the transition of H→CH_3. The effects of induction interactions in these complexes are insignificant and they cannot change the total interaction energies dramatically: their direct and indirect contributions vary from 0.0–0.2 kcal/mol in magnitude. Finally, it can be seen that the total interaction energies for homochiral and heterochiral PO complexes are very close to each other, meaning that the chirodiastaltic energy is very small and that is because the chiral discrimination effects are very small.

In Appendix B, Figures 4–10 show F-SAPT and F-SAPT difference analysis results for glycidol dimer complexes. The F-SAPT difference analysis is performed at the SAPT0 level and decomposes the SAPT0 components using eqns. 7 and 8 in Appendix B. Here, the F-SAPT difference analysis is started from an achiral ethylene oxide dimer and the hydroxymethyl groups are added one at a time to construct a glycidol dimer complex. Precisely speaking, the –CH_2OH functional group is replaced by a H atom pointed exactly in the same direction as the –CH_2OH carbon atom with a distance optimized at the DF-MP2/AVTZ level while the geometry of the rest of a complex remains fixed. In contrast to PO dimer complexes, there are two separate orderings in which hydroxymethyl groups are added to ethylene oxide dimers to form glycidol dimer complexes. Each F-SAPT difference analysis is separated into the direct and indirect effects of the –H/–CH_2OH substitution. The direct effect refers to the difference between the interaction of the –CH_2OH functional group with the entire other monomer and the analogous interaction of its substituted –H atom. The indirect effect is the energy difference between the oxirane backbone with the entire other molecule. The intermolecular interaction energies for glycidol dimer complexes are 2–3 times bigger than for PO dimers and it is reflected in all SAPT decomposed components as well. The chiral discrimination energy values vary from 0.044 kcal/mol to 1.725 kcal/mol and 0.206 kcal/mol to 1.690 kcal/mol for SAPT0

and SAPT2+3 levels, which are considerable in comparison to PO dimer structures, showing that the chiral discrimination effects are stronger in glycidol dimer structures. Also, Figures 4-10 of Appendix B show that there is a systematic increase in energy by the successive additions of the $–CH_2OH$ functional groups for eight-membered rings, approximately by 7-10 kcal/mol for electrostatic and exchange contributions and by less that 5 kcal/mol for the remaining induction and dispersion contributions. However, for the five-membered ring structures depending on which $–CH_2OH$ group is added first, there can be almost no increase in energy, or the maximum energetic difference happens at once.

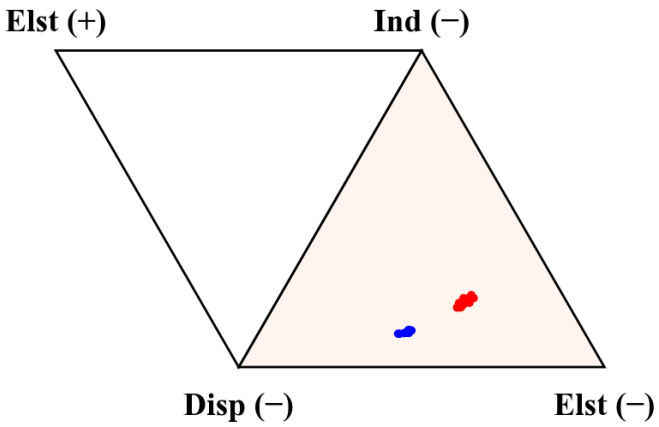

Figure 3.7: Ternary diagram of the attractive energy components for PO and Glycidol dimer structures.

The ternary diagram in Fig. 3.7 represents the relative contributions from the three attractive SAPT terms, electrostatics, induction, and dispersion, into the interaction energies in the PO and glycidol dimers.[21,31,96,97] As can be seen from Fig. 3.7, both propylene oxide and glycidol dimer structures are dispersion- and electrostatically dominated molecular complexes. It is also concluded that the dispersion component of SAPT contributes more in the PO dimer structures than in the glycidol dimer complexes, while the electrostatic contribution in the glycidol dimers plays a more constructive role than in the PO dimers, as expected because of the hydroxymethyl group in the glycidol molecule. Also, from Fig. 3.7, it can be concluded that all the structures for the same complex are so similar (shown by red and blues dots).

Last but not least, we have performed the frequency computations and the main focus is on the largest frequency shifts. Vibrational spectroscopy is an indispensable part of our study on

the PO–PO and glycidol–glycidol complexes. The harmonic frequencies for all 24 PO normal modes and all 27 glycidol normal modes were computed and are available in the Appendices A and B, respectively. The results show how the frequencies in an isolated PO and glycidol molecules are shifted and split into frequencies in homochiral and heterochiral PO and glycidol diastereomers. The main focus is on frequency shifts in a dimer relative to an isolated monomer.

Harmonic frequencies for the PO dimers were computed at the MP2/AVQZ level of theory and are shown in Figures 4 and 5 in Appendix A. These figures show how frequencies are shifted relative to an isolated PO monomer and split into two distinct frequencies in each of the RR and RS diastereomers. A pair of blue and green frequencies shown for all 12 PO dimer complexes corresponds to the symmetric and antisymmetric combination of the monomer vibrations for structures having a center of symmetry such as RS1, RS3, and RS6: otherwise, it corresponds to some linear combination of the same monomer modes. All subfigures in Figures 4 and 5 in Appendix A are sorted in an increasing order in frequency values, meaning that the first subfigure has the lowest frequency of 219.15 cm^{-1} which is a torsional mode, and the last subfigure displays the largest frequency of 3246.73 cm^{-1} pertaining to one of the C–H stretching modes. The largest frequency shifts are analyzed first. As can be seen from Figures 4 and 5 in Appendix A, the frequency shifts of over 10 cm^{-1} in either direction belong to the lowest frequency ν_1 =219.15 cm^{-1}, (up to 29.5 cm^{-1} for RR1), then to ν_{18} =1538.26 cm^{-1}, (up to -15.5 cm^{-1} for RS6), and lastly to ν_{22} =3163.52 cm^{-1}, (up to 11.8 cm^{-1} for RS2). The frequency for the ν_1 torsional mode, which is the methyl group rotation, is blue-shifted in most PO–PO complexes relative to the isolated monomer except for the RR4/RS4, RR5/RS5, and RR6/RS6 structures. This blue shift is expected because involvement in the secondary hydrogen bonds hinders the methyl group rotation. Also, it can be seen that for the RR5/RS5 and RR6/RS6 pairs, the energetic chiral differences are small, reflected in frequency shifts up to 2.6 cm^{-1} for ν_2 and RR6/RS6, which are attributed to small differences in geometric structures.

For glycidol complexes, the main focus was on the four most interesting modes which are available in Figure 11 in Appendix B and the remaining modes can be found in the supplementary information to Ref. 39. The selected normal modes are the rotation of the $–CH_2OH$ functional group around the C–C bond, the rotation of the alcohol hydrogen atom around the

C–O bond, the C–C–O bending involving the hydroxyl group oxygen, and the O–H stretching mode, pertaining to ν_1 =155.0 cm^{-1}, ν_4 =458.9 cm^{-1}, ν_5 =623.6 cm^{-1}, and ν_{27} =3778.4 cm^{-1}, respectively. The first normal mode considered here is ν_1, which corresponds to the rotation around the C–C bond between the oxirane backbone and the hydroxymethyl functional group. This mode is low-energy torsional mode which its value for the M1 monomer structure (top left in Fig. 3.4) is estimated around 155.0 cm^{-1}, which is in an acceptable range compared to the experimental value of 145(15) cm^{-1}.[77]

The next important frequency is ν_4 =458.9 cm^{-1}, where the H atom of the hydroxyl group rotates around the C–O bond (see Fig. 11 in Appendix B for more details). This rotational frequency shifts are large and the positivity of them shows these are blue-shifted. As can be seen, the patterns are different for eight-membered ring and five-membered ring structures. For five-membered ring structures, one of the monomers acts as a proton donor and an acceptor at the same time in H-bond formation, if is reflected in ν_4 rotational mode that one of the two frequency shifts is noticeably larger than than the other showing that a smaller ring in five-membered ring structures is severely affected by the distortion of the H atom of the hydroxyl group rotation. The ν_5 normal mode corresponds to the C–C–O bending motion that involves a ring carbon, a nonring carbon, and the hydroxyl oxygen. In this mode, an interesting but distinct pattern is observed for both eight-membered and five-membered rings, when a dimer consists of both M1 conformation, both frequency shifts are small. Once one monomer of M1 configuration and the other monomer with M2 configuration come together to make a dimer, one large shift and one small shift in frequencies are observed. Finally, when a complex is made up of both M2 configuration, there will be two large frequency shifts. It is worthwhile to mention that between the two minimum structures for an isolated glycidol molecule, M1 is the global minimum and M2 is the next local minimum; and all frequency shifts were computed and compared with the global minimum M1 conformation. The most important frequency is ν_{27}, where describes the O–H stretching mode. In this mode, the frequencies in a dimer are always smaller than the corresponding frequencies in a monomer (red-shifted), which is a typical signature of hydrogen bonds.

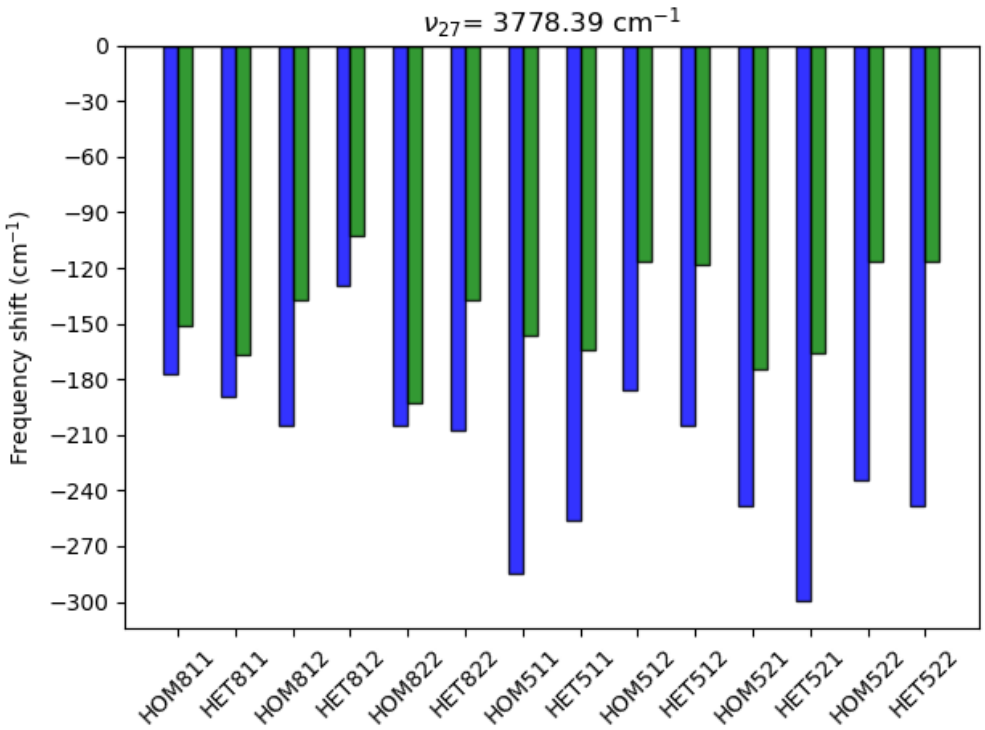

Figure 3.8: Vibrational frequency shifts of the O–H stretching mode of the 14 glycidol dimer structures relative to the isolated monomer frequencies.

As can be seen in Fig. 3.8, there is a distinct difference between the eight-membered ring and five-membered ring structures. In the eight-membered ring structures, the differences in frequency shifts are small because both H-bonds are formed by the same type of oxygen atom acceptor, in which belongs to the epoxide ring. But this not the case for five-membered ring structures. These frequency shifts are larger for five-membered ring structures because the two H-bonds are formed by different type of oxygen atoms; one of the acceptor oxygen atoms hinges the epoxide ring, while the other acceptor oxygen atom belongs to the alcohol group.

3.3 Summary

A comprehensive study of model complexes of two chiral molecules in a dimer form was performed using increasingly popular and efficient theoretical methods to investigate and describe intermolecular interactions and chirodiastaltic energies, and to get insight into the origin of chiral discrimination energy in noncovalently interacting molecules. The complexes at their

optimal geometries were analyzed with various computational methods such as DFT with different functionals, SAPT, F-SAPT, F-SAPT difference analysis, and normal mode calculations with the emphasis on differences between homochiral and heterochiral diastereomers. As expected, differences in interaction energies and, as a result, the chirodiastaltic energies, were considerably bigger for glycidol complexes than for PO dimers. Some "DFT plus dispersion" variants, in particular the B3LYP-D3 and B3LYP-D3M performed well on PO dimers with the average interaction energy errors slightly exceeding 0.1 kcal/mol. For the glycidol dimers in addition to the B3LYP-D3, the BLYP-D3M and PBE0-D3 functionals gave good results with the same average error as above. The chiral effects led to differences in interaction energies between the homochiral and heterochiral diastereomers ranging in magnitude from 0.0-0.13 kcal/mol for PO complexes and 0.1-1.6 kcal/mol for glycidol dimer structures. These differences were determined at several levels of theory up to the benchmark interaction energy values computed at the $\mathrm{MP2/(aQZ, a5Z)} + \Delta\mathrm{CCSD(T)/aTZ}$ level, that is, MP2 extrapolated to the complete basis set limit from aQZ and a5Z in the standard X^{-3} correlation energy extrapolation, with an additional term, $\Delta\mathrm{CCSD(T)}$, as a correction computed in the aTZ Dunning basis set.

For the molecular complexes studied here, symmetry-adapted perturbation theory leads to a systematic overbinding of all dimer structures, but for the accurate SAPT2+3 level this overbinding is less severe than it is for the SAPT0 level. Both SAPT0 and SAPT2+3 levels show the same trend in interaction energies and the correct sign for chirodiastaltic energy values, in agreement with the previous theoretical and experimental studies for both PO–PO and glycidol–glycidol complexes. SAPT results showed that for PO–PO complexes the dispersion component contributes the most to the binding in these structures. For glycidol–glycidol complexes, in addition to a sizable dispersion energy, almost the same amount of binding is provided by the induction contribution. The F-SAPT difference analysis results showed that the direct effects of either the H/CH_3 substitution in PO-PO or H/CH_2OH substitution in glycidol–glycidol overwhelm the indirect effects resulting from the electronic structure difference between the molecular backbones. For the glycidol case, these F-SAPT difference analysis is dominated by the hydrogen bond formation upon substitution. The difference is that for the

eight-membered ring structures these hydrogen bonds are always formed one at a time, while for the five-membered ring complexes, two hydrogen bonds can be formed one at a time or both at once, depending on which monomer in a dimer is chosen for substitution first.

The SAPT analysis were complemented by the computations of vibrational frequencies. As a result of the intermolecular interaction, two distinct shifts for each vibrational frequency of an isolated monomer were distinguished. The frequency shifts, splittings, and chiral differences of the intramolecular harmonic modes calculated at the MP2/aQZ level for PO–PO and DF-MP2/aTZ level for glycidol–glycidol complexes were analyzed.

Chapter 4

Intermolecular interactions of the Ethylene-Oxygen complex

In this chapter, we consider the ethylene-oxygen complex. Ethene (ethylene, C_2H_4) has a significant importance as a prototypical system in both theoretical and experimental chemistry. The stability of ethylene makes it possible to probe a variety of reactions. This molecule has a double bond between carbon atoms and the angles of H-C-H are experimentally determined to be almost 120° which implies that the carbon atoms hybridization is sp^2.

Ethylene is the simplest organic π-electron system that has been the subject of numerous experimental and theoretical studies.[98–104] This molecule with 16 electrons has the singlet ground state electronic configuration (^1A_g) in which the last two electrons are positioned in the π orbital as shown below (Fig. 4.1).

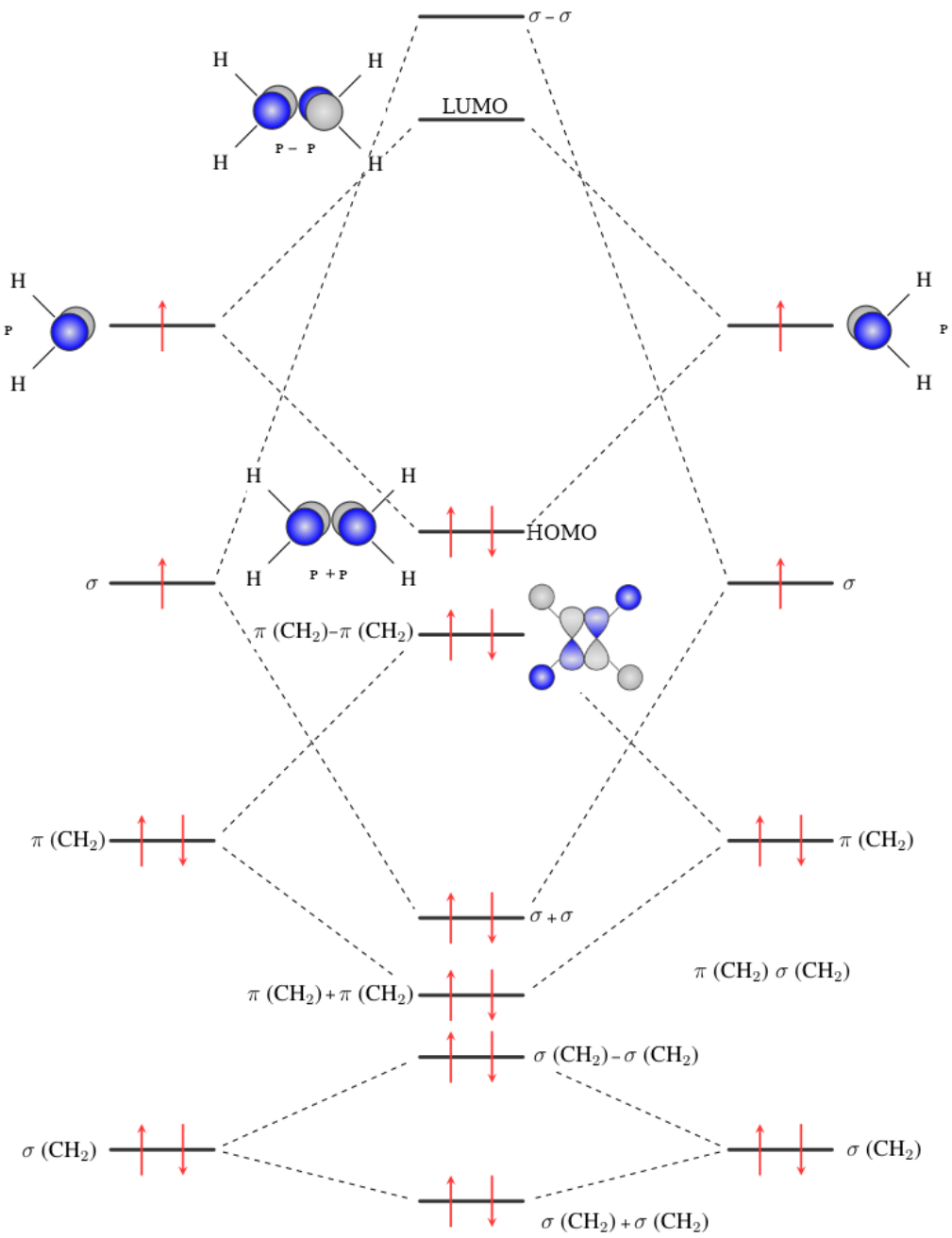

Figure 4.1: Molecular orbital diagram for ethylene.

In addition to the planar ethylene, we are interested in the twisted ethylene possessing the triplet state electronic configuration of ${}^3A_1$ and $\mathrm{D_{2d}}$ symmetry. The rotational barrier of ethylene has been the subject of many studies in the past.[105–107] In the twisted ethylene, the π-orbital overlap of the methylene groups decreases and the planar D_{2h} ethylene transforms to the D_{2d} symmetry.

In this study, the interaction partner of ethylene is the oxygen molecule, O_2, that has the electronic ground state $^3\Sigma_g^-$ (triplet sigma),[108] where the two electrons have parallel spins,

(core) $(\sigma_{2s})^2(\sigma^*_{2s})^2(\sigma_{2p_z})^2(\pi_{2p_x})^2(\pi_{2p_y})^2(\pi^*_{2p_x})^1(\pi^*_{2p_y})^1$

and the next two excited states have the electronic configurations as follows,

$^1\Delta_g$: (core) $(\sigma_{2s})^2(\sigma^*_{2s})^2(\sigma_{2p_z})^2(\pi_{2p_x})^2(\pi_{2p_y})^2[(\pi^*_{2p_x})^2(\pi^*_{2p_y})^0 + (\pi^*_{2p_x})^0(\pi^*_{2p_y})^2]$

$^1\Sigma_g^+$: (core) $(\sigma_{2s})^2(\sigma^*_{2s})^2(\sigma_{2p_z})^2(\pi_{2p_x})^2(\pi_{2p_y})^2[(\pi^*_{2p_x})^2(\pi^*_{2p_y})^0 - (\pi^*_{2p_x})^0(\pi^*_{2p_y})^2]$

where the first excited state shown by $^1\Delta_g$ is a singlet state which implies that the two electrons in the π^* molecular orbitals have opposite spins according to the Pauli exclusion principle. The lowest excited electronic state of O_2 ($^1\Delta_g$) has 94 kJ/mol more energy than its ground electronic state ($^3\Sigma_g^-$).[109] The second excited state which is 157.85 kJ/mol higher in energy than the ground state, has also accommodated the two electrons with opposite spins in π^* molecular orbitals[109] and therefore it is a singlet spin state, $^1\Sigma_g^+$. The oxygen molecule has also been the subject of many computational and experimental studies because of the trivial reason that the life on Earth heavily depends on oxygen. Furthermore, oxygen both in its open shell ground state and electronic excited states has interesting and unique chemistry that make it shine in the periodic table.[109–113] In this study, we are interested in exploring the potential energy curves of the C_2H_4–O_2 complex both in their ground state and excited states. For this matter, high-level *ab initio* methods are employed to get accurate and reliable results. In general, oxygen is highly reactive with ethylene, and this type of reaction is known as the ene reaction of singlet oxygen with olefins.[110] It is one of the important classes of reactions, with implications in biochemistry,[114] environmental chemistry,[115] and synthesis.[116]

Intermolecular complexes of O_2 with organic molecules have attracted great attention for decades. Studying a molecular cluster, in general, requires to analyze the isolated molecules first. Figure shows the ground electronic state and the next two excited states of isolated dioxygen and ethylene molecules. The lowest-lying excited electronic state, $^1\Delta_g$, is of particular importance for the photobiology perspective,[113] and it is referred to as singlet oxygen. This is an example of the importance of this type of molecular systems. Another application of the reaction of singlet oxygen with alkenes in addition to ene reactions and cycloaddition, is in the photodynamic therapy (PDT) treatments of tumors.[117] In photochemistry and photobiology, the

main process for generating singlet oxygen is sensitization where the sensitizer in an excited electronic state transfers its energy to the ground state triplet oxygen via collision. But this process has its own limitations, first because of the extremely low lifetime of the singlet oxygen in different solvents. In the literature, the lifetime of singlet oxygen depends mainly on solvents and varies from 900μs in tetrachloromethane (CCl_4) to 2μs in water (H_2O).[118–120] One of the intrinsic quantum physical properties of electrons is their spin. Molecular singlet oxygen, O_2, as mentioned earlier has two unpaired electrons, one with spin up (α) and the other with spin down (β). In general, chemical reactions cannot change the spin states of electrons. Hence, reactions between singlet spin states of ethylene and triplet spin states of oxygen are formally spin-forbidden, which means that they are slow. Normally, this is handled by using transition metals to activate and reduce O_2 because most transition metals have several unpaired electrons enabling them to react with triplet O_2. The other reason of usage of transition metals is that they are heavy atoms, which leads to strong spin-orbit coupling (SOC) which provides a quantum mechanical phenomenon known as spin-inversion in which the spin state of an electron changes. In this study, we are interested in knowing about the weak intermolecular interactions of the C_2H_4–O_2 complex. If this interaction leads to a reaction, this would be a spin-forbidden reaction because the spin states of ethylene and oxygen molecules are different. One possibility is the interaction of the first excited state of ethylene with the ground electronic state of O_2, where four unpaired electrons will be available. Depending on the relative direction of these sets of unpaired electrons coming from C_2H_4 and O_2, the resulting complex would have zero $(2-2)$ to four $(2+2)$ unpaired electrons meaning that the complex would possess a singlet, triplet or quintet spin state, respectively. Among these spin configurations, quintet is the single reference state, i.e. there is one possibility to construct this state, and the other spin states are not single-reference and require multireference calculations.

4.1 Potential energy curves (PEC)s for the Ethylene-Oxygen complex

The C_2H_4–O_2 complex in particular, or an M–O_2 molecular system in general where M is an alkene in general, establishes an interesting prototype which has unique and important chemical and physical properties. Perhaps one of the significant features of the C_2H_4–O_2 complex is that

it enables oxygen to get rid of some forbidden transitions in an isolated O_2 molecule, which we will see in the coming pages.

In this study we are interested in knowing the PECs for ground state and a few excited states of the ethylene-oxygen complex. Understanding weak intermolcular interactions between these two molecules just before their reaction is of great importance in biology. Among infinite configurations possible for the ground-state ethylene-oxygen complex, there were 9 with high symmetry that were investigated to find the most stable configuration for the C_2H_4–O_2 system, as shown in Figure 4.2.

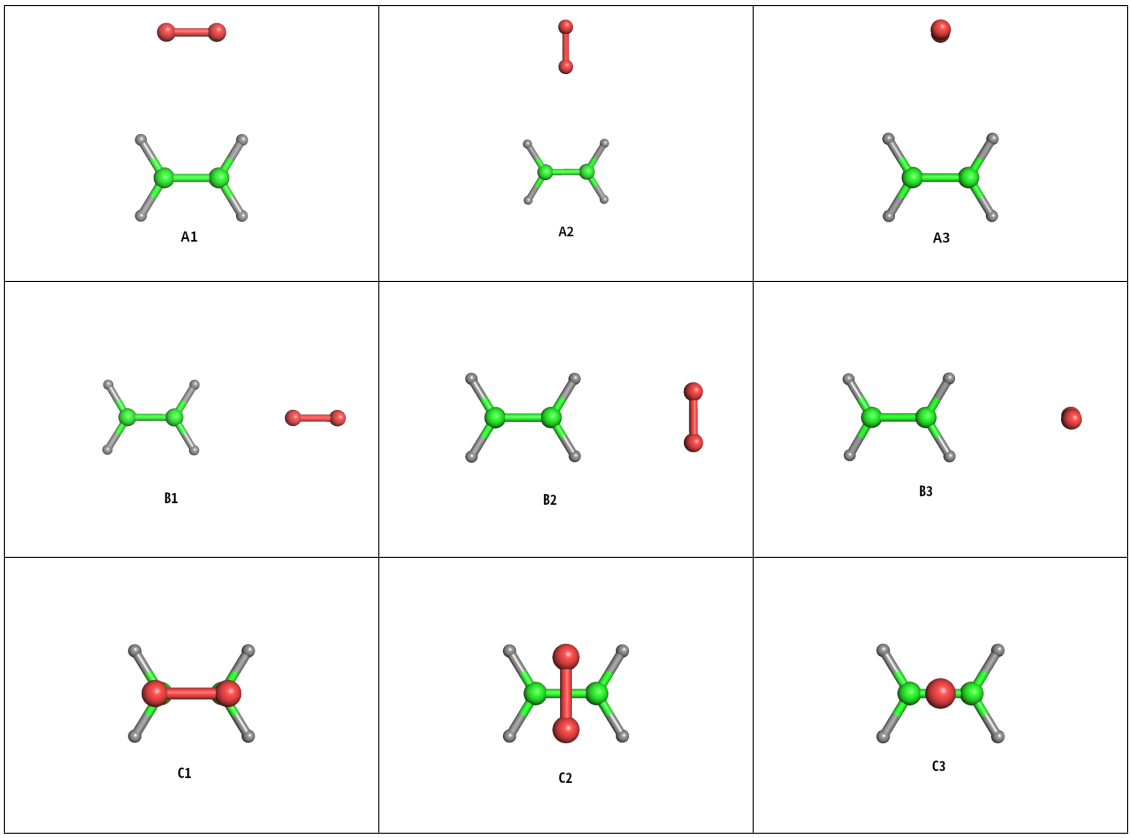

Figure 4.2: Possible ground-state C_2H_4–O_2 structures, optimized at the UMP2/aTZ level.

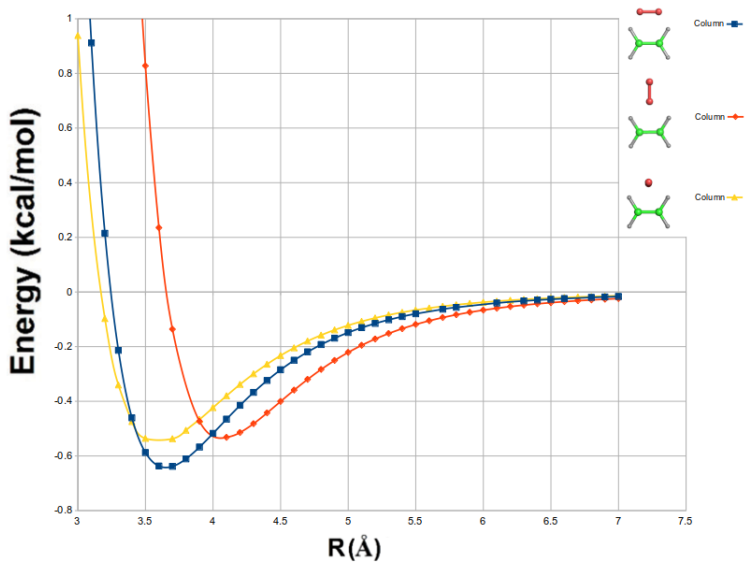

Figure 4.3: Potential energy curves for planar ethylene and oxygen at the RCCSD(T)/aTZ level.

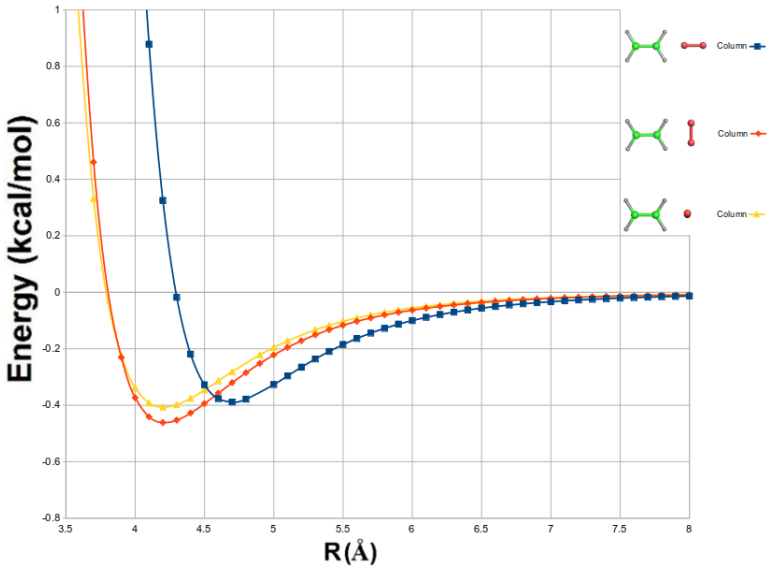

Figure 4.4: Potential energy curves for planar ethylene and oxygen at the RCCSD(T)/aTZ level.

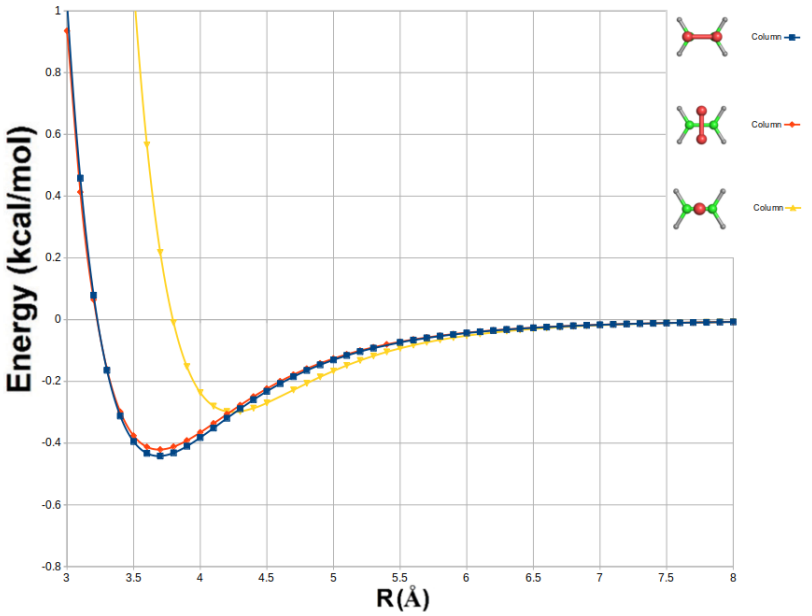

Figure 4.5: Potential energy curves for planar ethylene and oxygen at the RCCSD(T)/aTZ level.

In four of those structures, O_2 is in the same plane as the planar ethylene but with different orientations and in the remaining five structures, O_2 is out of the plane of the planar ethylene in three different directions. All 9 proposed geometries of the triplet C_2H_4-O_2 complex were optimized using the MP2/aug-cc-pVTZ level. Our optimized geometries were confirmed by the vibrational frequency calculations performed after geometry optimization computations, and the resulting PECs for the C_2H_4-O_2 complex are depicted in Fig. 4.3–4.5. For vibrational frequency calculations, the structure of interest must be minimized and the gradient at the minimum point must be zero. If a structure is at a saddle point or transition state, this situation is reflected in in the vibrational frequencies by getting imaginary numbers.

Because O_2 is an open-shell system, a spin restricted Hartree-Fock (ROHF) and the ROHF based coupled cluster (RCCSD(T)) calculations were performed. [121,122] The PECs for the C_2H_4–O_2 complex were constructed by varying the center of mass separation of C_2H_4 and O_2 molecules at the RCCSD(T) level using the augmented quadruple-ζ quality correlation consistent (aug-cc-pVQZ) basis set while other coordinates were fixed to their equilibrium positions. All the PECs shown here are attractive. For structures "A1" and "B2" all the normal modes are real numbers at the minimum structure, implying that the minimum points are true minimum. In addition,

the constructed PECs reveal that the "A1" C_2H_4-O_2 complex is the global minimum of -0.637 kcal/mol, which occurs at an 3.7 $\mathring{A}$ center of mass separation and the "B2" orientation is the next minimum (local minimum) structure with the energy of -0.461 kcal/mol, which occurs at around 4.3 $\mathring{A}$ center of mass separation. All the remaining structures are saddle points based on the frequency computations at their optimized structure.

Table 4.1 shows the SAPT computations performed at the SAPT0/aTZ level and its components as of electrostatics, first-order exchange, induction, and dispersion contributions. As can be seen, all interaction energies are negative as expected from the attractive PECs in Fig. 4.3–4.5. Also, this table confirms that the "A1" complex is the global minimum in the ground state. Because of the charge distributions of O_2, the electrostatic component contributes more in interaction energy than other SAPT0 terms.

Table 4.1: Interaction energy contributions and total interaction energies (in kcal/mol) predicted by SAPT0/aTZ for all possible C_2H_4–O_2 complexes in their ground state.

Structure	Elst	Exch	Ind	Disp	SAPT0
A1	-0.440	1.422	-0.140	-1.524	-0.682
A2	-0.253	0.944	-0.089	-1.221	-0.619
A3	-0.326	1.406	-0.107	-1.572	-0.599
B1	-0.161	0.615	-0.044	-0.872	-0.463
B2	-0.289	0.984	-0.065	-1.108	-0.478
B3	-0.213	0.889	-0.047	-1.064	-0.436
C1	-0.697	1.672	-0.093	-1.314	-0.433
C2	-0.648	1.543	-0.084	-1.214	-0.402
C3	-0.341	0.991	-0.103	-0.890	-0.342

For the next step in our study, the geometry optimization computations were carried out for triplet state of C_2H_4–O_2 complexes. But all that optimization calculations were failed and did not converged therefore the geometry optimization was performed for quintet twisted C_2H_4–O_2 complexes and all 6 possible structures were converged to a minimum and at the time of writing this dissertation, the pertinent frequency computations are running to confirm already obtained optimized geometries.

4.2 Summary

Various high level *ab initio* methods were utilized to compute the interaction energy for the C_2H_4–O_2 complex. The benchmark values were obtained at the RCCSD(T) level of theory combined with Dunning basis sets to investigate the ground and several excited electronic states. First, the planar C_2H_4–O_2 complex and twisted C_2H_4–O_2 were optimized at their relevant spin states. Then the interaction of singlet ethylene with triplet O_2 was studied and the PECs were constructed for different distances and different orientations. Subsequently, the interaction of triplet twisted ethylene with triplet O_2 was investigated and discussed, leading to a singlet, a triplet, and a quintet spin state for the complex. Finally, we investigate the triplet twisted ethylene with excite singlet O_2.

Chapter 5

Conclusions

In these studies, high-accuracy *ab initio* methods have been applied to simple prototype molecules in order to get insight into the chiral discrimination energy. Also, for the propylene oxide dimers and glycidol complexes, SAPT, F-SAPT, and F-SAPT difference analysis computations were performed to obtain the total intermolecular interaction energies along with their decomposed components and the influence of substituted functional groups on the chirodiastaltic energy. It was also a worthwhile task to carry out dispersion-corrected DFT calculations with a variety of functionals such as B3LYP, BLYP, and PBE0, and as it was shown that the B3LYP-D3M functional performed well on propylene oxide while the BLYP-D3M functional gave good results for the glycidol dimer structures, and the B3LYP-D3 functional represented reliable results for both systems of interest. In addition to the above computations, calculating normal modes is a demanding task especially for molecular systems containing secondary or true hydrogen bonds. Vibrational frequency shifts can reveal interesting and reliable characteristics of forming H-bonds in molecular clusters, and observing a frequency red-shifted of blue-shifted can be considered as a typical signature of the hydrogen bonds.

The $H_2C{=}CH_2{-}O_2$ complex was studied with CASSCF and MRCI methods to get the accurate potential energy surface (PES). As a standard procedure, the followed frequency calculations were performed to distinguish the true minimums from saddle points. It was shown that there are two C_2H_4-O_2 complexes with the lowest energy, where one of them is a global minimum and the next is a local minimum. Then the SAPT calculation was performed at the SAPT0/aTZ level to investigate the interaction energies in terms of different SAPT components (Section 4.1) and the benchmark interaction energy is going to be calculated.

5.1 Future and Outlook

There are many chiral molecules with unique chemistry that are capable to apply our findings and results to them in order to predict and investigate their chiral discrimination energy, such as nicotine ($C_{10}H_{14}N_2$). As mentioned earlier, the decomposition of the chirodiastaltic energy was carried out for the first time in the studies where they were explained in this thesis. Therefore, there are now open directions to apply these results to real world compounds as Korona and coworkers performed on some chiral drugs such as ibuprofen, norepinephrine, and baclofen.[84,85] Also, by awareness of the effect of individual functional groups into the chiral discrimination energy, the way we employed F-SAPT and F-SAPT difference analysis can dramatically reduce the time and cost for search and synthesis of any chiral drugs. Another aspect of our work that advances the state of the art is that our finding is applicable to enzyme substrate reactions. Enzymes are chiral molecules and by applying F-SAPT difference analysis, it would easier to analyze enzyme substrate interaction energies and distinguish where most of the interaction energy is coming from. Our plan for the C_2H_4-O_2 complex is to find optimized structures in the quintet state of C_2H_4-O_2 and get the PECs for that matter. Also, we are interested in investigating the spin splitting and spin inversion reactions where it could change the spin state of O_2. Also, it is a worthwhile task for investigate and analyze several low-lying excited states of the C_2H_4-O_2 complex, which is of great importance in biological applications.[123]

Bibliography

[1] Price, S. L. Quantifying intermolecular interactions and their use in computational crystal structure prediction. *Cryst. Eng. Comm.* **2004**, *6*, 344–353.

[2] Podeszwa, R.; Rice, B. M.; Szalewicz, K. On predicting structure of molecular crystals from first principles. *Phys. Rev. Lett.* **2008**, *101*, 115503.

[3] Lu, D.; Li, Y.; Rocca, D.; Galli, G. Ab initio Calculation of van der Waals Bonded Molecular Crystals. *Phys. Rev. Lett.* **2009**, *102*, 206411.

[4] Riley, K. E.; Hobza, P. Noncovalent interactions in biochemistry. *WIREs Comput. Mol. Sci.* **2011**, *1*, 3–17.

[5] Larson, A. M.; Groden, K.; Hannagan, R. T.; McEwen, J.-S.; Sykes, E. C. H. Understanding Enantioselective Interactions by Pulling Apart Molecular Rotor Complexes. *ACS Nano* **2019**, *13*, 5939–5946.

[6] Politzer, P.; Murray, J. S.; Peralta-Inga, Z. Molecular surface electrostatic potentials in relation to noncovalent interactions in biological systems. *Int. J. Quantum Chem.* **2001**, *85*, 676–684.

[7] Misiewicz, J. P.; Noonan, J. A.; Turney, J. M.; Schaefer, H. F. The non-covalently bound SO$\cdots$H2O system, including an interpretation of the differences between SO$\cdots$H2O and O2$\cdots$H2O. *Phys. Chem. Chem. Phys.* **2018**, *20*, 28840–28847.

[8] Wheeler, S. E.; Bloom, J. W. G. Toward a More Complete Understanding of Noncovalent Interactions Involving Aromatic Rings. *J. Phys. Chem. A* **2014**, *118*, 6133–6147.

[9] Řezáč, J.; Riley, K. E.; Hobza, P. S66: A Well-balanced Database of Benchmark Interaction Energies Relevant to Biomolecular Structures. *J. Chem. Theory Comput.* **2011**, *7*, 2427–2438.

[10] Faver, J. C.; Benson, M. L.; He, X.; Roberts, B. P.; Wang, B.; Marshall, M. S.; Kennedy, M. R.; Sherrill, C. D.; Merz, Jr., K. M. Formal Estimation of Errors in Computed Absolute Interaction Energies of Protein-Ligand Complexes. *J. Chem. Theory Comput.* **2011**, *7*, 790–797.

[11] Grimme, S. Semiempirical GGA-Type Density Functional Constructed with a Long-Range Dispersion Correction. *J. Comput. Chem.* **2006**, *27*, 1787–1799.

[12] Grimme, S.; Antony, J.; Ehrlich, S.; Krieg, H. A Consistent and Accurate Ab Initio Parametrization of Density Functional Dispersion Correction (DFT-D) for the 94 Elements H-Pu. *J. Chem. Phys.* **2010**, *132*, 154104.

[13] Becke, A. D.; Johnson, E. R. A Unified Density-Functional Treatment of Dynamical, Nondynamical, and Dispersion Correlations. *J. Chem. Phys.* **2007**, *127*, 124108.

[14] Tkatchenko, A.; Scheffler, M. Accurate Molecular Van Der Waals Interactions from Ground-State Electron Density and Free-Atom Reference Data. *Phys. Rev. Lett.* **2009**, *102*, 073005.

[15] Dion, M.; Rydberg, H.; Schröder, E.; Langreth, D. C.; Lundqvist, B. I. Van der Waals Density Functional for General Geometries. *Phys. Rev. Lett.* **2004**, *92*, 246401.

[16] Vydrov, O. A.; Van Voorhis, T. Nonlocal Van der Waals Density Functional: The Simpler the Better. *J. Chem. Phys.* **2010**, *133*, 244103.

[17] Lechner, C.; Sax, A. F. Adhesive Forces Between Aromatic Molecules and Graphene. *J. Phys. Chem. C* **2014**, *118*, 20970–20981.

[18] Møller, C.; Plesset, M. S. Note on an Approximation Treatment for Many-Electron Systems. *Phys. Rev.* **1934**, *46*, 618–622.

[19] Szabo, A.; Ostlund, N. S. *Modern Quantum Chemistry: Introduction to Advanced Electronic Structure Theory*, 1st ed.; Dover Publications, Inc., 1996.

[20] Cremer, D. Möller–Plesset perturbation theory: from small molecule methods to methods for thousands of atoms. *WIREs Comp. Mol. Sci.* **2011**, *1*, 509–530.

[21] Burns, L. A.; Marshall, M. S.; Sherrill, C. D. Appointing silver and bronze standards for noncovalent interactions: A comparison of spin-component-scaled (SCS), explicitly correlated (F12), and specialized wavefunction approaches. *J. Chem. Phys.* **2014**, *141*, 234111.

[22] Kodrycka, M.; Patkowski, K. Platinum, gold, and silver standards of intermolecular interaction energy calculations. *J. Chem. Phys.* **2019**, *151*, 070901.

[23] Dunning Jr., T. H. Gaussian-Basis Sets for Use in Correlated Molecular Calculations. 1. The Atoms Boron through Neon and Hydrogen. *J. Chem. Phys.* **1989**, *90*, 1007–1023.

[24] Kendall, R. A.; Jr., T. H. D.; Harrison, R. J. Electron Affinities of the 1st-Row Atoms Revisited-Systematic Basis Sets and Wave Functions. *J. Chem. Phys.* **1992**, *96*, 6796–6806.

[25] Woon, D. E.; Dunning, T. H. Gaussian basis sets for use in correlated molecular calculations. III. The atoms aluminum through argon. *J. Chem. Phys.* **1993**, *98*, 1358–1371.

[26] Jeziorski, B.; Moszyński, R.; Szalewicz, K. Perturbation Theory Approach to Intermolecular Potential Energy Surfaces of van der Waals Complexes. *Chem. Rev.* **1994**, *94*, 1887–1930.

[27] Szalewicz, K.; Patkowski, K.; Jeziorski, B. Intermolecular Interactions via Perturbation Theory: from Diatoms to Biomolecules. *Struct. Bonding (Berlin)* **2005**, *116*, 43–117.

[28] Szalewicz, K. Symmetry-adapted perturbation theory of intermolecular forces. *WIREs Comput. Mol. Sci.* **2012**, *2*, 254–272.

[29] Hohenstein, E. G.; Sherrill, C. D. Wavefunction Methods for Noncovalent Interactions. *WIREs Comput. Mol. Sci.* **2012**, *2*, 304–326.

[30] Patkowski, K. In *Annual Reports in Computational Chemistry*; Dixon, D. A., Ed.; Elsevier, Amsterdam, 2017; Vol. 13; pp 3–91.

[31] Patkowski, K. Recent developments in symmetry-adapted perturbation theory. *WIREs Comput. Mol. Sci.* **2020**, *10*, e1452.

[32] Parrish, R. M.; Sherrill, C. D. Spatial assignment of symmetry adapted perturbation theory interaction energy components: The atomic SAPT partition. *J. Chem. Phys.* **2014**, *141*, 044115.

[33] Parrish, R. M.; Parker, T. M.; Sherrill, C. D. Chemical Assignment of Symmetry-Adapted Perturbation Theory Interaction Energy Components: The Functional-Group SAPT Partition. *J. Chem. Theory Comput.* **2014**, *10*, 4417–4431.

[34] Bakr, B. W.; Sherrill, C. D. Analysis of transition state stabilization by non-covalent interactions in the Houk–List model of organocatalyzed intermolecular Aldol additions using functional-group symmetry-adapted perturbation theory. *Phys. Chem. Chem. Phys.* **2016**, *18*, 10297–10308.

[35] Bakr, B. W.; Sherrill, C. D. Analysis of transition state stabilization by non-covalent interactions in organocatalysis: application of atomic and functional-group partitioned symmetry-adapted perturbation theory to the addition of organoboron reagents to fluoroketones. *Phys. Chem. Chem. Phys.* **2018**, *20*, 18241–18251.

[36] Becke, A. D. Density-Functional Thermochemistry. 3. The Role of Exact Exchange. *J. Chem. Phys.* **1993**, *98*, 5648–5652.

[37] Perdew, J. P.; Burke, K.; Ernzerhof, M. Generalized Gradient Approximation Made Simple. *Phys. Rev. Lett.* **1996**, *77*, 3865–3868.

[38] Gu, Y.; Kar, T.; Scheiner, S. Fundamental Properties of the CH$\cdots$O Interaction:? Is It a True Hydrogen Bond? *J. Am. Chem. Soc.* **1999**, *121*, 9411–9422.

[39] Hemmati, R.; Patkowski, K. Ab Initio Study of Chiral Discrimination in the Glycidol Dimer. *J. Phys. Chem. A* **2020**, *124*, 9436–9450.

[40] Pirkle, W. H.; Pochapsky, T. C. Considerations of chiral recognition relevant to the liquid chromatography separation of enantiomers. *Chem. Rev.* **1989**, *89*, 347–362.

[41] Nagata, Y.; Takeda, R.; Suginome, M. Asymmetric Catalysis in Chiral Solvents: Chirality Transfer with Amplification of Homochirality through a Helical Macromolecular Scaffold. *ACS Cent. Sci.* **2019**, *5*, 1235–1240.

[42] Parker, D. NMR determination of enantiomeric purity. *Chem. Rev.* **1991**, *91*, 1441–1457.

[43] Born, M.; Oppenheimer, R. Zur Quantentheorie der Molekeln. *Annalen der Physik* **1927**, *389*, 457–484.

[44] Woolley, R.; Sutcliffe, B. Molecular structure and the born?Oppenheimer approximation. *Chemical Physics Letters* **1977**, *45*, 393–398.

[45] Cave, R. J.; Davidson, E. R. Quasidegenerate variational perturbation theory and the calculation of first? order properties from variational perturbation theory wave functions. *J. Chem. Phys.* **1988**, *89*, 6798–6814.

[46] McWeeny, R.; Sutcliffe, B. Fundamentals of Self-Consistent-Field (SCF), Hartree-Fock (HF), Multi-Configuration (MC)SCF and Configuration Interaction (CI) schemes. *Comput. Phys. Rep.* **1985**, *2*, 219–278.

[47] Szalay, P. G.; Müller, T.; Gidofalvi, G.; Lischka, H.; Shepard, R. Multiconfiguration Self-Consistent Field and Multireference Configuration Interaction Methods and Applications. *Chem. Rev.* **2012**, *112*, 108–181.

[48] Roos, B. O. The complete active space SCF method in a fock-matrix-based super-CI formulation. *Int. J. Quantum Chem.* **1980**, *18*, 175–189.

[49] Werner, H.-J.; Knowles, P. J. An Efficient Internally Contracted Multiconfiguration Reference CI Method. *J. Chem. Phys.* **1988**, *89*, 5803–5814.

[50] Knowles, P. J.; Werner, H.-J. An efficient method for the evaluation of coupling coefficients in configuration interaction calculations. *Chem. Phys. Lett.* **1988**, *145*, 514–522.

[51] Slater, J. C. Note on Hartree's Method. *Phys. Rev.* **1930**, *35*, 210–211.

[52] Čížek, J. On the Correlation Problem in Atomic and Molecular Systems. Calculation of Wavefunction Components in Ursell-Type Expansion Using Quantum-Field Theoretical Methods. *J. Chem. Phys.* **1966**, *45*, 4256–4266.

[53] Řezáč, J.; Šimová, L.; Hobza, P. CCSD[T] Describes Noncovalent Interactions Better than the CCSD(T), CCSD(TQ), and CCSDT Methods. *J. Chem. Theory Comput.* **2013**, *9*, 364–369.

[54] Woon, D. E.; Dunning Jr., T. H. *J. Chem. Phys.* **1994**, *100*, 2975–2988.

[55] Woon, D. E. Benchmark calculations with correlated molecular wave functions. V. The determination of accurate ab initio intermolecular potentials for He2, Ne2, and Ar2. *J. Chem. Phys.* **1994**, *100*, 2838.

[56] Peterson, K. A.; Dunning, T. H. Intrinsic Errors in Several ab Initio Methods: The Dissociation Energy of N2. *J. Phys. Chem.* **1995**, *99*, 3898–3901.

[57] Raghavachari, K.; Trucks, G. W.; Pople, J. A.; Head-Gordon, M. A 5th-Order Perturbation Comparison of Electron Correlation Theories. *Chem. Phys. Lett.* **1989**, *157*, 479–483.

[58] Hohenberg, P.; Kohn, W. Inhomogeneous Electron Gas. *Phys. Rev.* **1964**, *136*, B864–B871.

[59] Grimme, S. Density functional theory with London dispersion corrections. *WIREs Comput. Mol. Sci.* **2011**, *1*, 211–228.

[60] Chai, J.-D.; Head-Gordon, M. Long-range corrected hybrid density functionals with damped atom-atom dispersion corrections. *Phys. Chem. Chem. Phys.* **2008**, *10*, 6615–6620.

[61] Grimme, S. Accurate description of van der Waals complexes by density functional theory including empirical corrections. *J. Comput. Chem.* **2004**, *25*, 1463–1473.

[62] Zimmerli, U.; Parrinello, M.; Koumoutsakos, P. Dispersion corrections to density functionals for water aromatic interactions. *J. Chem. Phys.* **2004**, *120*, 2693–2699.

[63] Axilrod, B. M.; Teller, E. Interaction of the van der Waals Type Between Three Atoms. *J. Chem. Phys.* **1943**, *11*, 299–300.

[64] Marinescu, M.; Starace, A. F. Three-body dispersion coefficients for alkali-metal atoms. *Phys. Rev. A* **1997**, *55*, 2067–2074.

[65] Midzuno, Y.; Kihara, T. Non-additive Intermolecular Potential in Gases I. van der Waals Interactions. *J. Phys. Soc. Jpn.* **1956**, *11*, 1045–1049.

[66] Parrish, R. M. et al. PSI4 1.1: An Open-Source Electronic Structure Program Emphasizing Automation, Advanced Libraries, and Interoperability. *J. Chem. Theory Comput.* **2017**, *13*, 3185–3197.

[67] Parker, T. M.; Burns, L. A.; Parrish, R. M.; Ryno, A. G.; Sherrill, C. D. Levels of Symmetry Adapted Perturbation Theory (SAPT). I. Efficiency and Performance for Interaction Energies. *J. Chem. Phys.* **2014**, *140*, 094106.

[68] Dykstra, C. E.; Lisy, J. M. Experimental and theoretical challenges in the chemistry of noncovalent intermolecular interaction and clustering. *J. Mol. Struct. (Theochem)* **2000**, *500*, 375–390.

[69] Duan, G.; V.H. Smith, J.; Weaver, D. Validation of the applicability of force fields to reproduce *ab initio* noncovalent interactions involving aromatic groups. *Adv. Quant. Chem.* **2004**, *47*, 65–92.

[70] Murray, J. S.; Resnati, G.; Politzer, P. Close contacts and noncovalent interactions in crystals. *Faraday Discuss.* **2017**, *203*, 113–130.

[71] Boys, S. F.; Bernardi, F. The calculation of small molecular interactions by the differences of separate total energies. Some procedures with reduced errors. *Mol. Phys.* **1970**, *19*, 553–566.

[72] McGuire, B. A.; Carroll, P. B.; Loomis, R. A.; Finneran, I. A.; Jewell, P. R.; Remijan, A. J.; Blake, G. A. Discovery of the interstellar chiral molecule propylene oxide (CH3CHCH2O). *Science* **2016**, *352*, 1449–1452.

[73] Faure, A.; Dagdigian, P. J.; Rist, C.; Dawes, R.; Quintas-Sánchez, E.; Lique, F.; Hochlaf, M. Interaction of Chiral Propylene Oxide (CH3CHCH2O) with Helium: Potential Energy Surface and Scattering Calculations. *ACS Earth and Space Chem.* **2019**, *3*, 964–972.

[74] Su, Z.; Borho, N.; Xu, Y. Chiral Self-Recognition: Direct Spectroscopic Detection of the Homochiral and Heterochiral Dimers of Propylene Oxide in the Gas Phase. *J. Am. Chem. Soc.* **2006**, *128*, 17126–17131.

[75] Ōki, M.; Murayama, T. Intramolecular Interaction between the Hydroxyl Group and the Oxirane Ring. *Bull. Chem. Soc. Jpn.* **1973**, *46*, 259–263.

[76] Brooks, W. V. F.; Sastry, K. V. L. N. The Microwave Spectrum, Dipole Moment, and Structure of Glycidol. *Can. J. Chem.* **1975**, *53*, 2247–2251.

[77] Marstokk, K.-M.; Møllendal, H.; Stenstrøm, Y. Microwave Spectrum of Oxiranemethanol (Glycidol), the Assignment of a Second Hydrogen-Bonded Conformer and Conformational Composition in the Gas Phase and in Solution. *Acta Chem. Scand.* **1992**, *46*, 432–441.

[78] Portmann, S.; Inauen, A.; Lüthi, H. P.; Leutwyler, S. Chiral discrimination in hydrogen-bonded complexes. *J. Chem. Phys.* **2000**, *113*, 9577–9585.

[79] Borho, N.; Haber, T.; Suhm, M. A. Chiral self-recognition in the gas phase: the case of glycidol dimers. *Phys. Chem. Chem. Phys.* **2001**, *3*, 1945–1948.

[80] Borho, N.; Suhm, M. A. Glycidol dimer: anatomy of a molecular handshake. *Phys. Chem. Chem. Phys.* **2002**, *4*, 2721–2732.

[81] King, A. K.; Howard, B. J. A microwave study of the hetero-chiral dimer of butan-2-ol. *Chem. Phys. Lett.* **2001**, *348*, 343–349.

[82] Thomas, J.; Sunahori, F. X.; Borho, N.; Xu, Y. Chirality Recognition in the Glycidol$\cdots$Propylene Oxide Complex: A Rotational Spectroscopic Study. *Chem. Eur. J.* **2011**, *17*, 4582–4587.

[83] Dodziuk, H.; Ruud, K.; Korona, T.; Demissie, T. B. Chiral recognition by fullerenes: CHFClBr enantiomers in the C82 cage. *Phys. Chem. Chem. Phys.* **2016**, *18*, 26057–26068.

[84] Chojecki, M.; Rutkowska-Zbik, D.; Korona, T. On the applicability of functional-group symmetry-adapted perturbation theory and other partitioning models for chiral recognition — the case of popular drug molecules interacting with chiral phases. *Phys. Chem. Chem. Phys.* **2019**, *21*, 22491–22510.

[85] Chojecki, M.; Rutkowska-Zbik, D.; Korona, T. Description of Chiral Complexes within Functional-Group Symmetry-Adapted Perturbation Theory?The Case of (S/R)-Carvone with Derivatives of (?)-Menthol. *J. Phys. Chem. A* **2020**, *124*, 7735–7748.

[86] Pend'a, A. M.; Blanco, M. A.; Francisco, E. Two-electron integrations in the quantum theory of atoms in molecules. *J. Chem. Phys.* **2004**, *120*, 4581–4592.

[87] Pend'as, A. M.; Francisco, E.; Blanco, M. A. Two-electron integrations in the Quantum Theory of Atoms in Molecules with correlated wave functions. *J. Comput. Chem.* **2005**, *26*, 344–351.

[88] Parrish, R. M.; Sherrill, C. D. Quantum-Mechanical Evaluation of π-π versus Substituent-π Interactions in π Stacking: Direct Evidence for the Wheeler-Houk Picture. *J. Am. Chem. Soc.* **2014**, *136*, 17386–17389.

[89] Werner, H.-J. et al. MOLPRO, version 2012.1, a package of ab initio programs. 2012; see http://www.molpro.net (accessed June 2, 2016).

[90] Maris, A.; Giuliano, B. M.; Bonazzi, D.; Caminati, W. Molecular Recognition of Chiral Conformers: A Rotational Study of the Dimers of Glycidol. *J. Am. Chem. Soc.* **2008**, *130*, 13860–13861.

[91] Chałasiński, G.; Szczęśniak, M. M. State of the art and challenges of the *ab initio* theory of intermolecular interactions. *Chem. Rev.* **2000**, *100*, 4227–4252.

[92] Jurečka, P.; Šponer, J.; Černý, J.; Hobza, P. Benchmark database of accurate (MP2 and CCSD(T) complete basis set limit) interaction energies of small model complexes, DNA base pairs, and amino acid pairs. *Phys. Chem. Chem. Phys.* **2006**, *8*, 1985–1993.

[93] Helgaker, T.; Klopper, W.; Koch, H.; Noga, J. Basis-set convergence of correlated calculations on water. *J. Chem. Phys.* **1997**, *106*, 9639–9646.

[94] Halkier, A.; Helgaker, T.; Jørgensen, P.; Klopper, W.; Koch, H.; Olsen, J.; Wilson, A. K. Basis-Set Convergence in Correlated Calculations on Ne, N_2, and H_2O. *Chem. Phys. Lett.* **1998**, *286*, 243–252.

[95] Hemmati, R.; Patkowski, K. Chiral Self Recognition: Interactions in Propylene Oxide Complexes. *J. Phys. Chem. A* **2019**, *123*, 8607–8618.

[96] Smith, D. G. A.; Burns, L. A.; Patkowski, K.; Sherrill, C. D. Revised Damping Parameters for the D3 Dispersion Correction to Density Functional Theory. *J. Phys. Chem. Lett.* **2016**, *7*, 2197–2203.

[97] Singh, N. J.; Min, S. K.; Kim, D. Y.; Kim, K. S. Comprehensive Energy Analysis for Various Types of ?-Interaction. *J. Chem. Theory Comput.* **2009**, *5*, 515–529.

[98] Kaldor, U.; Shavitt, I. LCAO-SCF Computations for Ethylene. *J. Chem. Phys.* **1968**, *48*, 191–203.

[99] Merer, A. J.; Mulliken, R. S. Ultraviolet spectra and excited states of ethylene and its alkyl derivatives. *Chem. Rev.* **1969**, *69*, 639–656.

[100] Dunning, T. H.; Hunt, W. J.; Goddard, W. A. The theoretical description of the ($\pi\pi$*) excited states of ethylene. *Chem. Phys. Lett.* **1969**, *4*, 147–150.

[101] Mulliken, R. S. The excited states of ethylene. *J. Chem. Phys.* **1977**, *66*, 2448–2451.

[102] Barborini, M.; Sorella, S.; Guidoni, L. Structural Optimization by Quantum Monte Carlo: Investigating the Low-Lying Excited States of Ethylene. *J. Chem. Theory Comput.* **2012**, *8*, 1260–1269.

[103] Champenois, E. G.; Shivaram, N. H.; Wright, T. W.; Yang, C.-S.; Belkacem, A.; Cryan, J. P. Involvement of a low-lying Rydberg state in the ultrafast relaxation dynamics of ethylene. *J. Chem. Phys.* **2016**, *144*, 014303.

[104] McKellar, A. R. W.; Moazzen-Ahmadi, N. The Ethylene–Carbon Dioxide Complex and the Double Rotor Model. *J. Phys. Chem. A* **2020**, *124*, 684–689.

[105] Gemein, B.; Peyerimhoff, S. D. Radiationless Transitions between the First Excited Triplet State and the Singlet Ground State in Ethylene:? A Theoretical Study. *J. Phys. Chem.* **1996**, *100*, 19257–19267.

[106] Qi, F.; Sorkhabi, O.; Suits, A. G. Evidence of triplet ethylene produced from photodissociation of ethylene sulfide. *J. Chem. Phys.* **2000**, *112*, 10707–10710.

[107] Crawford, B. L.; Lancaster, J. E.; Inskeep, R. G. The Potential Function of Ethylene. *The Journal of Chemical Physics* **1953**, *21*, 678–686.

[108] Tudela, D.; Fernández, V. The Excited States of Molecular Oxygen. *J. Chem. Educ.* **2003**, *80*, 1381.

[109] Scurlock, R. D.; Wang, B.; Ogilby, P. R. Chemical Reactivity of Singlet Sigma Oxygen ($b^1\Sigma_g^+$) in Solution. *J. Am. Chem. Soc.* **1996**, *118*, 388–392.

[110] Harding, L. B.; Goddard, W. A. The mechanism of the ene reaction of singlet oxygen with olefins. *J. Am. Chem. Soc.* **1980**, *102*, 439–449.

[111] Hotokka, M.; Roos, B.; Siegbahn, P. CASSCF study of reaction of singlet molecular oxygen with ethylene. Reaction paths with C2v and Cs symmetries. *J. Am. Chem. Soc.* **1983**, *105*, 5263–5269.

[112] Ogilby, P. R. Singlet oxygen: there is indeed something new under the sun. *Chem. Soc. Rev.* **2010**, *39*, 3181–3209.

[113] Paterson, M. J.; Christiansen, O.; Jensen, F.; Ogilby, P. R. Overview of Theoretical and Computational Methods Applied to the Oxygen-Organic Molecule Photosystem. *J. Photochem. Photobiol.* **2006**, *82*, 1136–1160.

[114] Jensen, A. W.; Mohanty, D. K.; Dilling, W. L. The growing relevance of biological ene reactions. *Bioorg. Med. Chem.* **2019**, *27*, 686–691.

[115] Wayne, R. P. Singlet oxygen in the environmental sciences. *Res. Chem.* **1994**, *20*, 395–422.

[116] Mikami, K.; Shimizu, M. Asymmetric ene reactions in organic synthesis. *Chem. Rev.* **1992**, *92*, 1021–1050.

[117] Valentine, R. M.; Ibbotson, S. H.; Wood, K.; Brown, C. T. A.; Moseley, H. Modelling fluorescence in clinical photodynamic therapy. *Photochem. Photobiol. Sci.* **2013**, *12*, 203–213.

[118] Long, C.; Kearns, D. R. Selection rules for the intermolecular enhancement of spin forbidden transitions in molecular oxygen. *J. Chem. Phys.* **1973**, *59*, 5729–5736.

[119] Ogilby, P. R.; Foote, C. S. Chemistry of singlet oxygen. 34. Unexpected solvent deuterium isotope effects on the lifetime of singlet molecular oxygen ($^1\Delta_g$). *J. Am. Chem. Soc.* **1981**, *103*, 1219–1221.

[120] Sagadevan, A.; Hwang, K. C.; Su, M.-D. Singlet oxygen-mediated selective C–H bond hydroperoxidation of ethereal hydrocarbons. *Nat. Commun.* **2017**, *8*, 1812.

[121] Knowles, P. J.; Hampel, C.; Werner, H.-J. Coupled cluster theory for high spin, open shell reference wave functions. *J. Chem. Phys.* **1993**, *99*, 5219–5227.

[122] Knowles, P. J.; Hampel, C.; Werner, H.-J. Erratum: "Coupled cluster theory for high spin, open shell reference wave functions" [J. Chem. Phys. 99, 5219 (1993)]. *J. Chem. Phys.* **2000**, *112*, 3106–3107.

[123] Mirica, L. M.; Klinman, J. P. The nature of O2 activation by the ethylene-forming enzyme 1-aminocyclopropane-1-carboxylic acid oxidase. **2008**, *105*, 1814–1819.

Appendices

Appendix A

Chiral Self Recognition: Interactions in Propylene Oxide Complexes

THE JOURNAL OF PHYSICAL CHEMISTRY A

Article

Cite This: J. Phys. Chem. A 2019, 123, 8607−8618

pubs.acs.org/JPCA

Chiral Self Recognition: Interactions in Propylene Oxide Complexes

Reza Hemmati[†] and Konrad Patkowski*[,†]

[†]Department of Chemistry and Biochemistry, Auburn University, Auburn, Alabama 36849, United States

Supporting Information

ABSTRACT: We elucidate the subtle energetic effects that give rise to chiral recognition in the propylene oxide dimer. Specifically, we investigate six homochiral (*RRx*) and six heterochiral (*RSx*) structures of this complex, with the *RRn*−*RSn* pair sharing the same pattern of weak O···H−C hydrogen bonds but subtly differing in energy due to chiral effects. The interaction energies for the 12 structures are computed at various levels of electronic structure theory and basis set up to the complete basis set limit of the coupled-cluster approach with single, double, and perturbative triple excitations (CCSD(T)). These benchmark interaction energies are compared to the results of various approximate approaches, both density functional theory-based and wave function-based. We find that while the *RRn*−*RSn* diastereomeric energy differences exhibit a great deal of error cancellation between the individual interaction energies, most approximate methods have a hard time even reproducing the correct signs of these differences consistently. The origins of the *RRn*−*RSn* differences are elucidated by several symmetry-adapted perturbation theory (SAPT) analyses ranging from ordinary intermolecular SAPT to a functional-group SAPT (F-SAPT) decomposition of direct and indirect H → CH_3 substitution effects leading from achiral ethylene oxide complexes to chiral propylene oxide ones. It is shown that the largest diastereomeric energy differences are correlated to the variations in the electrostatic and dispersion SAPT contributions. Finally, the effect of chiral interactions on the vibrational frequencies of a propylene oxide molecule is investigated, showing that the interaction results in largest frequency shifts, splittings, and chiral discrimination effects in the lowest, torsional vibrational mode of the noninteracting monomer.

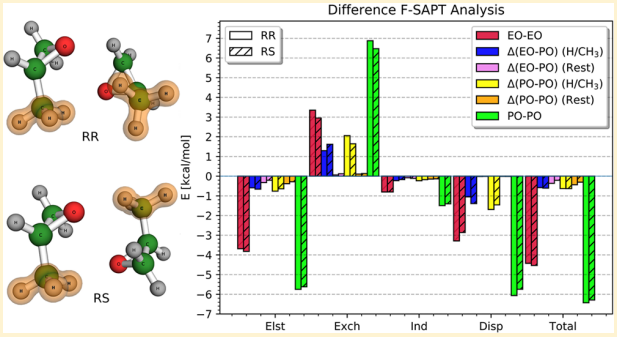

I. INTRODUCTION

The processes of life are inherently chiral, and nature—for reasons that are still under debate—has evolved in a near complete homochirality where only one of the enantiomers (L-amino acids, D-sugars, L-phospholipids, etc.) is ubiquitous in living organisms. This homochiral preference poses a significant challenge to the design and synthesis of biologically active compounds[1] as while one enantiomer exhibits desired therapeutic activity, the other one might be toxic. As a result, the phenomenon of chiral recognition, where the difference in energy and structure between diastereomeric complexes leads to a preferential binding of one enantiomer over the other, has become the keystone for such important and rapidly evolving disciplines as enantioselective organic synthesis[2,3] and the development of chiral materials.[4] On a fundamental level, chiral discrimination in the gas phase[5] and on surfaces[6] has been extensively studied using microscopic and spectroscopic techniques. It should be stressed that a quantitative investigation of chiral recognition effects by either theory or experiment is difficult as the underlying energetic effects are very small—the binding energy differences between diastereomers are often less than 1 kcal/mol. Moreover, while diastereomers of biologically relevant chiral molecules are typically stabilized by several hydrogen bonds, the strongest of these bonds are not necessarily decisive for the chiral recognition effect, which can originate from weaker bonds, steric repulsion, monomer relaxation, or other secondary effects.[7] The fact that one needs to recover small energy differences between diastereomers sets the bar high for *ab initio* electronic structure calculations in terms of both the theory level and the basis set employed.

As far as small systems (for which highly correlated electronic structure calculations are feasible) are concerned, the chiral discrimination phenomenon has been studied, both experimentally and theoretically, for gas-phase complexes such as the propylene oxide dimer,[8] glycidol dimer,[9] butan-2-ol dimer,[10] and propylene oxide−glycidol[11] complexes. The underlying chiral monomers vary greatly in terms of their flexibility, from the highly rigid propylene oxide molecule to the butan-2-ol molecule that can adopt a broad range of conformations. The key quantity being studied is the chirodiastaltic energy ΔE_{chir},[12] the energy difference between the homochiral and heterochiral complexes. The *ab initio* calculations of chirodiastaltic energies were typically performed using either density functional theory (DFT) or second-order Møller−Plesset perturbation theory (MP2) in a medium sized

Received: June 24, 2019
Revised: September 16, 2019
Published: September 17, 2019

DOI: 10.1021/acs.jpca.9b06028
J. Phys. Chem. A 2019, 123, 8607−8618

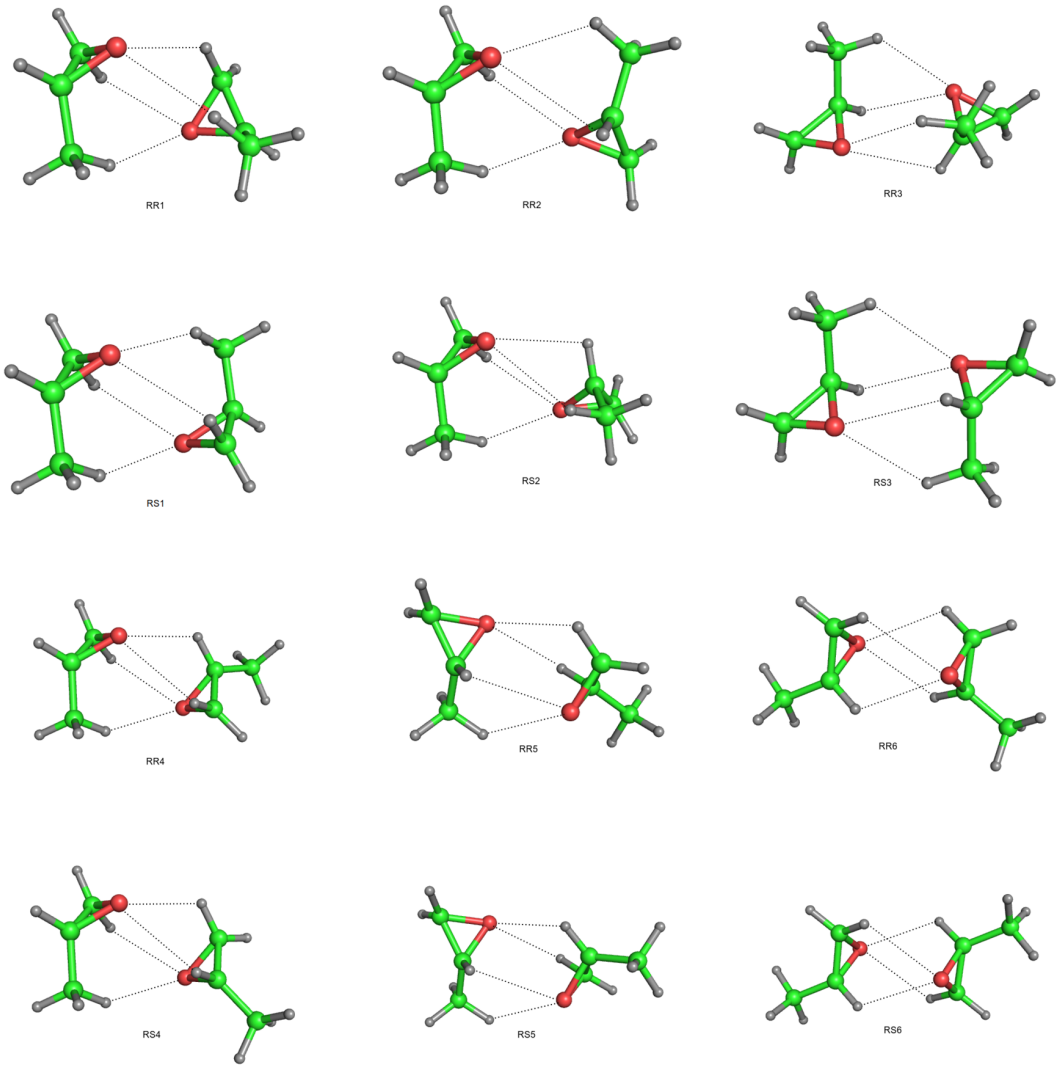

Figure 1. Optimized geometries of six homochiral (*RR*) and six heterochiral (*RS*) conformers of the PO dimer obtained at the DF-MP2/(aVTZ,aVQZ) extrapolated level.

basis set such as 6-311++G(d,p): a limited set of coupled-cluster calculations with single, double, and perturbative triple excitations (CCSD(T)) was performed in ref 7. While MP2 typically (but not universally) performs well for hydrogen-bonded dimers,[13] calculations in larger basis sets such as MP2/aug-cc-pVTZ[8,11] indicate that the results are far from being converged to the complete basis set (CBS) limit. Therefore, investigating these systems at higher theory and basis set levels is a worthwhile task.

Perhaps more importantly, computing chirodiastaltic energies as differences between supermolecular MP2/DFT/CCSD(T)/··· interaction energies affords little insight into the nature of the chiral recognition. In order to separate the chirodiastaltic energy into physically meaningful components, one needs an energy decomposition approach, preferably one that can analyze high-level effects of intra- and intermolecular electron correlation. Symmetry-adapted perturbation theory (SAPT)[14−16] is such an approach and provides interaction energy as a sum of well-defined electrostatic, induction, dispersion, and exchange corrections. A further level of interpretation has recently opened up through the introduction of atomic SAPT (A-SAPT)[17] and functional group SAPT (F-SAPT)[18] approaches. In these formalisms, each SAPT correction is further separated into terms arising from the interactions of a particular atom (A-SAPT)/group of atoms (F-SAPT) on molecule A with a particular atom/group on molecule B. The F-SAPT decomposition has recently been applied to elucidate the origins of enantioselectivity of some organocatalyzed reactions.[19,20] It should be noted that the SAPT decomposition is performed for the rigid interaction energy, defined with respect to noninteracting monomers in their geometries in the dimer. The flexible interaction energy, computed with respect to noninteracting monomers in their monomer-optimized geometries, can be obtained by adding the energy needed to bring the monomers into the conformations adopted in the complex. This monomer relaxation energy is obviously a unimolecular effect and does not lend itself to a SAPT interpretation.

In this study, we aim to obtain more insight into the origins of chiral discrimination effects in the propylene oxide (PO)

DOI: 10.1021/acs.jpca.9b06028
J. Phys. Chem. A 2019, 123, 8607−8618

dimer. We chose this complex as the propylene oxide molecule is small and rigid, and its bimolecular complex is stabilized solely by secondary O···H−C hydrogen bonds. As a result, high-level *ab initio* calculations are both feasible and necessary to recover the subtle chiral differences between diastereomers. Moreover, there is renewed interest in the interactions involving propylene oxide[21] as it recently became the first chiral organic molecule detected in the interstellar medium.[22] We start from the six pairs of homochiral (*RR*1−*RR*6) and heterochiral (*RS*1−*RS*6) structures obtained by Xu and co-workers.[8] We first perform a detailed investigation of the theory and basis set level needed to obtain accurate chirodiastaltic energies for all six pairs of structures, utilizing MP2 calculations in basis sets up to aug-cc-pV5Z and CCSD(T) calculations up to aug-cc-pVTZ. Having obtained benchmark interaction energies for the 12 conformations, we investigate the accuracy with which these energies are reproduced by lower-level methods such as density functional theory with atom-pairwise dispersion (DFT-D).[23] Last but not least, we perform SAPT calculations (at the SAPT0 and SAPT2+3 levels[24]) to quantify different physical contributions to chiral recognition energies (in addition to the monomer relaxation term) and subsequently refine the "global" SAPT analysis with the F-SAPT approach to identify the electrostatic, exchange, induction, and dispersion contributions arising from different fragments of the propylene oxide monomers. More specifically, we perform F-SAPT difference analysis[25] which refers to a process of partitioning a difference in interaction energies between substituted fragments. Here, we relate the diastereomeric PO−PO complexes to their achiral ethylene oxide−ethylene oxide (EO-EO) counterparts via an intermediate EO−PO step. As the entire chiral recognition effect stems from the difference between the interactions involving the methyl group and the hydrogen atom attached to the chiral center, a replacement of the former by another hydrogen atom renders the molecule achiral and limits the *RSn*−*RRn* energy differences to the relative energy of two points on the EO−EO potential energy surface. As the last step, the effects of *RR* and *RS* noncovalent interactions on the harmonic vibrational frequencies of the isolated propylene oxide molecule were investigated as well.

II. METHODS AND COMPUTATIONAL DETAILS

The MOLPRO program[26] was used to obtain the lowest energy geometry for all 12 dimer structures of propylene oxide investigated in ref 8. In each of these structures, each PO monomer serves as a donor for two and an acceptor for two secondary O···H−C hydrogen bonds. Therefore, the two PO monomers in a dimer are coupled via these four weak hydrogen bonds as shown in Figure 1. Because the PO molecule is chiral with the middle carbon atom serving as a stereogenic center, six of those 12 structures are homochiral (*RR* or *SS*) and the other six are heterochiral (*RS* or *SR*) conformers. The numbering *RRx*/*RSx* is dictated by the hydrogen atoms taking part in the hydrogen bonds and whether they come from the CH, CH_2, or CH_3 fragments. The corresponding *SS* and *SR* structures are enantiomeric (and thus isoenergetic) with the *RR* and *RS* structures, respectively, and we do not consider them explicitly.

All 12 geometries of the propylene oxide dimer have been reoptimized starting from the initial structures taken from ref 8 (where they were obtained at the MP2/6-311++G(d,p) level). We have reoptimized these structures at essentially the MP2 complete basis set limit, using the MP2/(aTZ,aQZ) level of theory and basis set. We have used the augmented correlation consistent Dunning bases[27,28] aug-cc-pVXZ ≡ aXZ, X = D, T, Q, 5. The notation method/(basis1,basis2) signifies that the interaction energy has been calculated using bases "basis1" and "basis2" and the standard X^{-3} correlation energy extrapolation for a given method.[29,30] It should be mentioned that the SCF interaction energy is computed from the larger of "basis1" and "basis2" sets and not from extrapolation. The different electronic structure approaches were utilized in the counterpoise-corrected supermolecular fashion; that is, the interaction energy is calculated as

$$E_{\text{int}} = E_{\text{AB}} - E_{\text{A}} - E_{\text{B}} \tag{1}$$

where E_{AB} denotes the total energy of a dimer and E_{A} and E_{B} show the energy of monomers A and B, respectively, all calculated in the full basis set of the interacting complex. The highest-level interaction energies computed by us, which will be used as benchmarks for all approximate methods, are the composite MP2/(aQZ,aSZ)+ΔCCSD(T)/aTZ values, with ΔCCSD(T) denoting the difference between the CCSD(T) and MP2 interaction energies computed in a given basis set. The accuracy of various approximate approaches is quantified by their mean unsigned errors (MUE), which are averages of the absolute deviations of calculated values from reference values according to the formula[31]

$$\text{MUE} = \frac{\sum_{i=1}^{n} |E^{i}_{\text{method}} - E^{i}_{\text{benchmark}}|}{n} \tag{2}$$

where n is the size of the data set. The approximate approaches tested in this work include a number of density functionals combined with the atom-pairwise dispersion corrections in the -D3,[32] -D3(BJ),[33] -D3M, and -D3M(BJ)[34] variants. We have also investigated approximate wave function and hybrid approaches: MP2, spin-component-scaled MP2 (SCS-MP2),[35] SAPT(DFT),[36,37] MP2C,[38] and direct RPA (dRPA).[39] The SAPT(DFT) interaction energies and the dispersion part of the MP2C values were obtained using the PBE0 functional[40,41] asymptotically corrected with the gradient-regulated scheme.[42] The dRPA calculations used PBE orbitals.[43]

Symmetry-adapted perturbation theory (SAPT)[14] offers a systematic way to calculate intermolecular interaction energies in a physically meaningful manner as a sum of electrostatic, induction, and dispersion interaction contributions along with their exchange counterparts, providing an attractive alternative to the supermolecular methods. In SAPT, the interaction energy is computed directly in terms of physically meaningful corrections in the perturbative series. Specifically, the SAPT interaction energy is represented as

$$E^{\text{SAPT}}_{\text{int}} = E^{(1)}_{\text{elst}} + E^{(1)}_{\text{exch}} + E^{(2)}_{\text{ind,resp}} + E^{(2)}_{\text{disp}} + E^{(2)}_{\text{exch-ind,resp}} + E^{(2)}_{\text{exch-disp}} + \delta E_{\text{HF}} \tag{3}$$

where the numbers in parentheses represent the order of the intermolecular interaction operator. The first four components of the r.h.s of the equation above are electrostatic, exchange, induction, and dispersion energies, respectively, and the additional subscript "resp" denotes the inclusion of monomer relaxation (response) effects. The last term δE_{HF} is the Hartree−Fock (HF) correction for higher than second-order

DOI: 10.1021/acs.jpca.9b06028
J. Phys. Chem. A 2019, 123, 8607−8618

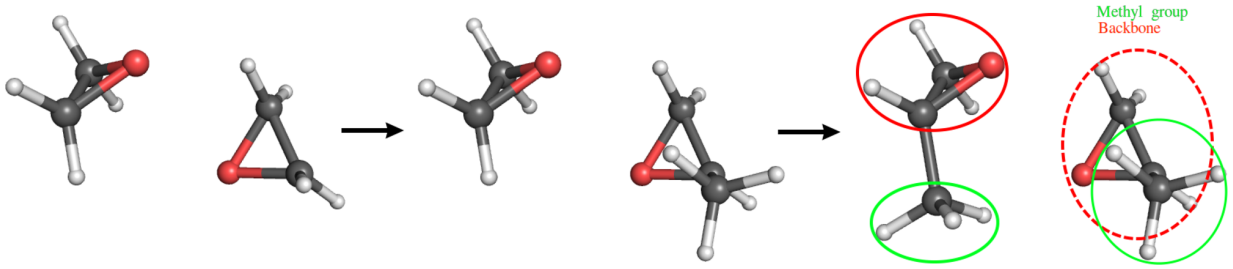

Figure 2. Fragmentation scheme applied for all 12 PO dimer structures in the F-SAPT analyses.

induction and exchange-induction contributions.[14] This correction can be calculated as

$$\delta E_{\mathrm{HF}} = E_{\mathrm{int}}^{\mathrm{HF}} - E_{\mathrm{elst}}^{(10)} - E_{\mathrm{exch}}^{(10)} - E_{\mathrm{ind,resp}}^{(20)} - E_{\mathrm{exch-ind,resp}}^{(20)} \tag{4}$$

where the second "0" superscript indicates that the intramolecular correlation effects have been neglected as implied at the SAPT0 level of theory.[24]

While SAPT provides a highly useful decomposition of the total interaction energy into contributions arising from different physical features of the interaction, functional group SAPT (F-SAPT)[18] adds another layer of information on top of SAPT. As each molecule is partitioned into groups of atoms, each SAPT correction splits into contributions arising from a particular functional group of molecule A interacting with a particular functional group of molecule B. Thus, we can identify the regions of A and B that are primarily responsible for a given type of interaction. The validity and usefulness of the F-SAPT decomposition depends on the way in which the monomers are partitioned: in particular, we found out that a splitting of the epoxide ring leads to unphysical behavior of individual F-SAPT terms. Therefore, we adopted a different partitioning, depicted in Figure 2, where the epoxide ring is intact: only the methyl group is distinguished as separate from the rest of the molecule (note that if the $-$H and $-$CH$_3$ substituents at the stereogenic center switch places, the *R* enantiomer is transformed to the *S* one and vice versa). Moreover, the partitioning of chirodiastaltic energy, which is a difference (*RR*−*RS*) of differences (supermolecular interaction energies), requires special care. In particular, substituent effects on F-SAPT components, or trends exhibited by these components across a class of similar systems, might be more meaningful than individual F-SAPT values. Therefore, we investigate the physical origins of chirodiastaltic energy via a difference F-SAPT analysis,[25] focusing on the substituent effects associated with the methyl group. In our difference analysis, the complete SAPT component of the PO−PO interaction energy in a given *RRx*/*RSx* structure is partitioned as

$$E_{\mathrm{SAPT}}^{\mathrm{PO-PO}} = E_{\mathrm{SAPT}}^{\mathrm{EO-EO}} + \Delta_{\mathrm{SAPT}}(\mathrm{EO-PO}) + \Delta_{\mathrm{SAPT}}(\mathrm{PO-PO}) \tag{5}$$

where $\Delta_{\mathrm{SAPT}}(\mathrm{EO-PO}) = E_{\mathrm{SAPT}}^{\mathrm{EO-PO}} - E_{\mathrm{SAPT}}^{\mathrm{EO-EO}}$ and $\Delta_{\mathrm{SAPT}}(\mathrm{PO-PO}) = E_{\mathrm{SAPT}}^{\mathrm{PO-PO}} - E_{\mathrm{SAPT}}^{\mathrm{EO-PO}}$ for any SAPT term. Furthermore, F-SAPT is employed to further partition the Δ_{SAPT} terms into the direct energetic effect of the H → CH$_3$ change (the difference between the interaction of a methyl group with the entire other molecule and the interaction of its replacement, a hydrogen atom, with the entire other molecule) and the indirect or electronic reorganization effect (the change brought by the part of the molecule whose geometry does not change upon the H → CH$_3$ substitution but the electron density does). The resulting F-SAPT difference analyses presented in section III were performed at the SAPT0/aTZ level. All of the SAPT and F-SAPT computations were performed using the Psi4 code.[44]

Harmonic vibrational frequency shifts were computed numerically using the MOLPRO code[26] and the MP2/aQZ level of theory. In the propylene oxide dimer, each monomer has 24 normal modes of vibration. Out of the 54 vibrational modes of the dimer, six correspond to low-frequency intermolecular motions and will not be analyzed further. The remaining 48 modes come in pairs resulting from the splitting of each doubly degenerate mode of two isolated PO molecules as the result of the intermolecular interaction. We will examine these intramolecular vibrational frequency shifts for the *RR*1−*RR*6 and *RS*1−*RS*6 structures, paying specific attention to the magnitudes of *shifts* (the differences between the complex and an isolated PO monomer), *splittings* (between the two frequencies arising from the same molecular mode) and *chiral discrimination effects* (the differences between shifts observed for the *RRx* and *RSx* complexes).

III. RESULTS AND DISCUSSION

The benchmark interaction energies for the *RR*1−*RR*6 and *RS*1−*RS*6 structures of the propylene oxide dimer are presented in Table 1. These energies are obtained at the MP2/(aQZ, a5Z)+ΔCCSD(T)/aTZ level of theory including the counterpoise correction. Here, ΔCCSD(T) refers to the coupled-cluster correction energy and is equal to

$$\Delta E_{\mathrm{int}}^{\mathrm{CCSD(T)}} = E_{\mathrm{int}}^{\mathrm{CCSD(T)}} - E_{\mathrm{int}}^{\mathrm{MP2}} \tag{6}$$

Table 1. Benchmark Interaction Energies (in kcal/mol) of the Propylene Oxide Dimer

system	MP2/(aQZ,a5Z)	ΔCCSD(T)	benchmark	ΔE_{chir} [a]
*RR*1	−5.185	0.094	−5.091	−0.133
*RR*2	−5.081	0.163	−4.918	−0.027
*RR*3	−4.881	0.247	−4.634	−0.049
*RR*4	−5.020	0.042	−4.978	0.048
*RR*5	−4.842	0.112	−4.730	−0.002
*RR*6	−4.940	−0.006	−4.946	−0.002
*RS*1	−5.050	0.092	−4.958	
*RS*2	−5.042	0.151	−4.891	
*RS*3	−4.789	0.203	−4.585	
*RS*4	−5.075	0.049	−5.026	
*RS*5	−4.828	0.100	−4.728	
*RS*6	−4.936	−0.008	−4.944	

[a]Defined as $\Delta E_{\mathrm{chir}} = E_{RRx}^{\mathrm{int}} - E_{RSx}^{\mathrm{int}}$

DOI: 10.1021/acs.jpca.9b06028
J. Phys. Chem. A 2019, 123, 8607−8618

Compared to ref 8, all 12 structures were reoptimized to minimize the counterpoise-corrected MP2/(aTZ,aQZ) energy. However, this reoptimization changed surprisingly little: the MP2/(aTZ,aQZ) interaction energies were altered by 0.002−0.030 kcal/mol compared to the ref 8 geometries optimized at the MP2/6-311++G(d,p) level, and the structures look virtually indistinguishable. The monomer deformation contributions to interaction energy amount to only 0.09−0.15 kcal/mol (at the benchmark MP2/(aQZ, aSZ)+ΔCCSD(T)/aTZ level). Thus, these contributions are very small compared to the total interaction energies but large in relation to the chirodiastaltic energies. However, the monomer deformation effects vary very little (by no more than 0.018 kcal/mol) between the *RRx* and *RSx* structures and thus were neglected in Table 1 and in all subsequent results.

According to the values in Table 1, the largest negative chirodiastaltic energy belongs to the *RR*1 and *RS*1 pair where the *RR* conformer is favored over the *RS*. On the other hand, the *RR*4 and *RS*4 pair has the largest positive chirodiastaltic energy which says that the heterochiral diastereomer is preferred over the homochiral one. The chirodiastaltic energy for the *RR*5/*RS*5 and *RR*6/*RS*6 pairs is essentially zero and we cannot give a definite answer about the sign of ΔE_{chir} even with such high-level calculations. The experimental study of ref 8 was able to assign rotational transitions to each complex in the *RR*2/*RS*2, *RR*4/*RS*4, and *RR*5/*RS*5 diastereomeric pairs (the other three pairs feature a nondipolar complex that cannot be observed by microwave spectroscopy) and, comparing the observed line intensities scaled by the respective dipole moments, concluded that ΔE_{chir} is negative for the *RR*2/*RS*2 pair, near zero for *RR*4/*RS*4, and positive for *RR*5/*RS*5. Our *ab initio* calculations are consistent with the experimental observation for the *RR*2/*RS*2 pair but not for the other two: interestingly, the MP2 calculations of ref 8 exhibited the same inconsistency with the experimental energy ordering. Our estimates of the differences in the monomer deformation and zero-point energies suggest that neither effect changes the computed ΔE_{chir} values appreciably. We can only speculate that a possible reason for the discrepancy with the experimental intensity pattern is that the relative abundances of different conformations in the experiment may come from the room-temperature distribution that is frozen in the molecular beam probed by the spectrometer.

In addition to interaction energies, we have computed the magnitudes of the electric dipole moment for each of the 12 configurations, using MP2 in bases up to aTZ as well as CCSD(T)/aDZ. The MP2 calculations used MOLPRO[26] while the CCSD(T) ones employed the CFOUR code.[45] The resulting dipole moments are presented in Table 2 and compared with the values computed at the MP2/6-311++G(d,p) level in ref 8. As expected, the nearly centrosymmetric *RS*1, *RS*3, and *RS*6 configurations have no dipole moment, and the very small value for the *RR*1 structure has precluded its identification in the microwave spectra of ref 8. While the results in Table 2 indicate a remarkable consistency between the aDZ and aTZ basis sets, and between MP2 and CCSD(T), the small-basis MP2 calculations[8] somewhat overestimate the dipole moments of nearly all complexes. The values obtained for the PO dimers are much smaller than the dipole moment of an isolated PO molecule, which amounts to 2.0 debye at the CCSD(T)/aDZ level, indicating an alignment of molecular dipoles that is close to antiparallel.

Table 2. Electric Dipole Moments (D) of the 12 Structures of the Propylene Oxide Dimer, Computed in This Work Using the MP2 and CCSD(T) Levels of Theory and the aDZ and aTZ Basis Sets[a]

	ref 8	this work		
complex	MP2/6-311++G(d,p)	MP2/aDZ	MP2/aTZ	CCSD(T)/aDZ
*RR*1	0.04	0.070	0.078	0.057
*RS*1	0.01	0.005	0.005	0.005
*RR*2	0.75	0.694	0.701	0.690
*RS*2	0.72	0.624	0.632	0.623
*RR*3	0.59	0.384	0.377	0.398
*RS*3	0.00	0.001	0.001	0.001
*RR*4	0.32	0.208	0.204	0.218
*RS*4	0.37	0.305	0.306	0.303
*RR*5	0.91	0.775	0.779	0.779
*RS*5	1.02	0.850	0.853	0.856
*RR*6	0.43	0.356	0.360	0.352
*RS*6	0.00	0.000	0.000	0.000

[a]The dipole moments obtained in ref 8 at the MP2/6-311++G(d,p) level are given for comparison.

In the discussion that follows, we will use three quantities to quantify the performance of approximate electronic structure theories relative to our benchmark values: the mean unsigned error (MUE) for the 12 interaction energies at the minima, MUE for the 6 chirodiastaltic energies (*RRx*−*RSx*), and the number $0 \le N_{correct} \le 6$ of chirodiastaltic energies predicted with the correct sign. For the latter number, we reward an approximate method for predicting negative signs for the first three chirodiastaltic energies, a positive sign for the fourth one, and a value close to zero (specifically, $|\Delta E_{chir}| < 0.01$ kcal/mol) for the *RR*5/*RS*5 and *RR*6/*RS*6 pairs. As the first step, we use these three quantities to examine the performance of the MP2 and CCSD(T) approaches in different basis sets below the benchmark level. The pertinent values are presented in Table 3.

Table 4 presents the MUE and $N_{correct}$ values, in the aTZ basis set, for several alternative approaches that exhibit similar computational scaling as MP2: spin-component-scaled MP2 (SCS-MP2),[35] SAPT(DFT),[36,37] MP2C,[38] and direct RPA.[39] The results in Table 4 show that the MP2C and SAPT(DFT) methods employing the PBE0 functional perform better on these complexes than the SCS-MP2 and dRPA methods.

Table 4 also lists the MUE and $N_{correct}$ values obtained by various dispersion-corrected DFT variants in the aTZ basis set. As can be seen from this table, B3LYP-D3 and -D3M functionals perform well for these complexes and they have the smallest values of MUE of interaction energies among the other methods in the table. However, a few other variants exhibit a more complete error cancellation between the *RRx* and *RSx* structures, leading to a slightly lower MUE of the chirodiastaltic energy. It is interesting to note that while all wave function and hybrid wave function/DFT approaches in Table 4 predict all six signs of chirodiastaltic energies correctly, none of the DFT variants are able to accomplish the same thing.

Before we present the SAPT decomposition of the interaction and chirodiastaltic energies, it is instructive to examine the performance of total wave function-based SAPT interaction energies, computed at different levels of theory and with different basis sets, in the same way as we have just done for DFT. Table 5 lists the pertinent values of MUE and $N_{correct}$.

DOI: 10.1021/acs.jpca.9b06028
J. Phys. Chem. A 2019, 123, 8607−8618

Table 3. Mean Unsigned Error (kcal/mol) of the Interaction Energy for the 12 Structures of Propylene Oxide Complexes at Different Basis Sets

	MUE for 12 interaction energy values			MUE for 6 chirodiastaltic energies			$N_{correct}$		
method	aDZ	aTZ	CBS	aDZ	aTZ	CBS	aDZ	aTZ	CBS
MP2	0.663	0.180	0.106	0.011	0.012	0.013	5	5	6
CCSD(T)	0.828	0.283		0.016	0.005		6	6	

Table 4. Mean Unsigned Error of the Interaction Energy for the 12 Structures of Propylene Oxide Complexes in the aTZ Basis Set Using Various MP2-Based and DFT-Based Methods[a]

method	MUE for 12 interaction energy values	MUE for 6 chiro-diastaltic energies	$N_{correct}$
SCS-MP2	1.307	0.019	6
SAPT(DFT)	0.970	0.007	6
MP2C	0.501	0.009	6
dRPA	1.092	0.027	6
B3LYP-D3(BJ)	0.681	0.019	3
B3LYP-D3M(BJ)	0.583	0.017	4
B3LYP-D3	0.131	0.021	4
B3LYP-D3M	0.122	0.028	4
BLYP-D3(BJ)	1.164	0.024	4
BLYP-D3M(BJ)	0.854	0.026	4
BLYP-D3	0.168	0.033	3
BLYP-D3M	0.385	0.037	4
PBE-D3(BJ)	0.996	0.028	4
PBE-D3M(BJ)	1.002	0.026	5
PBE-D3	0.709	0.034	4
PBE-D3M	1.181	0.026	5
PBE0-D3(BJ)	0.786	0.021	4
PBE0-D3M(BJ)	0.734	0.019	4
PBE0-D3	0.394	0.024	5
PBE0-D3M	0.773	0.019	4

[a]All energy values are in kcal mol^{-1}. Error statistics are computed relative to the MP2/(aQZ, a5Z) + ΔCCSD(T)/aTZ benchmark.

As can be observed, the SAPT2+3 level[24] yields smaller errors for these 12 structures than SAPT0.

Table 5. Mean Unsigned Error (kcal/mol) of the Total Interaction Energy of Propylene Oxide Complexes Computed at Different Levels of SAPT with Various Basis Sets

	MUE for 12 interaction energy values		MUE for 6 chiro-diastaltic energies		$N_{correct}$	
method	aDZ	aTZ	aDZ	aTZ	aDZ	aTZ
SAPT0	0.848	1.240	0.019	0.018	5	5
SAPT2+3	0.214	0.355	0.012	0.008	4	3

The interaction energy components computed at the SAPT0/aTZ and SAPT2+3/aTZ levels are displayed in Table 6. The splitting of various SAPT2+3 terms into the electrostatic, exchange, induction, and dispersion categories was performed exactly as defined in ref 24. As can be observed, for all 12 dimer complexes the electrostatic energies are almost as large in magnitude as the total interaction energies. However, the electrostatic energy values are quenched by the first-order exchange energies, which shows that the monomer wave functions for these minimum structures have substantial overlap. Furthermore, the largest attractive contribution to the total interaction energy of the propylene oxide complexes is the dispersion interaction. The largest differences between SAPT0 and SAPT2+3 arise in the exchange energy which is larger by 0.8−1.2 kcal/mol at the SAPT2+3/aTZ level, correcting the overbinding present in the SAPT0 total energies. While the second-order SAPT2+3 contributions are more negative than the SAPT0 ones (by up to 0.14 kcal/mol for the induction energy and 0.14−0.47 kcal/mol for the dispersion energy), the combined second-order differences do not overcome the difference in the first-order exchange repulsion.

SAPT decomposes molecular interactions into meaningful components corresponding to electrostatic, exchange, induction, and dispersion forces. F-SAPT[18] goes further and decomposes interaction energy components for each pair of user-defined functional groups of molecules. Here we apply F-SAPT at the SAPT0 level to quantify the strength of interaction energy and chirodiastaltic energy for the 12 structures of propylene oxide complexes. While one cannot expect F-SAPT (or any other fragmentation theory, for that matter) to give truly meaningful results when the epoxide ring is cut in half, we can examine the contributions to interaction energy brought about by the methyl group. After all, the differences between the noncovalent interactions involving the −H and $-CH_3$ substituents are the only reason for the chiral discrimination in this complex. A propylene oxide dimer which has been partitioned into the functional groups for F-SAPT analysis is shown in Figure 2.

Figure 3 shows the F-SAPT difference analysis of interaction energy via the decomposition defined in eq 5. The methyl groups were successively cut from both PO monomers and replaced with a hydrogen atom, pointing in the same direction as the carbon of the methyl group, but with the distance to the (formerly stereogenic) carbon optimized at the MP2/(aTZ,aQZ) level while keeping the rest of the complex frozen. We arbitrarily picked one of the two orderings in which the methyl groups of both monomers are cut off (both orderings are equivalent for the symmetric structures *RS*1, *RS*3, and *RS*6). The interaction energy component differences are further partitioned into direct (H/CH_3) and indirect (Rest) contributions as described in detail in section II. The data for the *RR*6/*RS*6 pair in Figure 3 shows, as expected, that the two methyl groups, both located far away from the interacting partner (cf. Figure 1), contribute very little to the overall interaction energy. The contributions of the methyl groups to individual SAPT components are also small but somewhat larger than the total interaction energy difference between the propylene oxide dimer and its corresponding ethylene oxide dimer structure, showing some cancellation between the enhanced dispersion energy and enhanced exchange energy in the presence of the $-CH_3$ groups. In the *RR*4, *RS*4, *RR*5, and *RS*5 conformations, one of the methyl groups is far away from the interacting partner. As a result, the addition of one of the methyl groups enhances the total noncovalent interaction much more than the addition of the other one: for the latter,

DOI: 10.1021/acs.jpca.9b06028
J. Phys. Chem. A 2019, 123, 8607−8618

Table 6. Different Components of Interaction Energy, in kcal/mol, Computed with SAPT0 (left) and SAPT2+3 (right) in the aTZ Basis Set[a]

structure	elst	exch	ind	disp	SAPT0	ΔE_{chir}	structure	elst	exch	ind	disp	SAPT2+3	ΔE_{chir}
*RR*1	−5.748	6.878	−1.496	−6.065	−6.431	−0.141	*RR*1	−5.535	8.083	−1.600	−6.469	−5.522	−0.137
*RS*1	−5.618	6.476	−1.405	−5.743	−6.290		*RS*1	−5.397	7.633	−1.504	−6.117	−5.385	
*RR*2	−5.423	6.392	−1.405	−5.777	−6.213	−0.016	*RR*2	−5.166	7.447	−1.487	−6.068	−5.273	−0.009
*RS*2	−5.394	6.352	−1.389	−5.765	−6.197		*RS*2	−5.157	7.427	−1.477	−6.057	−5.264	
*RR*3	−4.592	5.521	−1.150	−5.627	−5.848	−0.107	*RR*3	−4.326	6.350	−1.189	−5.767	−4.932	−0.067
*RS*3	−4.539	5.349	−1.114	−5.438	−5.741		*RS*3	−4.301	6.236	−1.168	−5.632	−4.865	
*RR*4	−5.474	6.266	−1.344	−5.656	−6.208	0.063	*RR*4	−5.268	7.457	−1.460	−6.090	−5.361	0.050
*RS*4	−5.537	6.360	−1.364	−5.730	−6.271		*RS*4	−5.330	7.562	−1.480	−6.163	−5.411	
*RR*5	−4.888	5.506	−1.160	−5.407	−5.950	−0.017	*RR*5	−4.622	6.515	−1.242	−5.698	−5.048	−0.009
*RS*5	−4.918	5.519	−1.173	−5.360	−5.933		*RS*5	−4.651	6.531	−1.257	−5.662	−5.039	
*RR*6	−5.262	5.795	−1.191	−5.461	−6.119	−0.004	*RR*6	−5.060	7.025	−1.330	−5.931	−5.296	−0.004
*RS*6	−5.260	5.788	−1.190	−5.453	−6.115		*RS*6	−5.057	7.018	−1.329	−5.924	−5.292	

[a]The ΔE_{chir} values pertain to the total SAPT energies.

the direct and indirect contributions in the F-SAPT difference analysis are non-negligible but cancel each other. For the six remaining structures (*RR*1−*RS*3), both methyl groups are directly involved in the interaction, and the addition of each one makes the binding stronger by a similar amount. Overall, the propylene oxide complexes are more stable than their ethylene oxide counterparts, which is a net effect of the increases in the attractive electrostatic and dispersion interactions and the increase in the repulsive exchange interaction when going from −H to $-CH_3$. The induction energy is less important for these systems, but it also becomes slightly more attractive when going from ethylene oxide to propylene oxide. More specifically, the addition of the two methyl groups increases the stability of the *RR*1, *RS*1, *RR*2, *RS*2, *RR*3, and *RS*3 conformations by about 2 kcal/mol each, and the stability of *RR*4, *RS*4, *RR*5, and *RS*5 by about 1 kcal/mol each, in direct correlation to the number of methyl groups that are located close to the other molecule and participate in the network of secondary hydrogen bonds.

The comparison of direct and indirect effects of the $-H/-CH_3$ substitution obtained from the F-SAPT difference analysis (Figure 3) is quite interesting. First of all, nearly the entire dispersion difference is a direct effect. This observation is a manifestation of the nearly atom-pairwise additive character of dispersion, which holds for ordinary closed-shell molecules such as propylene oxide but breaks down for zero- or small-gap systems such as metals or extended polycyclic aromatic hydrocarbons.[46,47] One should note that within a DFT+D method with a strictly pairwise additive dispersion such as DFT-D2,[48] the dispersion difference is 100% direct by construction, and even in DFT-D3[32] the only indirect contributions to dispersion are due to (likely small) changes of the chemical environment of the ethylene oxide backbone atoms upon the $-H/-CH_3$ substitution. Thus, our F-SAPT results confirm the validity of the pairwise-additive approach to dispersion for complexes of this type. The differences in the first-order exchange energy are similarly dominated by the direct effect of the $-H/-CH_3$ replacement, indicating that the overlap of the ethylene oxide backbone densities is only weakly affected by the presence or absence of the methyl group. The only F-SAPT contribution where the indirect effects are occasionally significant (although still smaller than the direct ones) is the electrostatic energy. Here, the effect likely stems from the small difference in the C−H and $C-CH_3$ bond polarity that slightly alters the partial charge on the ethylene oxide backbone.

The F-SAPT difference breakdown of chirodiastaltic energies is quite difficult as the diastereomeric differences are small in the first place. Quite interestingly, there is no correlation between the overall PO−PO chiral interaction energy difference and the corresponding difference between the two EO−EO backbone interactions in the configurations present in the *RRn* and *RSn* structures—note that the addition of the methyl groups flips the energetic order of the *RR*1/*RS*1 and *RR*3/*RS*3 pairs. As far as different conformations are concerned, the chirodiastaltic energy for the *RR*5/*RS*5 and *RR*6/*RS*6 ones is too tiny to be amenable to any analysis, and the interpretation of the next smallest *RR*2/*RS*2 difference is also problematic. For the remaining three pairs, the magnitude of the chirodiastaltic energy is 0.048 kcal/mol or more and Figure 3 can be used to shed some light on its origin. For these three pairs, the largest contributions to the chirodiastaltic energy arise from dispersion and first-order exchange. However, these two contributions cancel each other to a large extent. Overall, the energetic ordering of the *RRn* and *RSn* diastereomers is consistent with the ordering of the electrostatic and dispersion contributions and opposite to the ordering followed by first-order exchange. This observation is consistent with the preferred diastereomer adopting a slightly shorter intermolecular separation which enhances the attractive electrostatic and dispersion contributions at the expense of increased exchange repulsion.

Vibrational spectroscopy is one of the valuable tools for the elucidation of structural characteristics of molecules. *Ab initio* molecular electronic structure theory can predict the harmonic vibrational shifts of different frequencies due to the van der Waals interaction. The emphasis in this part is on frequency shifts in the dimer relative to the isolated monomer. The harmonic frequency shifts for all 12 structures and all 24 PO normal modes, computed at the MP2/aQZ level of theory, are presented in Figures 4 and 5. These figures show how the frequencies in an isolated PO molecule are shifted and split into two frequencies in the *RRx* and *RSx* dimers. A pair of similar frequencies shown in blue and green in Figures 4 and 5 corresponds to the symmetric and antisymmetric combinations of the monomer vibrations for structures possessing a center of symmetry (*RS*1, *RS*3, and *RS*6): otherwise, it corresponds to some more general linear combination of the same monomer modes. The 24 subfigures in Figures 4 and 5 are arranged in an

DOI: 10.1021/acs.jpca.9b06028
J. Phys. Chem. A 2019, 123, 8607−8618

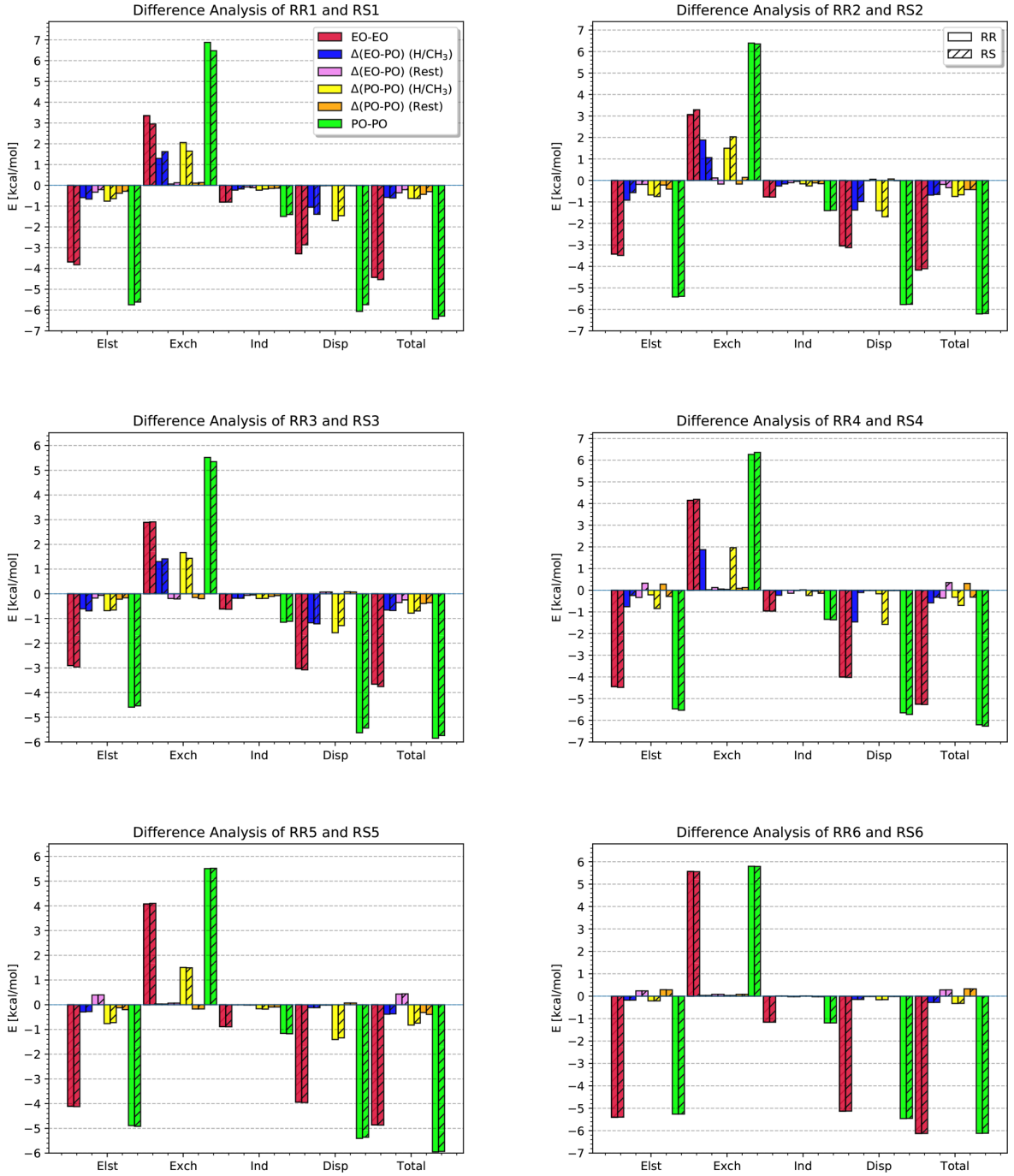

Figure 3. Energetic components of the interaction energy between each of the fragments predicted by F−SAPT difference analysis at the SAPT0/aTZ level of theory.

increasing order in frequency values. Thus, the first subfigure corresponds to the lowest frequency ν_1 which is a torsional mode (219.15 cm^{-1}), and the last subfigure represents the largest frequency ν_{24} = 3246.73 cm^{-1}, which is one of the C−H stretching modes. Note that when some monomer vibrational frequencies are very close together, it is not always trivial to assign the dimer modes to a particular parent monomer mode to properly define the shift. In the analysis below, the dimer and monomer frequencies are paired up solely on the basis of their ordering, which might occasionally switch the reference values for some shifts between different closely lying monomer frequencies.

We will focus first on the largest shifts in frequencies. As Figures 4 and 5 show, the only shifts of over 10 cm^{-1} in either direction occur for the lowest frequency ν_1 = 219.15 cm^{-1} (up to 29.5 cm^{-1} for *RR*1), ν_{18} = 1538.26 cm^{-1} (up to −15.5 cm^{-1} for *RS*6), and ν_{22} = 3163.52 cm^{-1} (up to 11.8 cm^{-1} for *RS*2). Also, in most cases, the two shifts point the same way. The frequency for the ν_1 torsional mode (methyl group rotation) is blue-shifted in most PO−PO structures relative to the isolated

DOI: 10.1021/acs.jpca.9b06028
J. Phys. Chem. A 2019, 123, 8607−8618

Figure 4. Vibrational frequency shifts ν_1−ν_{12} for 12 possible PO−PO structures relative to the isolated monomer frequencies. Because of the existence of two identical monomers, there are two frequency shifts pertinent to each monomer in the dimer system.

monomer, the exceptions being the *RR*4/*RS*4, *RR*5/*RS*5, and *RR*6/*RS*6 structures where the torsional mode of the methyl group that is far away from the other monomer is very slightly red-shifted. This blue shift is an expected result since the participation in the secondary hydrogen bonds somewhat hinders the methyl group rotation. The ν_{18} mode, which is dominated by the C−C stretching motion within the epoxide ring, is consistently red-shifted by the intermolecular interaction. This red shift is the strongest for the *RR*6/*RS*6 configurations, which is to be expected as nearly the entire interaction for these structures results from the epoxide backbone (in particular, unlike in *RR*1−5/*RS*1−5, all four C−H···O interactions in *RR*6/*RS*6 involve hydrogen atoms directly connected to the ring carbon atoms forming the bond being stretched). The ν_{22} frequency is one of the six C−H stretching modes in the PO molecule, and interestingly, the largest shifts, observed for the *RR*2/*RS*2, *RR*3/*RS*3, and *RR*5/*RS*5 structures, are always in the blue (positive) direction. The complete absence of large red shifts of the C−H stretching frequencies indicates that the C−H···O interactions present in the propylene oxide dimers have very little in common with regular hydrogen bonds that are not only stronger, but highly directional and markedly lowering the X−H stretching frequency. Indeed, the examination of the PO−PO structures in Figure 1 shows that the C, H, and O atoms defining the aforementioned interactions in the complex are far from collinear, with the relevant C−H···O angles in the 95−151 deg range (mostly about 120 deg).

We will now discuss the splittings that occur between the two dimer frequencies that are related to the same vibrational mode of an isolated PO monomer. The largest splittings within a frequency pair also occur for the ν_1 torsional mode, but this time for the *RR*4 and *RS*4 structures, amounting to 23.6 and 23.2 cm^{-1}, respectively. Such a large splitting is a consequence of the difference between the rotation of an interacting methyl group in one monomer and of a noninteracting methyl group in the other one. Interestingly, the corresponding ν_1 splittings for the *RR*5 and *RS*5 configurations, which also feature one methyl group that strongly interacts with the other PO molecule and one methyl group that does not, are substantially

DOI: 10.1021/acs.jpca.9b06028
J. Phys. Chem. A 2019, 123, 8607−8618

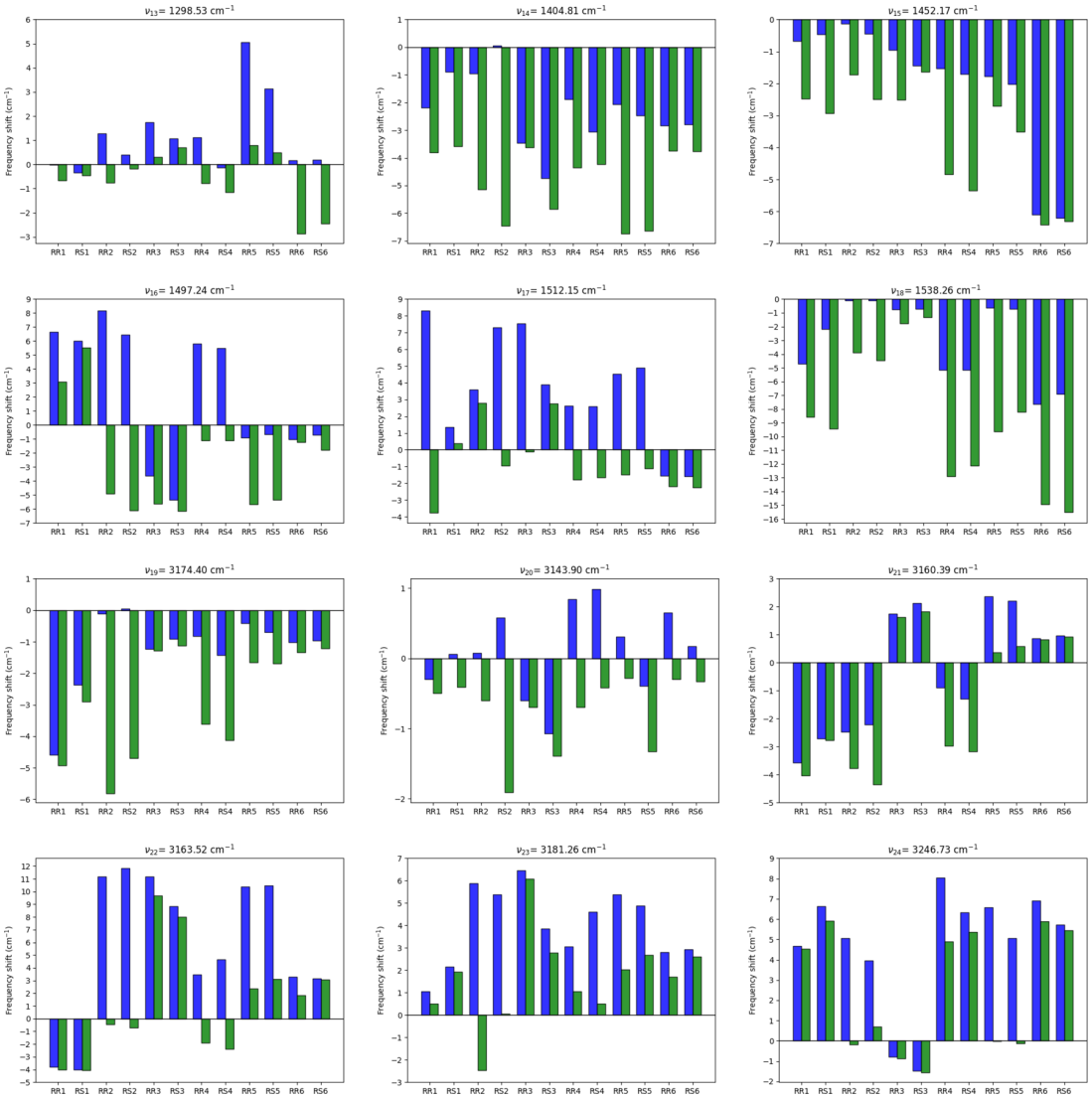

Figure 5. Vibrational frequency shifts ν_{13}–ν_{24} for 12 possible PO–PO structures relative to the isolated monomer frequencies. Because of the existence of two identical monomers, there are two frequency shifts pertinent to each monomer in the dimer system.

smaller at about 8–9 cm^{-1}. Quite a number of relatively large splittings, up to 14.7 cm^{-1} for ν_1, occur also for the *RR*2 and *RS*2 structures, indicating that various modes of both monomers are nonequivalent in these nonsymmetric dimers. The splittings in the *RR*1/*RR*1, *RR*3/*RS*3, and *RR*6/*RS*6 configurations, where the C–H···O contact pattern is symmetric, are generally small — the symmetric and antisymmetric coupling of the nearly equivalent modes is quite weak. The only notable exception is the bending ν_{17} mode with a splitting of 12.1 cm^{-1} for *RR*1 (but only 1.0 cm^{-1} for *RS*1). Finally, let us examine the chiral discrimination effects on harmonic vibrational frequencies, that is, the differences in frequency shifts between the *RRx* and *RSx* structures. Not surprisingly, the largest ΔE_{chir} magnitude within the *RR*1/*RS*1 pair (cf. Table 1) also leads to largest differences in vibrational frequencies, up to 7.0 cm^{-1} for ν_{17} and 6.9 cm^{-1} for ν_1. The chiral effects on frequency shifts in the other *RRn*/*RSn* pairs do not exceed 3.8 cm^{-1} (ν_{17} for *RR*2/*RS*2). The *RR*5/*RS*5 and *RR*6/*RS*6 pairs, where the energetic chiral differences are tiny, exhibit differences in frequency shifts up to 2.6 cm^{-1} (for the ν_2 mode and *RR*6/*RS*6). Such small discrepancies can likely be attributed to the difference in geometric structures.

IV. SUMMARY

We have investigated the subtle chiral recognition effects in the interaction of two propylene oxide molecules. This interaction gives rise to six pairs of diastereomeric structures *RRn*/*RSn* corresponding to six possible patterns of the four secondary O···H–C hydrogen bonds that hold the complex together. The chiral effects lead to interaction energy differences between the homochiral (*RRn*) and heterochiral (*RSn*) complexes ranging in magnitude from zero to 0.13 kcal/mol. These differences have been determined at several levels of theory up to the benchmark MP2/(aQZ,a5Z)+ΔCCSD(T)/aTZ result, using the local minimum structures reoptimized (at the MP2/(aTZ,aQZ) level of theory) from the configurations established in ref 8.

The electronic structure methods that offer better computational scaling than CCSD(T), either wave function- or DFT-

DOI: 10.1021/acs.jpca.9b06028
J. Phys. Chem. A 2019, 123, 8607–8618

based, exhibit mixed accuracy on the PO−PO interaction energies. Some "DFT plus dispersion" variants, most notably B3LYP-D3 and B3LYP-D3M, perform very well, with the average interaction energy errors only slightly exceeding 0.1 kcal/mol. Interestingly, the -D3(BJ) flavor of dispersion correction is quite inferior to the -D3 one: the lowest average error (for the B3LYP-D3M(BJ) variant) amounts to nearly 0.6 kcal/mol. None of the wave function approaches tested that exhibit MP2-like computational scaling exceed the accuracy of the simple MP2/aTZ approach. In absolute terms, the chirodiastaltic energies strongly benefit from error cancellation between the *RRn* and *RSn* structures for all methods considered. However, these energies are so small that most of the approximate approaches have serious difficulties recovering the correct signs of the chiral effects.

Symmetry-adapted perturbation theory leads to a systematic overbinding of all structures of the PO−PO complex. However, the higher SAPT2+3 level of theory overbinds much less than the more approximate SAPT0 one, primarily due to the inclusion of intramolecular correlation effects in the first-order exchange repulsion. Nevertheless, both SAPT levels give a reasonably accurate description of chirodiastaltic energies and can thus be used to shed more light on the physical origins of the chiral recognition. To this end, we further partitioned the SAPT interaction energy contributions by both a difference analysis (singling out the effects of the replacement of a hydrogen atom in ethylene oxide by a methyl group in propylene oxide) and the F-SAPT approach (distinguishing direct and indirect effects of the H → CH_3 substitution). The SAPT analyses show that the primary source of binding in the PO−PO complexes is dispersion, closely followed by electrostatics, and that the direct effects of the −H/−CH_3 F-SAPT energy difference overwhelm the indirect effects resulting from the electronic structure difference between the molecular backbones. Not all diastereomeric energy differences are large enough to be amenable to the F-SAPT analysis, but the largest ones are correlated with the variations in the electrostatic and dispersion contributions.

The interaction in a PO−PO homodimer results in a splitting of each vibrational frequency of an isolated PO molecule into two. We have analyzed the shifts, splittings, and chiral differences of the intramolecular harmonic frequencies computed at the MP2/aQZ level of theory for all 12 structures. The modes most strongly affected by the noncovalent interaction are the lowest-frequency mode arising from the methyl group rotation and several particular C−C and C−H stretching modes. While the magnitudes of frequency shifts relative to the noninteracting monomer extend up to nearly 30 cm^{-1} in some cases, they are mostly quite consistent within an *RRn*/*RSn* pair of structures. The largest diastereomeric differences between vibrational frequencies occur for the *RR*1/*RS*1 pair (which also exhibits the largest magnitude of chirodiastaltic energy) and extend up to 7.0 cm^{-1}.

We have chosen the propylene oxide dimer for this study due to its small size and rigidity which simplify both the benchmark interaction energy calculations and the SAPT energy decompositions. At the same time, the energetic differences between diastereomers are very small for this system which makes their accurate calculation with more approximate methods challenging. Nevertheless, the strategies used in this work to quantify and analyze the chiral effects are applicable to larger systems, where the calculations are more demanding but the required target accuracy is somewhat lower. As the next step, we are envisioning similar SAPT and F-SAPT interaction energy difference analyses for the glycidol dimer, where the chiral effects are stronger but monomer deformation plays a larger role and has to be considered as a separate interaction energy contribution alongside the SAPT decomposition.

■ ASSOCIATED CONTENT

Supporting Information

The Supporting Information is available free of charge on the ACS Publications website at DOI: 10.1021/acs.jpca.9b06028.

Cartesian geometries and vibrational frequencies of all 12 structures investigated in this work (TXT)

■ AUTHOR INFORMATION

Corresponding Author

*(K.P.) E-mail: patkowsk@auburn.edu.

ORCID

Reza Hemmati: 0000-0003-3258-1041

Konrad Patkowski: 0000-0002-4468-207X

Notes

The authors declare no competing financial interest.

■ ACKNOWLEDGMENTS

This work was supported by the U.S. National Science Foundation CAREER Award CHE-1351978.

■ REFERENCES

(1) Caner, H.; Groner, E.; Levy, L.; Agranat, I. Trends in the development of chiral drugs. *Drug Discovery Today* **2004**, *9*, 105−110.

(2) Noyori, R. Asymmetric Catalysis: Science and Opportunities (Nobel Lecture 2001). *Adv. Synth. Catal.* **2003**, *345*, 15−32.

(3) Mohr, J. T.; Krout, M. R.; Stoltz, B. M. Natural products as inspiration for the development of asymmetric catalysis. *Nature* **2008**, *455*, 323−332.

(4) Zhang, M.; Qing, G.; Sun, T. Chiral biointerface materials. *Chem. Soc. Rev.* **2012**, *41*, 1972−1984.

(5) Zehnacker, A.; Suhm, M. A. Chirality Recognition between Neutral Molecules in the Gas Phase. *Angew. Chem., Int. Ed.* **2008**, *47*, 6970−6992.

(6) Kühnle, A.; Linderoth, T. R.; Hammer, B.; Besenbacher, F. Chiral recognition in dimerization of adsorbed cysteine observed by scanning tunnelling microscopy. *Nature* **2002**, *415*, 891−893.

(7) Kraka, E.; Freindorf, M.; Cremer, D. Chiral Discrimination by Vibrational Spectroscopy Utilizing Local Modes. *Chirality* **2013**, *25*, 185−196.

(8) Su, Z.; Borho, N.; Xu, Y. Chiral Self-Recognition: Direct Spectroscopic Detection of the Homochiral and Heterochiral Dimers of Propylene Oxide in the Gas Phase. *J. Am. Chem. Soc.* **2006**, *128*, 17126−17131.

(9) Borho, N.; Suhm, M. A. Glycidol dimer: anatomy of a molecular handshake. *Phys. Chem. Chem. Phys.* **2002**, *4*, 2721−2732.

(10) King, A. K.; Howard, B. J. A microwave study of the heterochiral dimer of butan-2-ol. *Chem. Phys. Lett.* **2001**, *348*, 343−349.

(11) Thomas, J.; Sunahori, F. X.; Borho, N.; Xu, Y. Chirality Recognition in the Glycidol···Propylene Oxide Complex: A Rotational Spectroscopic Study. *Chem. - Eur. J.* **2011**, *17*, 4582−4587.

(12) Portmann, S.; Inauen, A.; Lüthi, H. P.; Leutwyler, S. Chiral discrimination in hydrogen-bonded complexes. *J. Chem. Phys.* **2000**, *113*, 9577−9585.

(13) Riley, K. E.; Pitoňák, M.; Jurečka, P.; Hobza, P. Stabilization and Structure Calculations for Noncovalent Interactions in Extended Molecular Systems Based on Wave Function and Density Functional Theories. *Chem. Rev.* **2010**, *110*, 5023−5063.

DOI: 10.1021/acs.jpca.9b06028
J. Phys. Chem. A 2019, 123, 8607−8618

(14) Jeziorski, B.; Moszyński, R.; Szalewicz, K. Perturbation Theory Approach to Intermolecular Potential Energy Surfaces of van der Waals Complexes. *Chem. Rev.* **1994**, *94*, 1887−1930.
(15) Szalewicz, K.; Patkowski, K.; Jeziorski, B. Intermolecular Interactions via Perturbation Theory: from Diatoms to Biomolecules. *Struct. Bonding (Berlin)* **2005**, *116*, 43−117.
(16) Hohenstein, E. G.; Sherrill, C. D. Wavefunction Methods for Noncovalent Interactions. *WIREs Comput. Mol. Sci.* **2012**, *2*, 304−326.
(17) Parrish, R. M.; Sherrill, C. D. Spatial assignment of symmetry adapted perturbation theory interaction energy components: The atomic SAPT partition. *J. Chem. Phys.* **2014**, *141*, 044115.
(18) Parrish, R. M.; Parker, T. M.; Sherrill, C. D. Chemical Assignment of Symmetry-Adapted Perturbation Theory Interaction Energy Components: The Functional-Group SAPT Partition. *J. Chem. Theory Comput.* **2014**, *10*, 4417−4431.
(19) Bakr, B. W.; Sherrill, C. D. Analysis of transition state stabilization by non-covalent interactions in the Houk-List model of organocatalyzed intermolecular Aldol additions using functional-group symmetry-adapted perturbation theory. *Phys. Chem. Chem. Phys.* **2016**, *18*, 10297−10308.
(20) Bakr, B. W.; Sherrill, C. D. Analysis of transition state stabilization by non-covalent interactions in organocatalysis: application of atomic and functional-group partitioned symmetry-adapted perturbation theory to the addition of organoboron reagents to fluoroketones. *Phys. Chem. Chem. Phys.* **2018**, *20*, 18241−18251.
(21) Faure, A.; Dagdigian, P. J.; Rist, C.; Dawes, R.; Quintas-Sánchez, E.; Lique, F.; Hochlaf, M. Interaction of Chiral Propylene Oxide (CH_3CHCH_2O) with Helium: Potential Energy Surface and Scattering Calculations. *ACS Earth Space Chem.* **2019**, *3*, 964−972.
(22) McGuire, B. A.; Carroll, P. B.; Loomis, R. A.; Finneran, I. A.; Jewell, P. R.; Remijan, A. J.; Blake, G. A. Discovery of the interstellar chiral molecule propylene oxide (CH_3CHCH_2O). *Science* **2016**, *352*, 1449−1452.
(23) Grimme, S.; Hansen, A.; Brandenburg, J. G.; Bannwarth, C. Dispersion-Corrected Mean-Field Electronic Structure Methods. *Chem. Rev.* **2016**, *116*, 5105−5154.
(24) Parker, T. M.; Burns, L. A.; Parrish, R. M.; Ryno, A. G.; Sherrill, C. D. Levels of Symmetry Adapted Perturbation Theory (SAPT). I. Efficiency and Performance for Interaction Energies. *J. Chem. Phys.* **2014**, *140*, 094106.
(25) Parrish, R. M.; Sherrill, C. D. Quantum-Mechanical Evaluation of π-π versus Substituent-π Interactions in π Stacking: Direct Evidence for the Wheeler-Houk Picture. *J. Am. Chem. Soc.* **2014**, *136*, 17386−17389.
(26) Werner, H.-J.; Knowles, P. J.; Knizia, G.; Manby, F. R.; Schütz, M. Molpro: a general-purpose quantum chemistry program package. *WIREs Comput. Mol. Sci.* **2012**, *2*, 242−253.
(27) Dunning, T. H., Jr. Gaussian-Basis Sets for Use in Correlated Molecular Calculations. 1. The Atoms Boron through Neon and Hydrogen. *J. Chem. Phys.* **1989**, *90*, 1007−1023.
(28) Kendall, R. A.; Dunning, T. H., Jr.; Harrison, R. J. Electron Affinities of the 1st-Row Atoms Revisited - Systematic Basis Sets and Wave Functions. *J. Chem. Phys.* **1992**, *96*, 6796−6806.
(29) Halkier, A.; Helgaker, T.; Jørgensen, P.; Klopper, W.; Koch, H.; Olsen, J.; Wilson, A. K. Basis-Set Convergence in Correlated Calculations on Ne, N_2, and H_2O. *Chem. Phys. Lett.* **1998**, *286*, 243−252.
(30) Helgaker, T.; Klopper, W.; Koch, H.; Noga, J. Basis-set convergence of correlated calculations on water. *J. Chem. Phys.* **1997**, *106*, 9639−9646.
(31) Řezáč, J.; Hobza, P. Benchmark Calculations of Interaction Energies in Noncovalent Complexes and Their Applications. *Chem. Rev.* **2016**, *116*, 5038−5071.
(32) Grimme, S.; Antony, J.; Ehrlich, S.; Krieg, H. A Consistent and Accurate Ab Initio Parametrization of Density Functional Dispersion Correction (DFT-D) for the 94 Elements H-Pu. *J. Chem. Phys.* **2010**, *132*, 154104.
(33) Grimme, S.; Ehrlich, S.; Goerigk, L. Effect of the Damping Function in Dispersion Corrected Density Functional Theory. *J. Comput. Chem.* **2011**, *32*, 1456−1465.
(34) Smith, D. G. A.; Burns, L. A.; Patkowski, K.; Sherrill, C. D. Revised Damping Parameters for the D3 Dispersion Correction to Density Functional Theory. *J. Phys. Chem. Lett.* **2016**, *7*, 2197−2203.
(35) Grimme, S. Improved Second-Order Møller-Plesset Perturbation Theory by Separate Scaling of Parallel- and Antiparallel-Spin Pair Correlation Energies. *J. Chem. Phys.* **2003**, *118*, 9095−9102.
(36) Hesselmann, A.; Jansen, G.; Schütz, M. Density-functional theory-symmetry-adapted intermolecular perturbation theory with density fitting: A new efficient method to study intermolecular interaction energies. *J. Chem. Phys.* **2005**, *122*, 014103.
(37) Misquitta, A. J.; Podeszwa, R.; Jeziorski, B.; Szalewicz, K. Intermolecular potentials based on symmetry-adapted perturbation theory including dispersion energies from time-dependent density functional calculations. *J. Chem. Phys.* **2005**, *123*, 214103.
(38) Hesselmann, A. Improved supermolecular second order Møller-Plesset intermolecular interaction energies using time-dependent density functional response theory. *J. Chem. Phys.* **2008**, *128*, 144112.
(39) Furche, F. Molecular tests of the random phase approximation to the exchange-correlation energy functional. *Phys. Rev. B: Condens. Matter Mater. Phys.* **2001**, *64*, 195120.
(40) Adamo, C.; Barone, V. Toward Reliable Density Functional Methods without Adjustable Parameters: The PBE0 Model. *J. Chem. Phys.* **1999**, *110*, 6158−6170.
(41) Ernzerhof, M.; Scuseria, G. E. Assessment of the Perdew-Burke-Ernzerhof Exchange-Correlation Functional. *J. Chem. Phys.* **1999**, *110*, 5029−5036.
(42) Grüning, M.; Gritsenko, O. V.; van Gisbergen, S. J. A.; Baerends, E. J. Shape corrections to exchange-correlation potentials by gradient-regulated seamless connection of model potentials for inner and outer region. *J. Chem. Phys.* **2001**, *114*, 652−660.
(43) Perdew, J. P.; Burke, K.; Ernzerhof, M. Generalized Gradient Approximation Made Simple. *Phys. Rev. Lett.* **1996**, *77*, 3865−3868.
(44) Parrish, R. M.; et al. Psi4 1.1: An Open-Source Electronic Structure Program Emphasizing Automation, Advanced Libraries, and Interoperability. *J. Chem. Theory Comput.* **2017**, *13*, 3185−3197.
(45) Stanton, J. et al. *CFOUR, a quantum chemical program package. containing the integral packages MOLECULE* (J. Almlöf and P.R. Taylor), PROPS (P.R. Taylor), ABACUS (T. Helgaker, H. J. Aa. Jensen, P. Jørgensen, and J. Olsen), and ECP routines by A. V. Mitin and C. van Wüllen. For the current version, see http://www.cfour.de (accessed June 2, 2016).
(46) Misquitta, A. J.; Spencer, J.; Stone, A. J.; Alavi, A. Dispersion Interactions between Semiconducting Wires. *Phys. Rev. B: Condens. Matter Mater. Phys.* **2010**, *82*, 075312.
(47) Gobre, V. V.; Tkatchenko, A. Scaling Laws for Van der Waals Interactions in Nanostructured Materials. *Nat. Commun.* **2013**, *4*, 2341.
(48) Grimme, S. Semiempirical GGA-Type Density Functional Constructed with a Long-Range Dispersion Correction. *J. Comput. Chem.* **2006**, *27*, 1787−1799.

DOI: 10.1021/acs.jpca.9b06028
J. Phys. Chem. A 2019, 123, 8607−8618

Appendix B

Ab Initio Study of Chiral Discrimination in the Glycidol Dimer

THE JOURNAL OF PHYSICAL CHEMISTRY A

pubs.acs.org/JPCA Article

Ab Initio Study of Chiral Discrimination in the Glycidol Dimer

Reza Hemmati and Konrad Patkowski*

Cite This: J. Phys. Chem. A 2020, 124, 9436−9450 Read Online

ACCESS | Metrics & More | Article Recommendations | Supporting Information

ABSTRACT: Chiral discrimination, the ability of a chiral molecule to exhibit different weak intermolecular interactions than its mirror image, is investigated for dimers of oxiranemethanol (glycidol). In this regard, high-level ab initio calculations were performed to study the chiral recognition effects in the homochiral and heterochiral dimers of glycidol. Fourteen dimer structures, seven homochiral and seven heterochiral, were studied: they all feature two intermolecular O−H···O hydrogen bonds. These structures have been determined with the second-order Møller−Plesset perturbation theory (MP2) using the aug-cc-pVTZ basis set and verified to pertain to actual local minima. The benchmark interaction energy values were computed using MP2 extrapolated from the aug-cc-pVQZ and aug-cc-pV5Z bases with a higher-level correction from a coupled-cluster calculation in the aug-cc-pVTZ basis. The global minimum structure is a homochiral one, with the two hydrogen bonds forming a part of a ring with eight heavy atoms. A similar heterochiral structure has a binding energy smaller by about 0.6 kcal/mol. The largest diastereomeric energy difference is about 1.0 kcal/mol. Further insight into the origins of chiral discrimination was provided by symmetry-adapted perturbation theory (SAPT) and a functional-group SAPT (F-SAPT) difference analysis to investigate the direct and indirect effects of two −H/−CH_2OH substitutions leading from an achiral ethylene oxide dimer to the chiral glycidol dimer. Last but not least, harmonic frequency shifts relative to a noninteracting glycidol molecule were calculated and analyzed for all conformations to get insight into the origins of chiral discrimination. It is found that the largest frequency shifts are related to the effect of hydrogen bonding on the O−H stretch mode, the stability of the ring involving both hydrogen bonds, and the transition between two nonequivalent minima of the glycidol molecule.

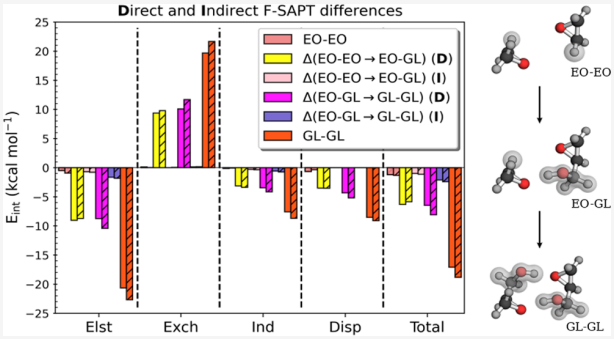

I. INTRODUCTION

Investigating and understanding weak intermolecular interactions involving chiral molecules is of great importance in biology and drug design. The two forms of a chiral molecule have the same chemical and physical properties, but they interact differently with other chiral molecules, which in turn leads to distinctive chiral recognition effects. A key feature to examine is chiral discrimination energy, which is defined as the energy difference between diastereomers. In the specific case of two identical chiral molecules, the chiral discrimination energy differentiates between a homochiral (RR/SS) and its counterpart heterochiral complex (RS/SR). The homochiral nature of the living organisms that almost exclusively use L-amino acids, D-sugars, and L-phospholipids makes molecular chiral discrimination a highly significant research topic in chemistry and biology. Moreover, the energetic and conformational differences between diastereomeric complexes may lead to privileged binding of one enantiomer over the other; this is the cornerstone of enantioselectivity in organic synthesis. The preferential production of one enantiomer is a highly sought after goal of enantioselective synthesis and has ultimately led to the observed homochirality of life through countless cycles of enantioselective processes, even though the source of the initial small enantiomeric excess might have been quite different.[1] A detailed description of the underlying intermolecular interactions of chiral diastereomers, leading to the chiral discrimination effects, is not yet fully established. This paper aims to provide such a first-principles description for a model diastereomeric complex, the glycidol dimer.

In the last few years, the chiral discrimination effects have been investigated,[2−9] theoretically and experimentally, for several representative gas-phase intermolecular complexes. The systems studied include glycidol dimer,[2] butan-2-ol dimer,[10] propylene oxide dimer,[4,8] and the propylene oxide−glycidol[6] complex. Techniques such as Fourier transform microwave (FTMW) spectroscopy have been applied to investigate the conformational and dynamical characteristics of several of these chiral complexes.[4,7] Moreover, some of the important vibrational modes of these complexes were analyzed by infrared spectroscopy.[2]

Received: August 25, 2020
Revised: October 15, 2020
Published: November 4, 2020

https://dx.doi.org/10.1021/acs.jpca.0c07764
J. Phys. Chem. A 2020, 124, 9436−9450

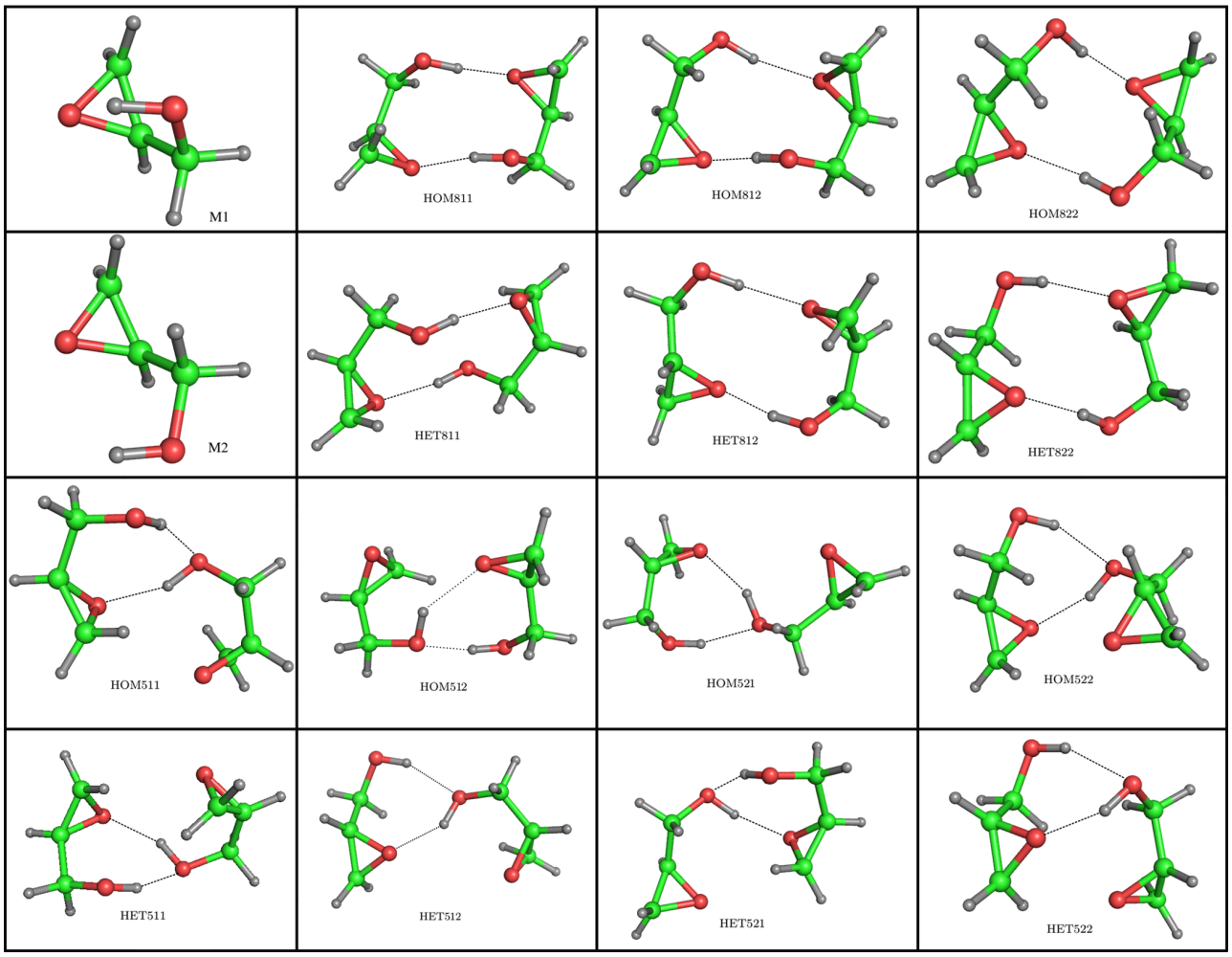

Figure 1. Optimized geometries of seven homochiral (HOM) and seven heterochiral (HET) conformers of the glycidol dimer obtained at the DF-MP2/AVTZ level. The two monomer conformations M1 (global minimum) and M2 are also shown. The structures are grouped in pairs corresponding to the same patterns of hydrogen bonding and monomer conformations.

From a theoretical perspective, the chiral discrimination phenomenon is quite hard to study. First, the supermolecular interaction energies for individual complexes are computed as differences between the energy of the complex and the energies of the noninteracting molecules (monomers)

$$E^{\mathrm{int}} = E_{\mathrm{AB}} - E_{\mathrm{A}} - E_{\mathrm{B}} \tag{1}$$

Then, the chiral discrimination energy (chirodiastaltic energy), measuring the relative stability of the homo- and heterochiral complexes, is a difference of differences[11]

$$\Delta E^{\mathrm{int}}_{\mathrm{chir}} = E^{\mathrm{int}}_{\mathrm{RR}} - E^{\mathrm{int}}_{\mathrm{RS}} \tag{2}$$

Even further, it might be advantageous to discuss the effect of various substituents on chiral discrimination, and one can examine the variation of $\Delta E^{\mathrm{int}}_{\mathrm{chir}}$ between the substituted and unsubstituted monomers, leading to differences of differences of differences. It is well known that computing interaction energies accurately requires not just a size-consistent method to allow for error cancellation between E_{AB} and $E_{\mathrm{A}} + E_{\mathrm{B}}$, but an accurate, high-level account of electron correlation and, at the same time, a large enough basis set to overcome the slow convergence of electron correlation effects such as dispersion. The coupled-cluster approach with single, double, and perturbative triple excitations, CCSD(T), has been the method of choice to generate benchmark high-accuracy interaction energies, and the basis set requirements for calculating values sufficiently converged to the CCSD(T) complete basis set limit (CBS) have been well established.[12,13] It is quite likely that a carefully selected more approximate approach, such as a variant of density functional theory (DFT), might exhibit consistent error cancellation and provide accurate $\Delta E^{\mathrm{int}}_{\mathrm{chir}}$ values for all systems relevant to a particular study, but such behavior should never be taken for granted and a comparison to CCSD(T)-level benchmark values is required for validation.

An additional drawback of the supermolecular method, eqs 1 and 2, is that the resulting numbers, E^{int} and $\Delta E^{\mathrm{int}}_{\mathrm{chir}}$, provide little insight into the origins of the chiral discrimination. Therefore, it is advantageous to supplement supermolecular calculations with ones that provide some form of interaction energy decomposition. Symmetry-adapted perturbation theory (SAPT)[14−16] can provide both accurate total interaction energies and a meaningful energy decomposition. Moreover, a finer-grained partitioning of SAPT corrections is afforded by the functional-group SAPT (F-SAPT) modification,[17] where each SAPT term (electrostatics, induction, dispersion, and exchange) is further split into contributions originating from a specific pair of

https://dx.doi.org/10.1021/acs.jpca.0c07764
J. Phys. Chem. A 2020, 124, 9436−9450

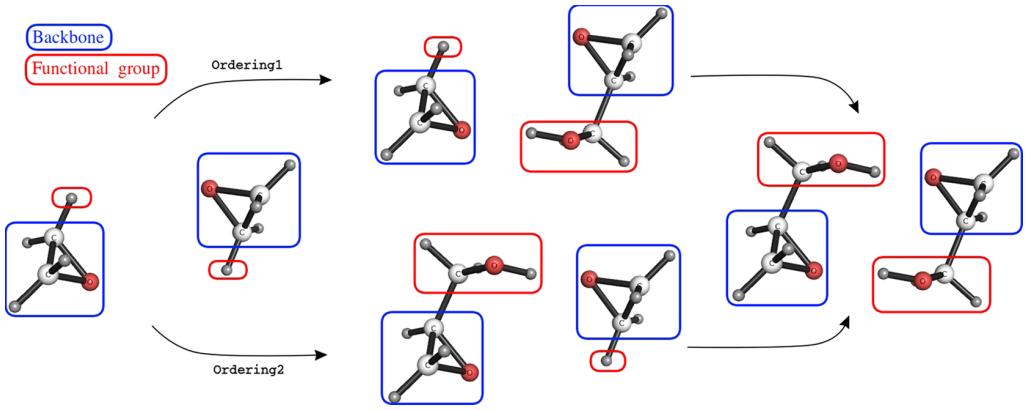

Figure 2. Two different pathways leading to a chiral glycidol dimer structure from an achiral ethylene oxide dimer structure, and the fragmentation pattern in the F-SAPT calculations.

functional groups on the two molecules. F-SAPT has been applied to provide a unique insight into several problems of practical interest, from the origins of substituent effects in $\pi-\pi$ stacking[18] to the stabilization of a specific transition state stereoisomer in some organocatalyzed reactions.[19,20]

Very recently, SAPT and F-SAPT decompositions have been applied to elucidate the origins of chiral discrimination. In our previous study,[8] the interactions between two propylene oxide (PO) molecules led to 12 dimer conformations, which represented six homochiral and six heterochiral local minima. The coupled-cluster, DFT, SAPT, and F-SAPT approaches were utilized to compute the PO−PO intermolecular interaction energies. In contrast with the current study, propylene oxide is a very rigid molecule: the monomer deformation energy was minuscule and could be ignored in all calculations. Some "DFT plus dispersion" variants, especially B3LYP-D3 and B3LYP-D3M,[21] performed very well on this system. The results of other methods such as SAPT showed a systematic overbinding of all dimer structures, but the SAPT2+3 approach[22] overbinds much less than the more approximate SAPT0 level, mainly because of the inclusion of intramolecular correlation effects in the first-order exchange-repulsion term. The analysis of SAPT results showed that the main origin of binding in the PO−PO dimers is dispersion followed by electrostatics. The F-SAPT analyses showed that the direct effects of the $-H/-CH_3$ substitution dominate over the indirect effects resulting from the electron density change in the rest of the molecule. Last but not least, vibrational frequency calculations were performed on the 12 PO−PO structures to investigate the frequency shifts, splittings, and chiral differences. The modes most affected by the noncovalent interactions are the lowest-frequency mode coming from the methyl group rotation and some specific C−H and C−C stretching modes.

Another study[9] from last year, similar to ours in methods but different in molecular systems, gives deep insights into the applicability of F-SAPT and other methods to chiral recognition effects. Korona and co-workers performed a comprehensive study on three chiral drug molecules, ibuprofen, norepinephrine, and baclofen, with two chiral phases of phenethylamine and proline. They concluded that the interaction energy differences between the RR and RS complexes are significant for structures containing phenethylamine but not necessarily for those with proline. Another study of the same group[23] examined the dimerization process of methyl chlorophyllide *a*, and the F-SAPT analysis showed the crucial role of the magnesium ions in the stabilization of the dimer.

As the chiral monomer for the present study, glycidol was chosen for two main reasons. First, it has a polar hydroxyl group that can rotate around the C−O bond, which gives an opportunity to explore the influence of monomer deformation on the chiral discrimination effects. Second, it is a relatively small molecule that can be used as a prototype for bigger molecular systems, and the glycidol dimer can be studied accurately using high-level electronic structure methods. In this work, we aim at a quantitative analysis of the origins of chiral discrimination in the glycidol dimers at the molecular level. To this end, we first determine accurate CCSD(T)-level benchmark interaction energies that can in turn be used to assess the accuracy of more approximate methods such as different flavors of DFT with dispersion. Similar to our earlier PO−PO study,[8] we then reveal the details of the chiral discrimination process using SAPT, F-SAPT, and a differential F-SAPT analysis of the effects of replacing hydrogen atoms by the $-CH_2OH$ groups, going from an achiral ethylene oxide dimer to the chiral glycidol dimer.

Glycidol possesses two functional groups: a rigid oxirane ring and a methanol unit. Therefore, it is able to form both intra- and intermolecular hydrogen bonds. The intramolecular interaction of the hydroxyl group with the oxirane ring has been studied previously by Ōki and Murayama.[24,25] The two lowest energy conformers denoted by M1 and M2 (Figure 1) were identified in the infrared spectroscopic study,[26] and between these two, M1 is the global minimum structure. For the glycidol dimers, some conformers have been studied spectroscopically by Caminati and co-workers,[7] who also identified the remaining local minima (for a total of seven homochiral and seven heterochiral ones) using MP2/6-311++G** calculations.

This article is organized as follows: in Section II, we describe the theoretical background; in Section III, the results and their discussion are given; and the summary follows in Section IV.

II. METHODS AND COMPUTATIONAL DETAILS

We considered 14 dimer structures, initially proposed in ref 7, with two glycidol subunits held together through weak intermolecular interactions. Among these structures, there are seven homochiral dimers labeled "HOM" consisting of two R or two S subunits, and seven heterochiral dimers which are labeled "HET" arising from a complex between an R enantiomer and an S one. These complexes can be additionally divided into two groups, according to Borho and Suhm,[2] as shown in Figure 1. One group

https://dx.doi.org/10.1021/acs.jpca.0c07764
J. Phys. Chem. A 2020, 124, 9436−9450

Table 1. Benchmark DF-MP2/(AVQZ,AV5Z) + ΔCCSD(T)/AVTZ Interaction Energies (in kcal/mol) for the Glycidol Dimer

structure	DF-MP2/CBS	ΔCCSD(T)	benchmark	ΔE_{chir}^{int} [a]
HOM811	−14.499	0.144	−14.355	1.620
HET811	−16.059	0.084	−15.975	
HOM812	−12.702	0.135	−12.567	−1.469
HET812	−11.251	0.153	−11.098	
HOM822	−11.987	0.185	−11.802	−0.181
HET822	−11.813	0.192	−11.621	
HOM511	−10.235	0.187	−10.048	1.474
HET511	−11.663	0.142	−11.522	
HOM512	−10.154	0.174	−9.980	−0.093
HET512	−9.998	0.111	−9.887	
HOM521	−10.374	0.115	−10.259	0.737
HET521	−11.174	0.178	−10.996	
HOM522	−12.404	0.155	−12.249	−0.410
HET522	−11.972	0.132	−11.839	

[a]Defined as $\Delta E_{chir}^{int} = E_{homodimer}^{int} - E_{heterodimer}^{int}$

forms hydrogen bonds that involve a ring of eight heavy atoms and is labeled "8" in addition to either HOM or HET. In the second group, the hydrogen bonds form a ring involving only five heavy atoms, and it is labeled "5". In each eight-membered ring structure, each glycidol monomer serves as a donor for one O−H···O hydrogen bond and as an acceptor for the second hydrogen bond with the involvement of both its oxygen atoms. However, in five-membered ring systems, a single OH group in one of the glycidol monomers acts as a hydrogen bond donor and an acceptor at the same time, as illustrated in Figure 1. The last two-digit coding in the name of a structure denotes the type of monomer conformation, which is shown in the top left of Figure 1. There is a caveat for some five-membered ring structures: to distinguish the minima involving a five-membered ring and one monomer in each conformation, we call them HOM512, HET512, HOM521, and HET521. The ordering of digits indicates that in HOM512, as an example, one functional group of M1 and two functional groups of M2 are involved in the hydrogen bonding, while in HOM521, two functional groups of M1 and one functional group of M2 form hydrogen bonds. The same applies to HET512 and HET521.

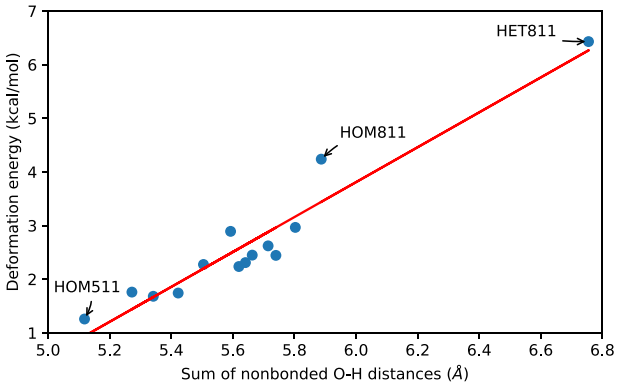

Figure 3. Monomer deformation energies for all 14 glycidol dimer structures versus the sum of the two intramolecular nonbonded OH distances.

Table 3. Mean Unsigned Errors of the Interaction Energy (kcal/mol) for the 14 Structures of Glycidol Dimer for Various Methods and Basis Sets

	MUE for 14 interaction energy values			MUE for 7 chirodiastaltic energies		
method	AVDZ	AVTZ	CBS	AVDZ	AVTZ	CBS
MP2	1.516	0.516	0.149	0.150	0.079	0.040
CCSD(T)	1.810	0.665		0.146	0.057	
SAPT0	1.544	2.321		0.161	0.222	
SAPT2+3	0.939	0.390		0.073	0.082	

All 14 geometries of the glycidol dimer were reoptimized starting from the initial structures taken from ref 7, where they were obtained at the MP2/6-311++G** level. We reoptimized them using the DF-MP2/AVTZ level, where AVTZ≡ aug-cc-pVTZ denotes the augmented correlation consistent triple-zeta Dunning basis.[27,28] While the structures used in all single-point energy calculations were obtained by minimizing the counterpoise-corrected interaction energy including the monomer deformation corrections, for the frequency calculations, one must use a structure that minimizes the total dimer energy rather than the interaction energy. Such a change in the optimization

Table 2. Calculated Monomer Deformation Energies, Binding Energies (D_e), Vibrational Zero-Point Energy Differences (ΔZPE), and Dissociation Energies (D_0) at the DF-MP2/(AVQZ,AV5Z) + ΔCCSD(T)/AVTZ Level (in kcal/mol) of the Glycidol Dimer

structure	E_{int}	$E_{deformation}$	D_e	ΔD_e^{chir} [a]	ΔZPE	D_0
HOM811	−14.355	4.238	10.117	0.571	1.049	9.068
HET811	−15.975	6.429	9.546		1.114	8.432
HOM812	−12.567	2.966	9.601	0.952	1.084	8.517
HET812	−11.098	2.449	8.649		0.881	7.768
HOM822	−11.802	2.310	9.492	0.315	1.253	8.239
HET822	−11.621	2.444	9.177		1.138	8.039
HOM511	−10.048	1.258	8.790	−1.050	1.137	7.653
HET511	−11.522	1.682	9.840		1.305	8.535
HOM512	−9.980	1.760	8.220	0.075	0.958	7.262
HET512	−9.887	1.742	8.145		0.940	7.205
HOM521	−10.259	2.237	8.022	−0.699	1.038	6.984
HET521	−10.996	2.275	8.721		1.201	7.520
HOM522	−12.249	2.622	9.627	0.680	1.334	8.293
HET522	−11.839	2.892	8.947		1.291	7.656

[a]Defined as $\Delta D_e^{chir} = D_{e,homodimer} - D_{e,heterodimer}$

https://dx.doi.org/10.1021/acs.jpca.0c07764
J. Phys. Chem. A 2020, 124, 9436−9450

Table 4. Mean Unsigned Errors (MUE) of the Interaction Energy for 14 Structures of the Glycidol Dimer in the AVTZ Basis Set Using Various DFT Functionals[a]

method	MUE for 14 interaction energy values	MUE for 7 chiro-diastaltic energies
B3LYP-D3(BJ)	0.219	0.105
B3LYP-D3M(BJ)	0.133	0.100
B3LYP-D3	0.117	0.108
B3LYP-D3M	0.373	0.115
BLYP-D3(BJ)	0.806	0.171
BLYP-D3M(BJ)	0.254	0.166
BLYP-D3	0.245	0.108
BLYP-D3M	0.095	0.156
PBE-D3(BJ)	0.416	0.170
PBE-D3M(BJ)	0.450	0.171
PBE-D3	0.222	0.142
PBE-D3M	0.660	0.180
PBE0-D3(BJ)	0.286	0.106
PBE0-D3M(BJ)	0.256	0.104
PBE0-D3	0.112	0.098
PBE0-D3M	0.295	0.111

[a]All energy values are in kcal/mol. Error statistics are computed relative to the DF-MP2/(AVQZ,AV5Z) + ΔCCSD(T)/AVTZ benchmark.

target resulted in insignificant changes to the geometry, and the frequency calculations confirmed that each of the 14 structures is a local minimum.

The counterpoise-corrected supermolecular approach, eq 1, has been applied to the electronic structure methods used in this work, with all three quantities E_{AB}, E_A, and E_B computed in the full dimer basis set. Our benchmark interaction energies are the composite DF-MP2/(AVQZ,AV5Z)+ΔCCSD(T)/AVTZ values, where the ΔCCSD(T) term represents the difference between the CCSD(T) and MP2 interaction energies computed with a desired basis set

$$\Delta E_{\text{int}}^{\text{CCSD(T)}} = E_{\text{int}}^{\text{CCSD(T)}} - E_{\text{int}}^{\text{MP2}} \tag{3}$$

Also, to quantify the accuracy of various approximate methods relative to the benchmark, the mean unsigned errors (MUE) relative to reference values have been computed using the following formula[29]

$$\text{MUE} = \frac{\sum_{i=1}^{n} |E_{\text{method}}^{i} - E_{\text{benchmark}}^{i}|}{n} \tag{4}$$

where n is the size of the data set. The MUE statistics were obtained for a number of approximate methods, mostly based on DFT. The DFT calculations utilized the functionals B3LYP, BLYP, PBE, and PBE0 with the atom-pairwise dispersion corrections in the -D3,[30] -D3(BJ),[31] -D3M, and -D3M(BJ)[21] variants. All calculations in this work have been performed using the Molpro[32] and Psi4[33] programs.

The SAPT approach[14−16] offers a systematic way to calculate intermolecular interaction energies decomposed into physically meaningful components, and we used SAPT to analyze the

Table 5. Interaction Energy Components for All 14 Optimized Glycidol Structures Computed with SAPT0 (Top Panel) and SAPT2+3 (Bottom Panel) in the AVTZ Basis Set, Along with the Resulting Chirodiastaltic Energies[a]

structure	elst.	exch.	ind.	disp.	SAPT0	$\Delta E_{\text{chir}}^{\text{int}}$
HOM811	−20.652	19.683	−7.612	−8.523	−17.104	1.725
HET811	−22.677	21.663	−8.703	−9.111	−18.829	
HOM812	−19.296	19.755	−7.082	−8.450	−15.073	−1.196
HET812	−16.537	16.152	−6.110	−7.382	−13.877	
HOM822	−18.655	20.836	−6.711	−9.471	−14.002	0.044
HET822	−18.090	19.411	−6.437	−8.930	−14.046	
HOM511	−17.543	20.400	−6.194	−8.688	−12.025	1.890
HET511	−20.058	22.614	−6.890	−9.582	−13.915	
HOM512	−15.277	16.209	−5.012	−7.743	−11.824	−0.069
HET512	−16.241	16.933	−5.516	−6.931	−11.755	
HOM521	−18.162	19.766	−6.637	−7.136	−12.168	0.968
HET521	−19.145	22.034	−6.934	−9.091	−13.136	
HOM522	−19.539	20.807	−6.378	−9.704	−14.814	−0.686
HET522	−18.767	20.866	−6.248	−9.978	−14.128	
structure	elst.	exch.	ind.	disp.	SAPT2+3	$\Delta E_{\text{chir}}^{\text{int}}$
HOM811	−19.869	23.280	−8.367	−9.813	−14.769	1.690
HET811	−21.922	25.509	−9.546	−10.499	−16.459	
HOM812	−18.629	23.218	−7.791	−9.753	−12.955	−1.391
HET812	−15.378	18.819	−6.614	−8.391	−11.564	
HOM822	−18.480	24.654	−7.452	−10.938	−12.216	−0.206
HET822	−17.616	22.964	−7.122	−10.235	−12.010	
HOM511	−17.685	24.304	−6.946	−10.053	−10.380	1.575
HET511	−19.872	26.570	−7.643	−11.010	−11.955	
HOM512	−15.088	19.158	−5.550	−8.816	−10.296	−0.209
HET512	−15.893	19.937	−6.103	−8.028	−10.087	
HOM521	−17.998	23.250	−7.359	−8.386	−10.492	0.877
HET521	−19.241	26.151	−7.754	−10.526	−11.369	
HOM522	−19.125	24.476	−7.064	−11.064	−12.778	−0.452
HET522	−18.624	24.696	−6.961	−11.437	−12.326	

[a]All values are in units of kcal/mol.

https://dx.doi.org/10.1021/acs.jpca.0c07764
J. Phys. Chem. A 2020, 124, 9436−9450

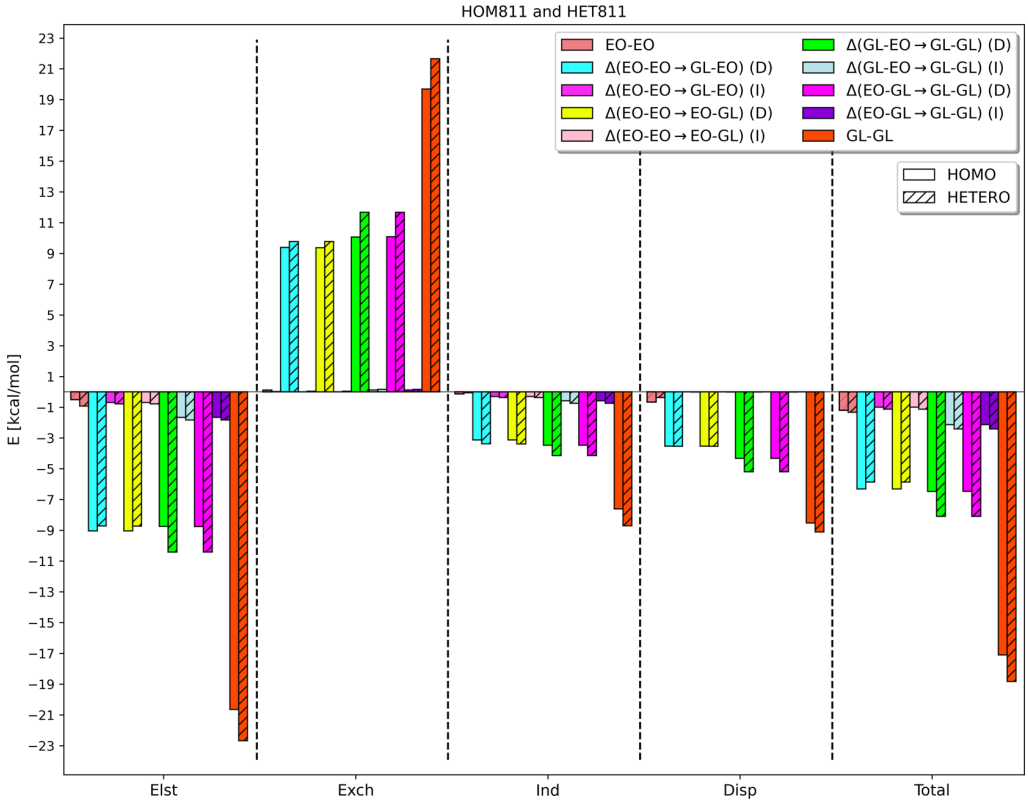

Figure 4. Interaction energy components for the HOM811/HET811 pair of glycidol dimer structures as predicted by the F-SAPT difference analysis at the SAPT0/AVTZ level of theory. The bars marked EO−EO denote the energy components for the ethylene oxide (EO) dimer, which in subsequent steps is expanded into the glycidol dimer by replacing one hydrogen atom at a time by a $-CH_2OH$ functional group, as explained in detail in the text. The effects of this replacement are partitioned into the direct energy difference (denoted "D") between the molecule−CH_2OH and molecule−H interactions and the indirect effect (denoted "I") stemming from an altered interaction with the ethylene oxide backbone.

glycidol−glycidol interactions. In SAPT, the interaction energy is calculated directly as a sum of terms in the perturbative series. In our case, this sum extends through the second order in the intermolecular interaction operator

$$E_{\text{int}}^{\text{SAPT}} = (E_{\text{elst}}^{(1)})_{\text{elst}} + (E_{\text{exch}}^{(1)})_{\text{exch}} + (E_{\text{ind,resp}}^{(2)} + E_{\text{exch-ind,resp}}^{(2)} + \delta E_{\text{HF}})_{\text{ind}} + (E_{\text{disp}}^{(2)} + E_{\text{exch-disp}}^{(2)})_{\text{disp}} \quad (5)$$

where the order of each component is represented by its superscript and the groupings of terms into the four commonly used SAPT contributions are indicated by parentheses. The first two of these contributions are the first-order electrostatic and exchange energy components, respectively, and the next two are the second-order induction and dispersion terms together with their exchange counterparts. The δE_{HF} term in eq 5 represents the remaining higher-order induction components approximated using a supermolecular Hartree−Fock (HF) calculation as

$$\delta E_{\text{HF}} = E_{\text{int}}^{\text{HF}} - E_{\text{elst}}^{(10)} - E_{\text{exch}}^{(10)} - E_{\text{ind,resp}}^{(20)} - E_{\text{exch-ind,resp}}^{(20)} \quad (6)$$

where the second "0" in the superscript indicates that the intramolecular correlation effects have been neglected, as done at the SAPT0 level of theory.[16,22] In this work, we will employ two levels of SAPT: the simplest SAPT0 variant, neglecting intramolecular correlation, and the much more sophisticated SAPT2+3 one, including a large variety of intramolecular correlation effects through second order as well as the leading intermolecular interaction effects through third order.[22] In addition to conventional SAPT, we add another layer of useful information and insight by employing the functional-group-pairwise partitioning denoted as F-SAPT.[17,34] F-SAPT decomposes each SAPT0 interaction energy component into contributions arising from the interaction of a given functional group on monomer A with a particular functional group on monomer B. The F-SAPT analysis is based on the key assumption that the functional groups are chemically separable units connected by only single σ bonds.[17] Accordingly, we separate each glycidol monomer into two units, the $-CH_2OH$ functional group and the $-C_2H_3O$ backbone.

The fragmentation scheme applied for the glycidol dimer is shown in Figure 2. This figure also illustrates another layer of abstraction in the form of the F-SAPT difference analysis.[19,20,34] In the current study, we are interested in the substituent effects on the F-SAPT interaction energy components across a class of similar systems. For this reason, similar to our earlier study,[8] we started with the (achiral) ethylene oxide (EO) dimer and substituted the $-CH_2OH$ functional groups in two consecutive steps, replacing a hydrogen atom in each ethylene oxide monomer to arrive at a glycidol dimer structure. In this manner, a particular SAPT component of the glycidol−glycidol (GL−GL) interaction in a given homo- or heterochiral structure is partitioned as

$$E_{\text{GL-GL}}^{\text{SAPT}} = E_{\text{EO-EO}}^{\text{SAPT}} + \Delta_{\text{SAPT}}(\text{EO} - \text{GL}) + \Delta_{\text{SAPT}}^{1}(\text{GL} - \text{GL}) \quad (7)$$

https://dx.doi.org/10.1021/acs.jpca.0c07764
J. Phys. Chem. A 2020, 124, 9436−9450

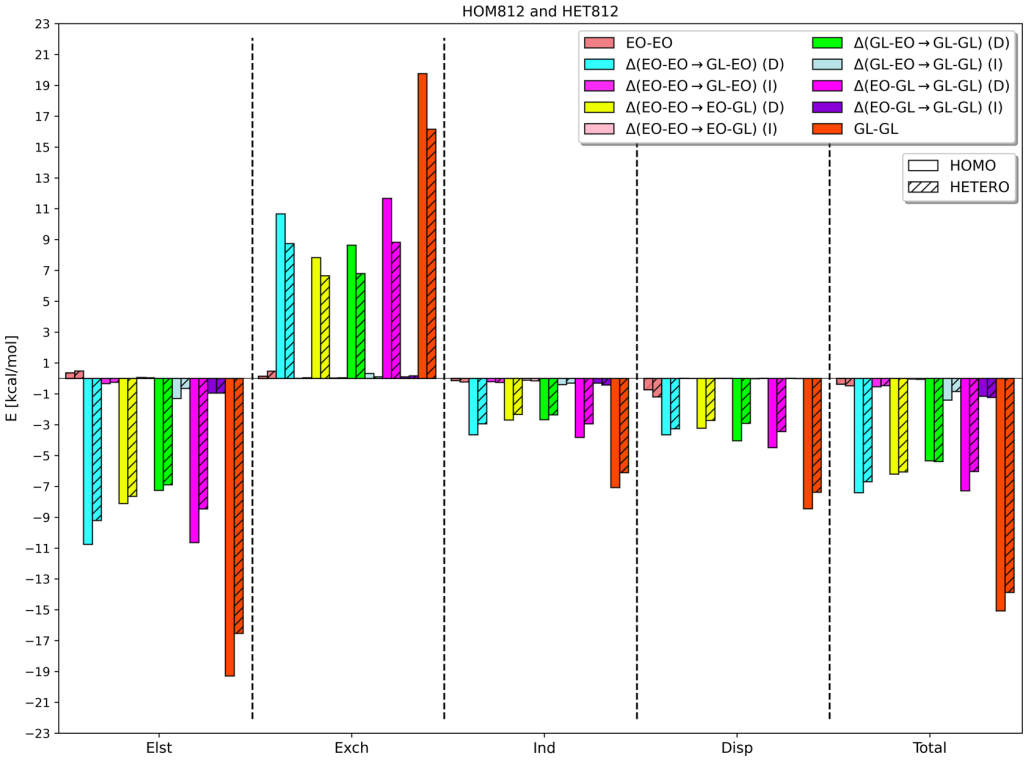

Figure 5. Interaction energy components for the HOM812/HET812 pair of glycidol dimer structures as predicted by the F-SAPT difference analysis at the SAPT0/AVTZ level of theory. The bars marked EO−EO denote the energy components for the ethylene oxide (EO) dimer, which in subsequent steps is expanded into the glycidol dimer by replacing one hydrogen atom at a time by a $-CH_2OH$ functional group, as explained in detail in the text. The effects of this replacement are partitioned into the direct energy difference (denoted "D") between the molecule$-CH_2OH$ and molecule−H interactions and the indirect effect (denoted "I") stemming from an altered interaction with the ethylene oxide backbone.

and

$$E^{\mathrm{SAPT}}_{\mathrm{GL-GL}} = E^{\mathrm{SAPT}}_{\mathrm{EO-EO}} + \Delta_{\mathrm{SAPT}}(\mathrm{GL-EO}) + \Delta^2_{\mathrm{SAPT}}(\mathrm{GL-GL}) \quad (8)$$

depending on which monomer accepts the substituent hydroxymethyl group first. In eqs 7 and 8, $\Delta_{\mathrm{SAPT}}(\mathrm{EO-GL}) = E^{\mathrm{SAPT}}_{\mathrm{EO-GL}} - E^{\mathrm{SAPT}}_{\mathrm{EO-EO}}$, $\Delta^1_{\mathrm{SAPT}}(\mathrm{GL-GL}) = E^{\mathrm{SAPT}}_{\mathrm{GL-GL}} - E^{\mathrm{SAPT}}_{\mathrm{EO-GL}}$, $\Delta_{\mathrm{SAPT}}(\mathrm{GL-EO}) = E^{\mathrm{SAPT}}_{\mathrm{GL-EO}} - E^{\mathrm{SAPT}}_{\mathrm{EO-EO}}$, and $\Delta^2_{\mathrm{SAPT}}(\mathrm{GL-GL}) = E^{\mathrm{SAPT}}_{\mathrm{GL-GL}} - E^{\mathrm{SAPT}}_{\mathrm{GL-EO}}$ for any SAPT term. The ordering of the two glycidol monomers is arbitrary, but it is kept consistent in a pair of homo- and heterochiral structures.

The last quantities that we investigated were the normal modes of the 14 dimer structures, where we examined the frequency shifts to get more insight into the weak intermolecular interactions leading to chiral discrimination. The vibrational modes of all 14 glycidol dimer configurations were computed at the DF-MP2/AVTZ level of theory, and the frequency shifts were calculated with respect to the harmonic vibrational frequencies of an isolated glycidol monomer at its global minimum (M1 in Figure 1). Every dimer structure has 60 normal modes, but six of them are low-frequency intermolecular motions and will not be considered further. The remaining 54 normal modes come in pairs (originating from the same monomer mode) and lead to two distinct frequency shifts pertaining to some combination of these modes in the two interacting monomers.

III. RESULTS AND DISCUSSION

III.I. Benchmark Interaction and Binding Energies. In this section, we describe the results of various wave function and DFT methods and see which ones perform well for our diastereomeric complexes. Table 1 presents the benchmark interaction energies for all 14 glycidol dimer structures. These energies are calculated at the DF-MP2/(AVQZ,AV5Z) + ΔCCSD(T)/AVTZ level of theory including the counterpoise correction.

The chirodiastaltic energies $\Delta E^{\mathrm{int}}_{\mathrm{chir}}$, eq 2, in Table 1 show that the largest positive value belongs to the HOM811 and HET811 pair, where the heterochiral conformer is preferred over the homochiral one as far as the interaction energy is concerned. The largest negative chirodiastaltic energy occurs for the HOM812 and HET812 pair that implies that the homochiral structure is favored over its heterochiral counterpart.

All $\Delta E^{\mathrm{CCSD(T)}}_{\mathrm{int}}$ corrections are in the 0.08−0.2 kcal/mol range, indicating that the DF-MP2/CBS method performs well for these hydrogen-bonded systems. Overall, the interaction energies at the minima range from −9.9 kcal/mol for HET512 to −16.0 kcal/mol for HET811, in an expected range for a system held together by two hydrogen bonds. The HOM811/HET811 pair clearly represents the most favorable configuration of two glycidol molecules, and most structures involving an eight-member hydrogen-bonded ring are slightly more stable than those with a five-membered ring.

In contrast to our previous work[8] on the propylene oxide dimer, the monomer deformation contribution cannot be neglected for the glycidol complex because this molecule is much more flexible than propylene oxide. Not only the hydroxyl group can rotate around the C−O bond, but also the entire hydroxymethyl group can undergo a rotation around the C−C bond, giving more degrees of freedom to the glycidol molecule.

https://dx.doi.org/10.1021/acs.jpca.0c07764
J. Phys. Chem. A 2020, 124, 9436−9450

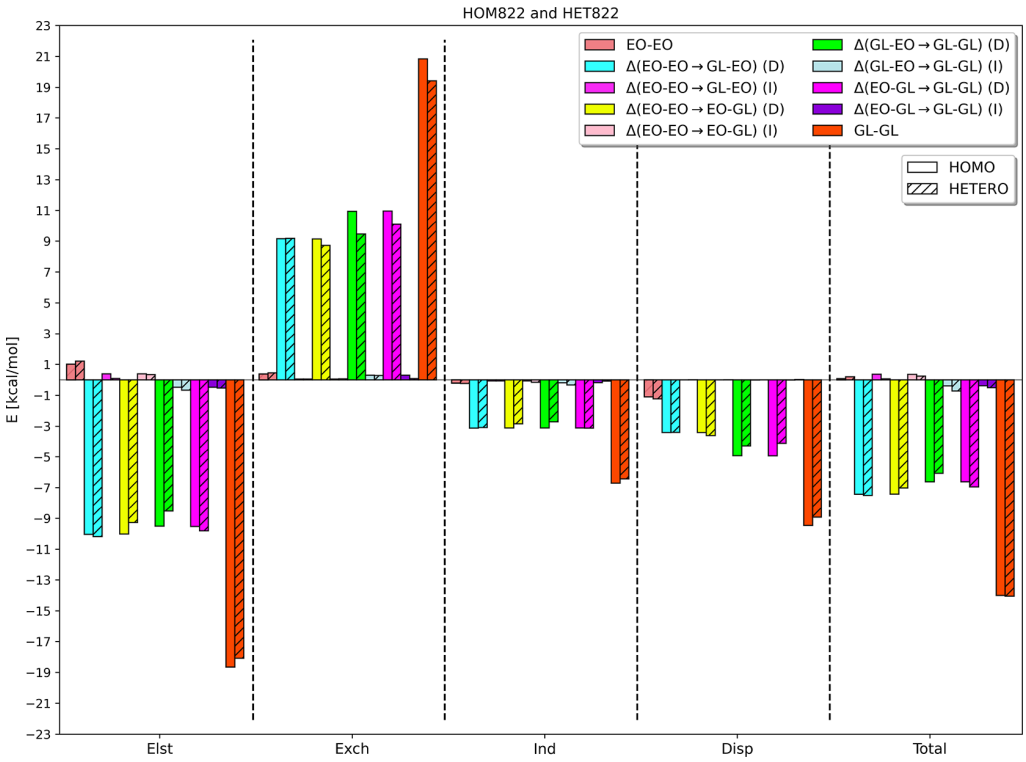

Figure 6. Interaction energy components for the HOM822/HET822 pair of glycidol dimer structures as predicted by the F-SAPT difference analysis at the SAPT0/AVTZ level of theory. The bars marked EO−EO denote the energy components for the ethylene oxide (EO) dimer, which in subsequent steps is expanded into the glycidol dimer by replacing one hydrogen atom at a time by a $-CH_2OH$ functional group, as explained in detail in the text. The effects of this replacement are partitioned into the direct energy difference (denoted "D") between the molecule$-CH_2OH$ and molecule−H interactions and the indirect effect (denoted "I") stemming from an altered interaction with the ethylene oxide backbone.

Moreover, the intermolecular interaction, the driving force for possible deformation, is substantially stronger. The monomer deformation energy[35] is calculated as the difference between the energy of monomers in the dimer geometry and in the optimized monomer geometry[35] and it is always calculated at the same DF-MP2/(AVQZ,AV5Z) + ΔCCSD(T)/AVTZ level as the interaction energy, but with monomer basis sets.

The resulting monomer deformation energies along with the binding energy values

$$D_e = |E^{int} + E^{deformation}| \quad (9)$$

for all 14 glycidol dimer structures are presented in Table 2. As can be seen, the monomer deformation energies are in the 1−3 kcal/mol range for the glycidol dimer structures except for the HOM811 and HET811 complexes. Further investigation revealed that these relatively large deformation effects result from the fact that in an isolated glycidol molecule in the M1 configuration, the hydrogen atom of the hydroxyl group is attracted to the epoxide ring oxygen. Therefore, the OH···O contact, while not a perfect linear intramolecular hydrogen bond, is definitely a favorable interaction. When a glycidol molecule approaches another glycidol molecule, this favorable interaction is reduced to a different extent as the hydroxyl hydrogen atom rotates toward the oxygen atoms of the adjacent glycidol molecule. This conformational change is particularly pronounced for the HET811 structure, as evidenced by Figure 3, which shows that the deformation energy strongly correlates with the sum of the two intramolecular nonbonded O(oxirane)−H(alcohol) distances, showing that the dominant energetic penalty incurred in the dimer is associated with the rotation of the hydroxyl hydrogen atoms away from the intramolecular OH···O contact. In addition, binding energies show that the HOM811 conformation has the most favorable interaction, which is in complete agreement with the previous studies that showed HOM811 as the global minimum.[2,7] Actually, the RR/SS diastereomer is the more stable one in all eight-membered ring structures. Overall, the inclusion of the monomer deformation energy has two interesting effects on the relative stability of different conformations in Table 2. First, HOM811 becomes the global minimum as the HET811 structure, favored on the interaction energy grounds, requires a particularly large distortion of the monomers. Second, the binding energies for all 14 minima are in a narrower range than interaction energies, with no clear preference for the HOM811/HET811 pair (actually, HET511 is slightly more stable than HET811). It is interesting to note that glycidol molecules adjust to their structures in the complex primarily by the hydrogen atom rotation around the C−O bond. The other possible torsional motion, the rotation of the whole hydroxymethyl group around the C−C bond, is less pronounced as all glycidol molecules in the complexes retain either their M1 or M2 conformation, as illustrated in Figure 1.

Table 2 also contains the dissociation energies D_0, obtained from D_e by the addition of the vibrational zero-point energy (ZPE) correction ΔZPE = ZPE(AB) − ZPE(A) − ZPE(B). The ΔZPE values for different structures are in a fairly narrow 0.9−1.3 kcal/mol range, and the ordering of D_0 values for different structures follows the ordering of D_e.

III.II. Performance of Approximate Approaches. In the discussion that follows, we quantify the performance of some approximate electronic structure theories relative to our benchmark

https://dx.doi.org/10.1021/acs.jpca.0c07764
J. Phys. Chem. A 2020, 124, 9436−9450

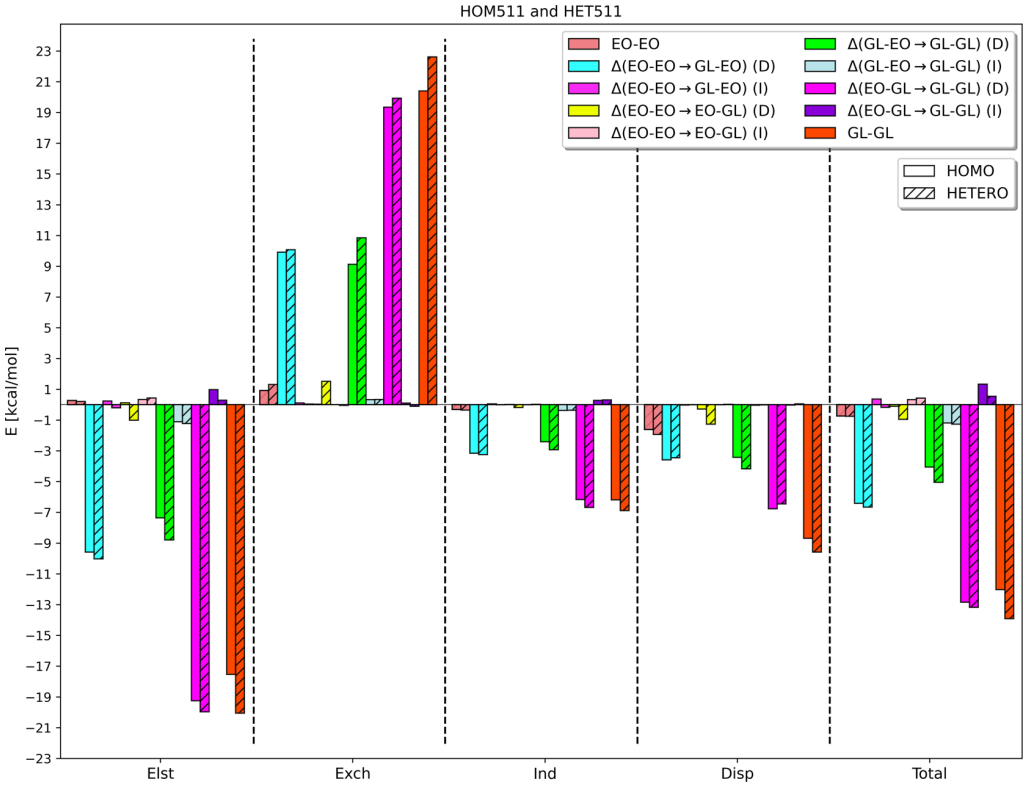

Figure 7. Interaction energy components for the HOM511/HET511 pair of glycidol dimer structures as predicted by the F-SAPT difference analysis at the SAPT0/AVTZ level of theory. The bars marked EO−EO denote the energy components for the ethylene oxide (EO) dimer, which in subsequent steps is expanded into the glycidol dimer by replacing one hydrogen atom at a time by a $-CH_2OH$ functional group, as explained in detail in the text. The effects of this replacement are partitioned into the direct energy difference (denoted "D") between the molecule$-CH_2OH$ and molecule−H interactions and the indirect effect (denoted "I") stemming from an altered interaction with the ethylene oxide backbone.

energies using two quantities: the mean unsigned error (MUE) for all 14 interaction energies at the minima and the MUE for seven chirodiastaltic energies. Table 3 presents the comparison of the resulting errors for several wave function methods. As can be seen from this table, SAPT2+3 and MP2 have the smallest MUE values of interaction energies in the aug-cc-pVTZ basis set, but neither method is converged to CBS at this level. It can be concluded that the accuracy of the results is strongly dependent on both the method and the basis set, as large basis sets including diffuse functions are vital to get reliable results for hydrogen-bonded complexes.[36,37] Among the four methods shown in Table 3, SAPT2+3 shows the most complete error cancellation between the RR(SS) and RS(SR) structures at the AVDZ level, which leads to an MUE of 0.073 kcal/mol for the chirodiastaltic energy. At the AVTZ level, the chirodiastaltic energy errors from MP2 and CCSD(T) become slightly smaller.

The MUE values for different dispersion-corrected DFT variants relative to the DF-MP2/(AVQZ,AV5Z) + ΔCCSD(T)/AVTZ benchmark are listed in Table 4 both for the interaction energy and the chirodiastaltic energy, as computed in the aug-cc-pVTZ basis set. As this table shows, the BLYP-D3M, PBE0-D3, and B3LYP-D3 functionals perform well for glycidol dimer complexes with the MUE of 0.095, 0.112, and 0.117 kcal/mol, respectively. However, in contrast to the MUE values for the interaction energy, the most complete error cancellation for chirodiastaltic energy occurs in the PBE0-D3 dispersion-corrected functional, followed by the B3LYP-D3M(BJ) and PBE0-D3M(BJ) ones.

III.III. SAPT and F-SAPT Results. Table 5 shows the interaction energy components calculated using the SAPT0 and SAPT2+3[14,22] approaches and the resulting chirodiastaltic energies in the aug-cc-pVTZ basis set. SAPT provides the splitting of the total interaction energy into electrostatics, exchange, induction, and dispersion, which can be analyzed individually. All 14 dimer structures have considerable large and negative electrostatic energies, which are comparable in magnitude to the positive first-order exchange component. The large magnitude of electrostatic energy is not surprising for a hydrogen-bonded complex. The exchange part compensates the electrostatic part, and as a result, the total interaction energy is dominated by the two remaining terms, induction and dispersion.

The comparison of SAPT0 and SAPT2+3 reveals that the former method overestimates the binding (gives interaction energies that are too negative). However, the SAPT0 chirodiastaltic energies are in reasonably good agreement with SAPT2+3 (and with the benchmark values in Table 1), which is important as our subsequent F-SAPT difference analysis is performed at the SAPT0 level of theory. The biggest differences between SAPT0 and SAPT2+3 arise from the first-order exchange, which is more repulsive by 2.7−4.1 kcal/mol at the higher theory level. The electrostatic energy is also generally less negative for SAPT2+3, but by a smaller amount, up to 1.2 kcal/mol. On the other hand, the SAPT2+3 energy decomposition gives stronger attraction in the induction and dispersion parts, with the respective differences in the 0.5−0.8 and 1.0−1.5 kcal/mol ranges.

Figures 4−10 show the functional-group SAPT (F-SAPT) difference analysis using the decomposition defined in eqs 7 and 8. Here, F-SAPT was applied at the SAPT0 level to evaluate the components of interaction energies and chirodiastaltic energies

https://dx.doi.org/10.1021/acs.jpca.0c07764
J. Phys. Chem. A 2020, 124, 9436−9450

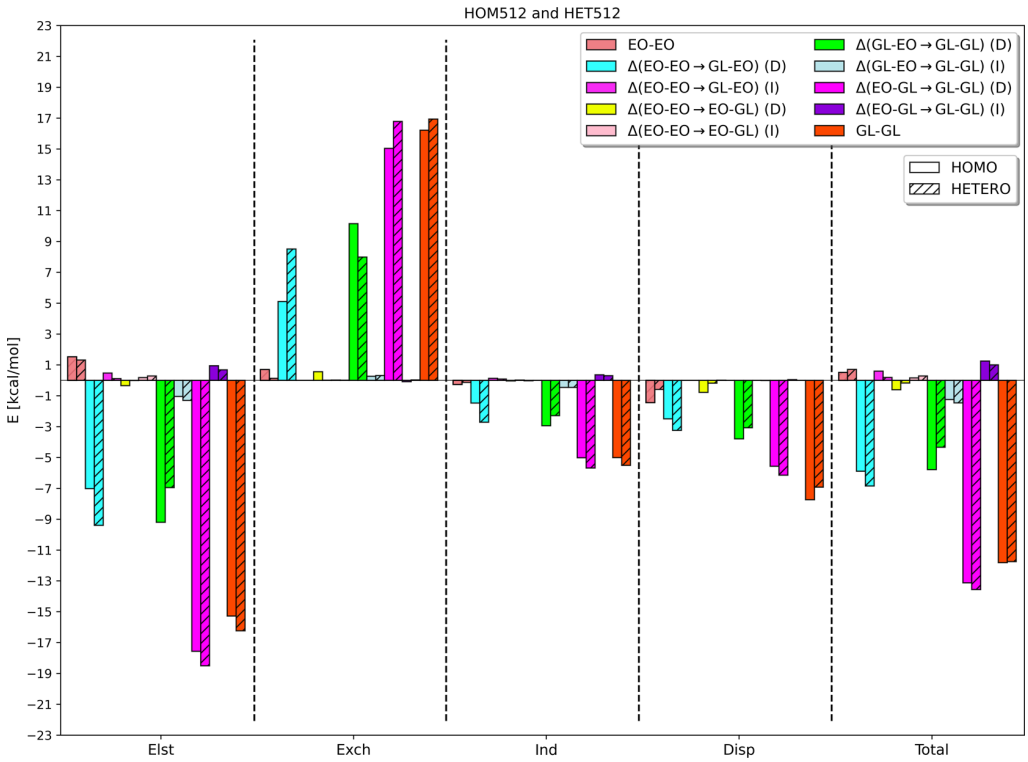

Figure 8. Interaction energy components for the HOM512/HET512 pair of glycidol dimer structures as predicted by the F-SAPT difference analysis at the SAPT0/AVTZ level of theory. The bars marked EO−EO denote the energy components for the ethylene oxide (EO) dimer, which in subsequent steps is expanded into the glycidol dimer by replacing one hydrogen atom at a time by a $-CH_2OH$ functional group, as explained in detail in the text. The effects of this replacement are partitioned into the direct energy difference (denoted "D") between the molecule$-CH_2OH$ and molecule$-$H interactions and the indirect effect (denoted "I") stemming from an altered interaction with the ethylene oxide backbone.

for all 14 glycidol dimer structures. F-SAPT allowed us to compute the SAPT component contributions from each pair of user-defined functional groups, which in this case are the epoxide ring and the hydroxymethyl. The hydroxymethyl groups were sequentially added to a reduced structure featuring two achiral ethylene oxide molecules. Specifically, the $-CH_2OH$ group replaced a hydrogen atom pointed exactly in the same direction as the $-CH_2OH$ carbon atom, with the distance optimized at the DF-MP2/AVTZ level, keeping the remaining part of the complex invariant. There are two distinct orderings in which the hydroxymethyl groups are added to form the glycidol dimer out of the ethylene oxide dimer. Except for the symmetric dimer structures such as HET811, these two orderings are not equivalent and the F-SAPT differences for both orderings are presented in Figures 4−10. Each F-SAPT difference is split into the direct and indirect effects of the $-H \rightarrow -CH_2OH$ substitution. The direct energetic effect refers to the difference between the interaction of the $-CH_2OH$ group with the entire other molecule and the corresponding interaction of its replacement −H atom. The remaining indirect effect is defined as the energy difference brought by the oxirane backbone, whose geometry does not change upon the $-H \rightarrow -CH_2OH$ replacement but the electron density does. Thus, it is the difference between the interaction of the entire other molecule and the oxirane backbone in glycidol versus the same oxirane backbone in ethylene oxide.

Figures 4−10 illustrate that the glycidol dimer structures are much more stable than their ethylene oxide dimer counterparts, as the increase in the attractive electrostatic, induction, and dispersion interactions is not nearly compensated by the growth in the repulsive exchange interaction upon the $-H \rightarrow -CH_2OH$ replacement. In sharp contrast with the propylene oxide dimer,[8] the induction energy is very important for glycidol complexes, providing nearly the same amount of net attraction as the dispersion energy. The HOM811 and HET811 data in Figures 4−10 reveal that the direct effects are similar each time the $-CH_2OH$ group is added, as in each addition one new hydrogen bond is formed. This is the common trend for all eight-membered rings, and it is completely different from the behavior of five-membered ring structures. Among the eight-membered rings, in particular for the HOM811 and HET811 pair, the changes for the two possible pathways (Figure 2) are highly consistent since these particular structures are close to symmetric. In the case of HOM822, there is no symmetry and the results for the two orderings are not exactly equal, but the trends of the direct and indirect energetic effects are similar to what we see for HOM811 and HET811. In other words, each $-H \rightarrow -CH_2OH$ replacement creates a relatively strong hydrogen bond (a large direct effect) and the two resulting bonds are similar in strength. If we look at the five-membered rings, there is quite a distinct behavior of the F-SAPT differences. We have the option to choose which monomer in the EO−EO structure undergoes the $-H \rightarrow -CH_2OH$ replacement first. One of the orderings of adding the functional groups gives a hydrogen bond the first time and a second hydrogen bond the second time, while the other ordering gives no hydrogen bonds the first time and both hydrogen bonds the second time. This is expected as in the case of five-membered rings, one of the oxygen atoms acts as a hydrogen bond donor and acceptor simultaneously. Moreover, by looking at the individual components in each figure, it becomes clear that the direct effects have much larger contributions

https://dx.doi.org/10.1021/acs.jpca.0c07764
J. Phys. Chem. A 2020, 124, 9436−9450

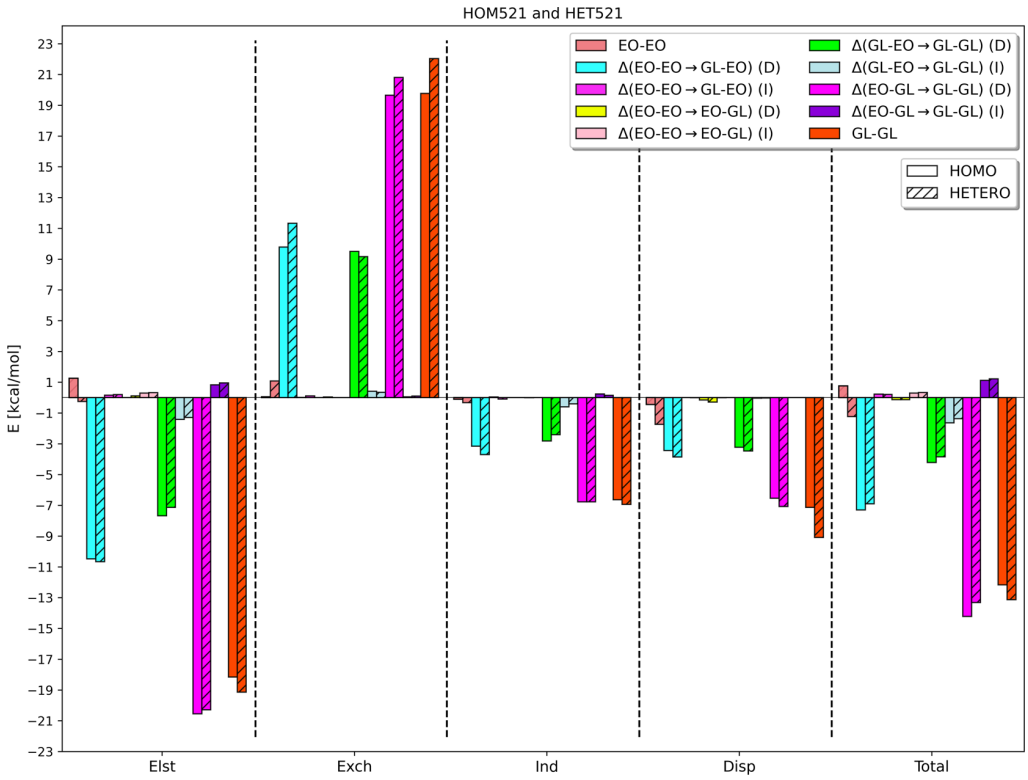

Figure 9. Interaction energy components for the HOM521/HET521 pair of glycidol dimer structures as predicted by the F-SAPT difference analysis at the SAPT0/AVTZ level of theory. The bars marked EO−EO denote the energy components for the ethylene oxide (EO) dimer, which in subsequent steps is expanded into the glycidol dimer by replacing one hydrogen atom at a time by a $-CH_2OH$ functional group, as explained in detail in the text. The effects of this replacement are partitioned into the direct energy difference (denoted "D") between the molecule−CH_2OH and molecule−H interactions and the indirect effect (denoted "I") stemming from an altered interaction with the ethylene oxide backbone.

to the total interaction energy than the indirect effects, especially for the homochiral structures. The indirect effects are quite small at all stages of substitution, especially the dispersion ones (indicating a near pairwise additivity of dispersion[38] for this system, similar to our earlier study[8]). The only noticeable indirect F-SAPT contributions arise from the electrostatic energy. In any case, the bulk of the chirodiastaltic energy comes from the direct effects of the hydroxymethyl group insertion.

It is quite difficult to ascribe the chirodiastaltic energies to individual F-SAPT differences. Figures 4−10 show that the addition of $-CH_2OH$ groups flips the energetic ordering of quite a few HOM/HET pairs, showing that there is no correlation between the overall GL−GL chiral interaction energy differences and the corresponding differences between the EO−EO backbone arrangements. Figures 4−10 also show that for all pairs of diastereomeric structures, the contributions of all individual SAPT components to the chirodiastaltic energy are large. However, the differences in the first-order repulsive exchange energy are largely canceled by the attractive electrostatic, induction, and dispersion contributions. Altogether, the energetic ordering of the RR and RS diastereomers follows the ordering of the electrostatic contributions except for the HOM822/HET822 and HOM512/HET512 pairs.

III.IV. Vibrational Frequency Shifts. We conclude this section by examining the frequency shifts of the normal modes of an isolated glycidol molecule resulting from the intermolecular interaction. We focus on the four most interesting modes in Figure 11 that exhibit the largest shifts (the numerical data for all other modes are presented in the Supporting Information). They are the rotation of the $-CH_2OH$ group around the C−C bond, the rotation of the alcohol hydrogen atom around the C−O bond, the C−C−O bending involving the hydroxyl group oxygen, and the O−H stretching, corresponding to $\nu_1 = 155.0\ cm^{-1}$, $\nu_4 = 458.9\ cm^{-1}$, $\nu_5 = 623.6\ cm^{-1}$, and $\nu_{27} = 3778.4\ cm^{-1}$, respectively.

For the O−H stretching mode, the frequencies in the dimers are always lower relative to the monomer (red-shifted), which is the typical characteristic of the hydrogen bonds. An examination of the frequency values for the stretching mode reveals a clear difference between the structures with eight-membered rings and those with five-membered rings. In the eight-membered ring structures, both hydrogen bonds are similar because they are formed with the same type of oxygen atom acceptor belonging to the epoxide ring. Therefore, the differences between the two frequency shifts are small. However, for the five-membered rings, these differences are larger because the two hydrogen bonds are not equivalent: one of the acceptor oxygen atoms belongs to the epoxide ring, while the second acceptor is the alcohol group oxygen.

We now turn to the ν_5 normal mode that describes the C−C−O bending motion involving a ring carbon, a nonring carbon, and the hydroxyl oxygen. There is an interesting pattern in this mode for both eight-membered and five-membered rings: when the two molecules in a dimer are in the M1 conformation from Figure 1, both frequency shifts are small. Once one of the monomers in the complex has the M1 conformation and the other the M2 one, there will be one big shift and one small shift in frequencies. Finally, when both monomers in the dimer are in the M2

https://dx.doi.org/10.1021/acs.jpca.0c07764
J. Phys. Chem. A 2020, 124, 9436−9450

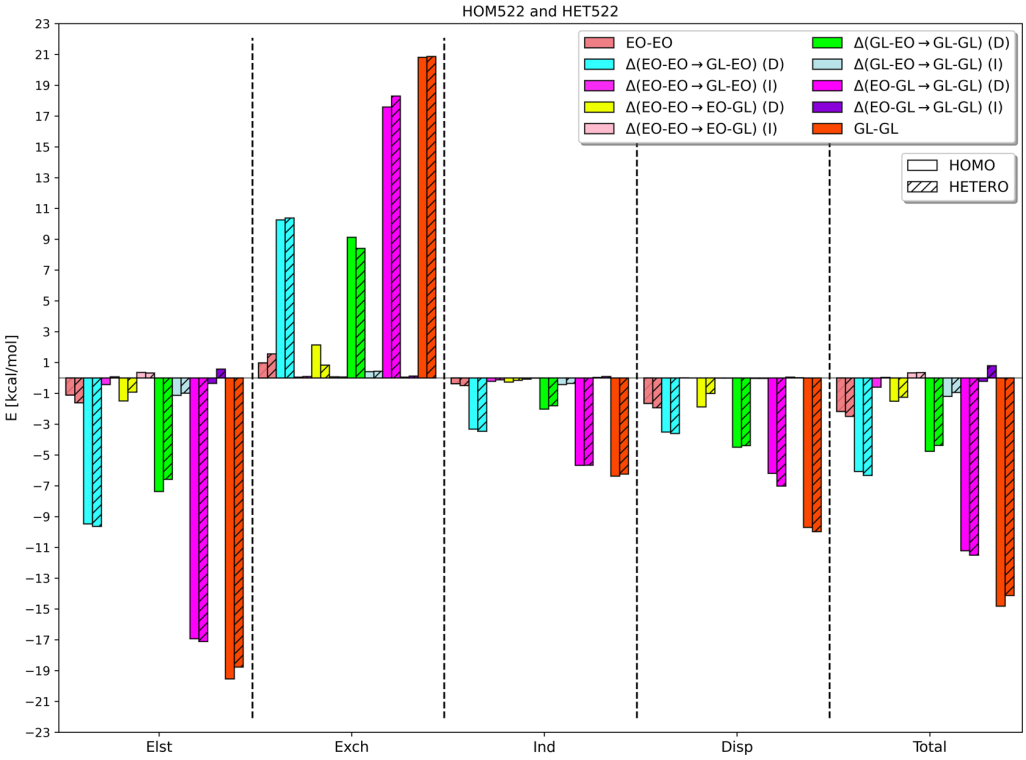

Figure 10. Interaction energy components for the HOM522/HET522 pair of glycidol dimer structures as predicted by the F-SAPT difference analysis at the SAPT0/AVTZ level of theory. The bars marked EO−EO denote the energy components for the ethylene oxide (EO) dimer, which in subsequent steps is expanded into the glycidol dimer by replacing one hydrogen atom at a time by a $-CH_2OH$ functional group, as explained in detail in the text. The effects of this replacement are partitioned into the direct energy difference (denoted "D") between the molecule$-CH_2OH$ and molecule−H interactions and the indirect effect (denoted "I") stemming from an altered interaction with the ethylene oxide backbone.

conformation, we see two large frequency shifts. Among the two possible minimum structures for an isolated glycidol molecule, M1 is the global minimum while M2 is the next accessible local minimum; note that we are comparing all frequency shifts against the global minimum monomer conformation M1. Because of this observation, we calculated the normal modes for the local minimum M2 structure and found that the ν_5 mode has a frequency of 521.7 cm^{-1}, a −102.0 cm^{-1} shift relative to the global minimum, and a similar shift to those observed in Figure 11. Thus, the large ν_5 shifts displayed in Figure 11 arise entirely out of the monomer transformation from the M1 conformation to the M2 one, and any effects of the intermolecular interaction, beyond facilitating this transformation, are minor.

The next important frequency in Figure 11 is ν_4, which corresponds to the H atom of the hydroxyl group rotating around the C−O bond. As can be seen, the frequency shifts are large and positive (blue-shifted) for this mode. At the equilibrium, there is a hydrogen bond between the H atom of the alcohol group and the O atom of the adjacent glycidol monomer. However, when this H atom starts to rotate out of position, it breaks the hydrogen bond; as a result, the energy increases and this leads to a steeper potential well and an increase in the frequency. As a result, we observe a larger vibrational frequency in the dimer than in the monomer, and the frequency shifts themselves are large too, big enough to reorder the frequencies of normal modes relative to the isolated monomer. It is notable that one of the two ν_4 frequency shifts is particularly large, up to about 400 cm^{-1}, for all structures with five-membered rings, indicating that a smaller ring is particularly sensitive to the distortion associated with the H atom rotation.

The last normal mode highlighted in Figure 11 is ν_1, which is a low-energy torsional mode corresponding to the rotation around the C−C bond between the oxirane backbone and the hydroxymethyl group. In the case of the M1 monomer structure, the lowest harmonic vibrational mode has been estimated around 155.0 cm^{-1}, which is in an acceptable agreement with the experimental value of 145(15) cm^{-1}.[26] Moreover, this C−C torsional mode frequency is in good agreement with side bands of the experimental gas-phase spectrum in Figure 1 of ref 2.

As Figure 11 shows, almost all of the ν_1 frequencies are blue-shifted. The examination of this normal mode in the complex structures shows that this is a mixed torsional mode. As a result, instead of finding two frequencies with a pronounced C−C torsional character, there were three such modes. This means that the ν_1 mode is mixed with something else in the dimer (specifically, with an intermolecular vibration), and that is why there are three frequency shift bars for ν_1 in Figure 11. Two of these bars always indicate blue shifts, showing that the intramolecular torsional motion is somewhat hindered by the intermolecular hydrogen bonding, while the last frequency is either unchanged or slightly red-shifted.

IV. SUMMARY

In this study, we have elucidated the chiral discrimination effects in the interaction between two glycidol molecules using high-accuracy ab initio calculations. These weak noncovalent interactions give rise to 14 diastereomeric structures, consisting of seven homochiral and seven heterochiral conformations, categorized into eight-membered ring and five-membered ring

https://dx.doi.org/10.1021/acs.jpca.0c07764
J. Phys. Chem. A 2020, 124, 9436−9450

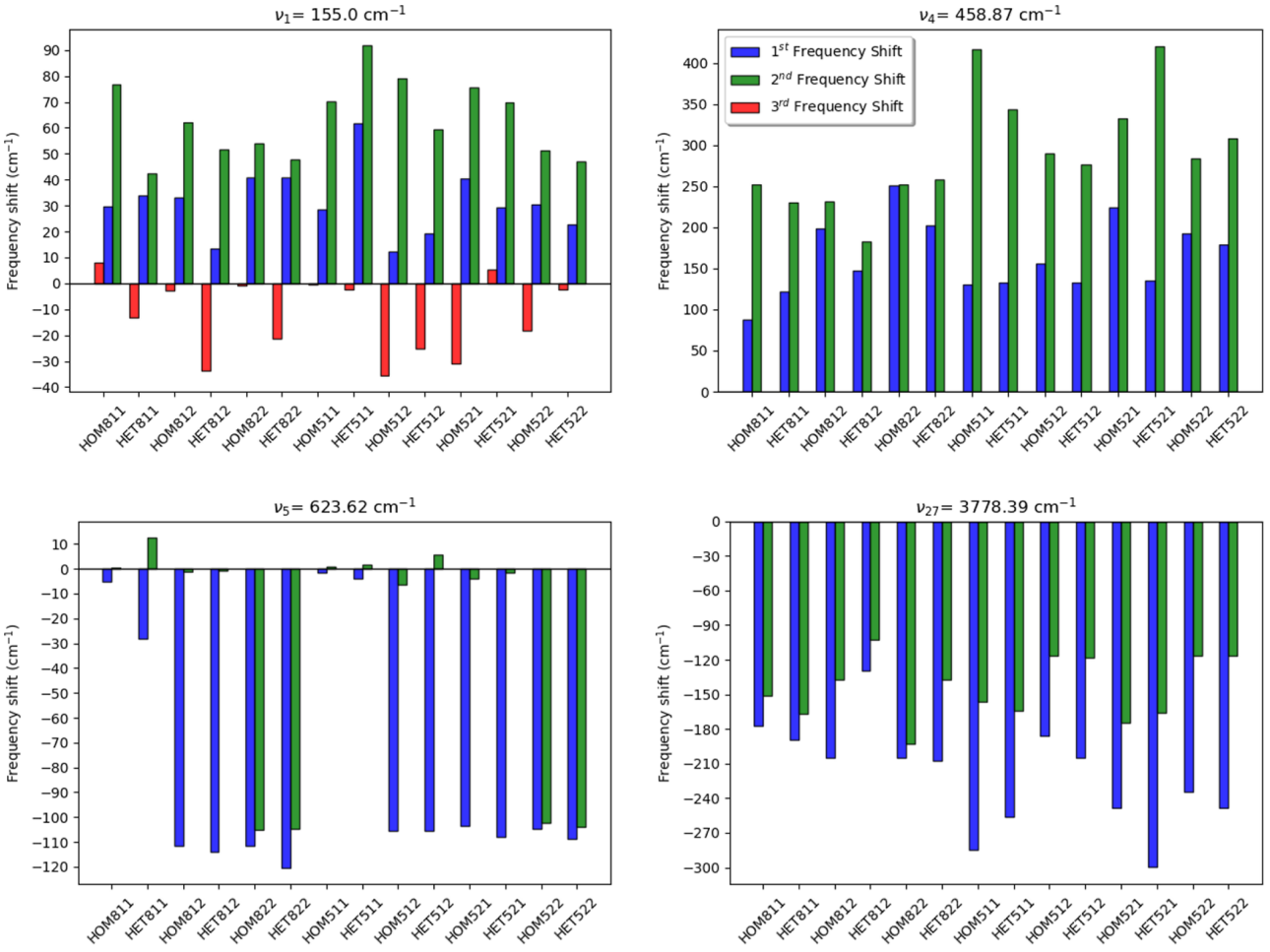

Figure 11. Vibrational frequency shifts of the most important normal modes of the 14 glycidol dimer structures relative to the isolated monomer frequencies. Because of the existence of two identical monomers, there are two frequency shifts pertinent to each monomer in the complex. The ν_1 mode is strongly coupled to an intermolecular mode and heavily contributes to the three frequencies shown.

structures, occurring in pairs that exhibit the same pattern of hydrogen bonding and the same monomer conformations. The effects of chirality of the glycidol molecules lead to diastereomeric energy differences between homo- and heterochiral complexes in the range of 0.1−1.6 kcal/mol for the interaction energy and 0.1−1.1 kcal/mol for the binding energy (the latter includes monomer deformation). The geometries of dimers were taken from ref 7 and reoptimized at the DF-MP2 level with the AVTZ basis set, and the benchmark interaction energy values for all 14 structures were calculated at the DF-MP2 level and extrapolated to the complete basis set limit from AVQZ and AV5Z in the standard X^{-3} extrapolation of the correlation part,[39] with an added ΔCCSD(T) correction computed in the AVTZ basis set.

Both supermolecular approaches such as dispersion-corrected density functional theory (DFT+D)[30,40] and perturbative methods such as SAPT[14] were used to calculate the interaction energies in the 14 glycidol dimer structures. Among different flavors of DFT+D, the BLYP-D3M, B3LYP-D3, and PBE0-D3 variants perform very well on the interaction energies with the lowest average error around 0.1 kcal/mol. As the MUE values show, the chirodiastaltic energies benefit from error cancellation between the homo- and heterochiral dimer structures for most variants and methods considered. Approximate approaches such as DFT+D recover the chiral energy differences with an accuracy of about 0.1 kcal/mol.

The symmetry-adapted perturbation theory leads to a systematic overbinding of all glycidol dimer structures, but at the more accurate SAPT2+3 level, the overbinding is less severe than at the SAPT0 level. Both SAPT0 and SAPT2+3 show similar interaction energy trends and nearly always predict the correct sign for the chirodiastaltic energy values. The acceptably accurate SAPT0 description of the chirodiastaltic energy can be used to get insight into the origins of the chiral recognition in the glycidol complexes. Accordingly, we fine-grained the SAPT data by performing F-SAPT calculations with each glycidol molecule partitioned into the oxirane backbone and the hydroxymethyl group. Moreover, we carried out a difference analysis in which the effects of a hydrogen atom replacement in ethylene oxide by a hydroxymethyl group in glycidol can be singled out and analyzed. In this way, the direct (functional group interaction) and indirect (backbone electronic reorganization) effects of the −H → −CH_2OH substitution are distinguishable. The SAPT results show a typical pattern for a complex held together by two hydrogen bonds: while the electrostatic energy is the largest attractive term, it is more than offset by the repulsive first-order exchange energy so that the total first-order effect is repulsive. In second order, in addition to a sizable dispersion energy, nearly the same amount of stabilization is provided by induction. Moreover, the direct effects of the −H→ −CH_2OH substitution in the

https://dx.doi.org/10.1021/acs.jpca.0c07764
J. Phys. Chem. A 2020, 124, 9436−9450

F-SAPT energy differences overwhelm the indirect effects. The dominant contributions in the F-SAPT difference analysis arise from the hydrogen bond formation upon substitution. For the eight-membered ring structures, hydrogen bonds are always formed one at a time, while for the five-membered ring ones, two bonds can be formed one at a time or both at once, depending on which $-CH_2OH$ group is added first.

As a result of the intermolecular interaction, two distinguishable shifts of each vibrational frequency of an isolated glycidol molecule are obtained from calculations. These two frequency shifts were analyzed at the DF-MP2/AVTZ level for all 14 structures. The largest shifts caused by the noncovalent interactions are arising from the C−C torsional mode (where one of the C atoms is out of the epoxide ring), the C−O torsional mode within the $-CH_2OH$ group, the C−C−O bending mode (two of those atoms are out of the epoxide ring), and the O−H stretching mode. The O−H stretching frequencies are around 3600−3700 cm^{-1}, in acceptable agreement with experiment.[26] Because of the nature of the hydrogen bonding in the eight-membered and five-membered ring structures, the differences between the two frequency shifts in this O−H stretching mode are small for the eight-membered ring conformations while there is a larger difference up to 140 cm^{-1} for the five-membered ring structures. There was an interesting pattern in the C−C−O bending mode, which makes it possible to distinguish which monomer conformations (M1, M2, or both) are present in the complex. Compared to the previously studied propylene oxide dimer,[8] the interaction energies, monomer flexibility effects, and frequency shifts are all much bigger due to the presence of two conventional O−H···O hydrogen bonds rather than the weaker C−H···O contacts.

■ ASSOCIATED CONTENT

Supporting Information

The Supporting Information is available free of charge at https://pubs.acs.org/doi/10.1021/acs.jpca.0c07764.

Cartesian coordinates for the 14 optimized configurations of the glycidol dimer (TXT)

Vibrational frequencies for all 14 complexes and for an isolated glycidol molecule (TXT)

■ AUTHOR INFORMATION

Corresponding Author

Konrad Patkowski − *Department of Chemistry and Biochemistry, Auburn University, Auburn, Alabama 36849, United States;* orcid.org/0000-0002-4468-207X; Email: patkowsk@auburn.edu

Author

Reza Hemmati − *Department of Chemistry and Biochemistry, Auburn University, Auburn, Alabama 36849, United States;* orcid.org/0000-0003-3258-1041

Complete contact information is available at: https://pubs.acs.org/10.1021/acs.jpca.0c07764

Notes

The authors declare no competing financial interest.

■ ACKNOWLEDGMENTS

This work was supported by the U.S. National Science Foundation awards CHE-1351978 and CHE-1955328. A part of the calculations was carried out at the Auburn University Hopper Research Cluster. We thank Dr. Assimo Maris for supplying us with the Cartesian geometries from ref 7.

■ REFERENCES

(1) Bailey, J.; Chrysostomou, A.; Hough, J. H.; Gledhill, T. M.; McCall, A.; Clark, S.; Ménard, F.; Tamura, M. Circular Polarization in Star-Formation Regions: Implications for Biomolecular Homochirality. *Science* **1998**, *281*, 672−674.

(2) Borho, N.; Suhm, M. A. Glycidol dimer: anatomy of a molecular handshake. *Phys. Chem. Chem. Phys.* **2002**, *4*, 2721−2732.

(3) Borho, N.; Haber, T.; Suhm, M. A. Chiral self-recognition in the gas phase: the case of glycidol dimers. *Phys. Chem. Chem. Phys.* **2001**, *3*, 1945−1948.

(4) Su, Z.; Borho, N.; Xu, Y. Chiral Self-Recognition: Direct Spectroscopic Detection of the Homochiral and Heterochiral Dimers of Propylene Oxide in the Gas Phase. *J. Am. Chem. Soc.* **2006**, *128*, 17126−17131.

(5) Yang, G.; Xu, Y. The effects of self-aggregation on the vibrational circular dichroism and optical rotation measurements of glycidol. *Phys. Chem. Chem. Phys.* **2008**, *10*, 6787−6795.

(6) Thomas, J.; Sunahori, F. X.; Borho, N.; Xu, Y. Chirality Recognition in the Glycidol···Propylene Oxide Complex: A Rotational Spectroscopic Study. *Chem. - Eur. J.* **2011**, *17*, 4582−4587.

(7) Maris, A.; Giuliano, B. M.; Bonazzi, D.; Caminati, W. Molecular Recognition of Chiral Conformers: A Rotational Study of the Dimers of Glycidol. *J. Am. Chem. Soc.* **2008**, *130*, 13860−13861.

(8) Hemmati, R.; Patkowski, K. Chiral Self Recognition: Interactions in Propylene Oxide Complexes. *J. Phys. Chem. A* **2019**, *123*, 8607−8618.

(9) Chojecki, M.; Rutkowska-Zbik, D.; Korona, T. On the applicability of functional-group symmetry-adapted perturbation theory and other partitioning models for chiral recognition — the case of popular drug molecules interacting with chiral phases. *Phys. Chem. Chem. Phys.* **2019**, *21*, 22491−22510.

(10) King, A. K.; Howard, B. J. A microwave study of the hetero-chiral dimer of butan-2-ol. *Chem. Phys. Lett.* **2001**, *348*, 343−349.

(11) Portmann, S.; Inauen, A.; Lüthi, H. P.; Leutwyler, S. Chiral discrimination in hydrogen-bonded complexes. *J. Chem. Phys.* **2000**, *113*, 9577−9585.

(12) Burns, L. A.; Marshall, M. S.; Sherrill, C. D. Appointing silver and bronze standards for noncovalent interactions: A comparison of spin-component-scaled (SCS), explicitly correlated (F12), and specialized wavefunction approaches. *J. Chem. Phys.* **2014**, *141*, No. 234111.

(13) Kodrycka, M.; Patkowski, K. Platinum, gold, and silver standards of intermolecular interaction energy calculations. *J. Chem. Phys.* **2019**, *151*, No. 070901.

(14) Jeziorski, B.; Moszyński, R.; Szalewicz, K. Perturbation Theory Approach to Intermolecular Potential Energy Surfaces of van der Waals Complexes. *Chem. Rev.* **1994**, *94*, 1887−1930.

(15) Hohenstein, E. G.; Sherrill, C. D. Wavefunction Methods for Noncovalent Interactions. *Wiley Interdiscip. Rev.: Comput. Mol. Sci.* **2012**, *2*, 304−326.

(16) Patkowski, K. Recent developments in symmetry-adapted perturbation theory. *Wiley Interdiscip. Rev.: Comput. Mol. Sci.* **2020**, *10*, No. e1452.

(17) Parrish, R. M.; Parker, T. M.; Sherrill, C. D. Chemical Assignment of Symmetry-Adapted Perturbation Theory Interaction Energy Components: The Functional-Group SAPT Partition. *J. Chem. Theory Comput.* **2014**, *10*, 4417−4431.

(18) Parrish, R. M.; Sherrill, C. D. Quantum-Mechanical Evaluation of π-π versus Substituent-π Interactions in π Stacking: Direct Evidence for the Wheeler-Houk Picture. *J. Am. Chem. Soc.* **2014**, *136*, 17386−17389.

(19) Bakr, B. W.; Sherrill, C. D. Analysis of transition state stabilization by non-covalent interactions in the Houk-List model of organo-catalyzed intermolecular Aldol additions using functional-group symmetry-adapted perturbation theory. *Phys. Chem. Chem. Phys.* **2016**, *18*, 10297−10308.

(20) Bakr, B. W.; Sherrill, C. D. Analysis of transition state stabilization by non-covalent interactions in organocatalysis: application of atomic

and functional-group partitioned symmetry-adapted perturbation theory to the addition of organoboron reagents to fluoroketones. *Phys. Chem. Chem. Phys.* **2018**, *20*, 18241−18251.
(21) Smith, D. G. A.; Burns, L. A.; Patkowski, K.; Sherrill, C. D. Revised Damping Parameters for the D3 Dispersion Correction to Density Functional Theory. *J. Phys. Chem. Lett.* **2016**, *7*, 2197−2203.
(22) Parker, T. M.; Burns, L. A.; Parrish, R. M.; Ryno, A. G.; Sherrill, C. D. Levels of Symmetry Adapted Perturbation Theory (SAPT). I. Efficiency and Performance for Interaction Energies. *J. Chem. Phys.* **2014**, *140*, No. 094106.
(23) Chojecki, M.; Rutkowska-Zbik, D.; Korona, T. Dimerization Behavior of Methyl Chlorophyllide a as the Model of Chlorophyll a in the Presence of Water Molecules−Theoretical Study. *J. Chem. Inf. Model.* **2019**, *59*, 2123−2140.
(24) Oki, M.; Murayama, T. Intramolecular Interaction between the Hydroxyl Group and the Oxirane Ring. *Bull. Chem. Soc. Jpn.* **1973**, *46*, 259−263.
(25) Oki, M.; Iwamura, H.; Murayama, T.; Oka, I. Intramolecular Interaction between the Hydroxyl Group and the Cyclopropane Ring. *Bull. Chem. Soc. Jpn.* **1969**, *42*, 1986−1991.
(26) Marstokk, K.-M.; Møllendal, H.; Stenstrøm, Y.; et al. Microwave Spectrum of Oxiranemethanol (Glycidol), the Assignment of a Second Hydrogen-Bonded Conformer and Conformational Composition in the Gas Phase and in Solution. *Acta Chem. Scand.* **1992**, *46*, 432−441.
(27) Dunning, T. H., Jr. Gaussian-Basis Sets for Use in Correlated Molecular Calculations. 1. The Atoms Boron through Neon and Hydrogen. *J. Chem. Phys.* **1989**, *90*, 1007−1023.
(28) Kendall, R. A.; Dunning, T. H., Jr.; Harrison, R. J. Electron Affinities of the 1st-Row Atoms Revisited - Systematic Basis Sets and Wave Functions. *J. Chem. Phys.* **1992**, *96*, 6796−6806.
(29) Řezáč, J.; Hobza, P. Benchmark calculations of interaction energies in noncovalent complexes and their applications. *Chem. Rev.* **2016**, *116*, 5038−5071.
(30) Grimme, S.; Antony, J.; Ehrlich, S.; Krieg, H. A Consistent and Accurate Ab Initio Parametrization of Density Functional Dispersion Correction (DFT-D) for the 94 Elements H-Pu. *J. Chem. Phys.* **2010**, *132*, No. 154104.
(31) Grimme, S.; Ehrlich, S.; Goerigk, L. Effect of the Damping Function in Dispersion Corrected Density Functional Theory. *J. Comput. Chem.* **2011**, *32*, 1456−1465.
(32) Werner, H.-J.; Knowles, P. J.; Knizia, G.; Manby, F. R.; Schütz, M. Molpro: a general-purpose quantum chemistry program package. *Wiley Interdiscip. Rev.: Comput. Mol. Sci.* **2012**, *2*, 242−253.
(33) Parrish, R. M.; Burns, L. A.; Smith, D. G. A.; Simmonett, A. C.; DePrince, A. E., III; Hohenstein, E. G.; Bozkaya, U.; Sokolov, A. Yu.; Di Remigio, R.; Richard, R. M.; et al. Psi4 1.1: An Open-Source Electronic Structure Program Emphasizing Automation, Advanced Libraries, and Interoperability. *J. Chem. Theory Comput.* **2017**, *13*, 3185−3197.
(34) Parrish, R. M.; Sherrill, C. D. Spatial assignment of symmetry adapted perturbation theory interaction energy components: The atomic SAPT partition. *J. Chem. Phys.* **2014**, *141*, No. 044115.
(35) Patkowski, K. Benchmark Databases of Intermolecular Interaction Energies: Design, Construction, and Significance. In *Annual Reports in Computational Chemistry*, Dixon, D. A., Ed.; Elsevier: Amsterdam, 2017; Vol. *13*, pp 3−91.
(36) Boese, A. D. Assessment of Coupled Cluster Theory and more Approximate Methods for Hydrogen Bonded Systems. *J. Chem. Theory Comput.* **2013**, *9*, 4403−4413.
(37) Řezáč, J. Non-Covalent Interactions Atlas Benchmark Data Sets: Hydrogen Bonding. *J. Chem. Theory Comput.* **2020**, *16*, 2355−2368.
(38) Grimme, S.; Hansen, A.; Brandenburg, J. G.; Bannwarth, C. Dispersion-Corrected Mean-Field Electronic Structure Methods. *Chem. Rev.* **2016**, *116*, 5105−5154.
(39) Halkier, A.; Helgaker, T.; Jørgensen, P.; Klopper, W.; Koch, H.; Olsen, J.; Wilson, A. K. Basis-Set Convergence in Correlated Calculations on Ne, N_2, and H_2O. *Chem. Phys. Lett.* **1998**, *286*, 243−252.
(40) Grimme, S. Semiempirical GGA-Type Density Functional Constructed with a Long-Range Dispersion Correction. *J. Comput. Chem.* **2006**, *27*, 1787−1799.

https://dx.doi.org/10.1021/acs.jpca.0c07764
J. Phys. Chem. A 2020, 124, 9436−9450